

RELATIONSHIP BETWEEN FIELD-CALCULATED SILICATE DISSOLUTION
RATES AND CARBON DIOXIDE PARTIAL PRESSURE

by
Alexis K. Navarre

A thesis submitted to the Faculty and Board of Trustees of the Colorado School of Mines in partial fulfillment of the requirements for the degree of Master of Science (Geochemistry).

Golden, Colorado

Date _____

Signed: _____

Alexis K. Navarre

Approved: _____

Dr. Geoffrey Thyne
Thesis Advisor

Golden, Colorado School of Mines

Date _____

Dr. Murray Hitzman
Professor and Head,
Department of Geology and
Geological Engineering

ABSTRACT

Weathering rates for plagioclase, alkali feldspar, biotite, and hornblende were calculated from field data collected in a series of canyons near Indian Wells Valley, CA. Flow in these canyons is intermittent and most of the discharge is through alluvium that fills the bottoms of the canyons. This alluvium is derived from the weathering of granite and granodiorite. Carbon dioxide concentrations in the stream waters have been measured and a range of values for PCO_2 was found from $10^{-1.3}$ to $10^{-2.65}$. Preliminary models of the system show a strong positive correlation between total dissolved solids (TDS) in the stream water and partial pressure of carbon dioxide (PCO_2). Slope and vegetation type do not change dramatically between these canyons, while changes in lithology and residence time can be accounted for, leading to the hypothesis that higher TDS is a result of faster weathering due to elevated CO_2 . Equations to correct weathering rates for increased partial pressures of CO_2 have been developed from laboratory experiments showing an increase in weathering rates proportional to approximately $PCO_2^{0.3}$.

Paces (1983) approach to calculating weathering rates was employed for data from the study area. A relationship between plagioclase dissolution rate and PCO_2 was developed and it shows that dissolution rate is proportional to $PCO_2^{0.58}$. This relationship is similar to the relationship previously reported from laboratory studies.

TABLE OF CONTENTS

	Page
ABSTRACT	iii
LIST OF FIGURES	vi
LIST OF TABLES	viii
ACKNOWLEDGMENTS	ix
Chapter 1. INTRODUCTION.....	1
Purpose.....	2
Concepts of Mass Balance Modeling	3
Previous Mineral Dissolution Studies.....	5
Previous PCO ₂ -Dependent Rate Studies.....	10
Chapter 2. DISCRIPTION OF STUDY AREA.....	12
Location	12
Physiography.....	12
Climate.....	15
Vegetation.....	15
Regional Geologic Setting and History	16
Study Area Mineralogy.....	17
Chapter 3. RESEARCH METHODS.....	21
Field Methods	21
Chemical Analysis	23
X-Ray Diffraction.....	24
Petrographic Analyses	25
Electron Microprobe Analyses	26
Geochemical Analyses.....	26
Inverse Modeling	26
Mass Balance Equations	29
Chapter 4. PRELIMINARY MODELING	36
Preliminary Observations.....	36
Geochemical Modeling with PHREEQC.....	38

Dissolution Rate Calculations.....	42
Chapter 5. RESULTS AND DISCUSSION	46
General Discussion	46
Plagioclase	49
Alkali-Feldspar	50
Hornblende.....	51
Biotite.....	51
Uncertainty in Calculation of Rates.....	53
Rate Dependency on PCO_2	58
Mechanism of Increased Rates	60
Chapter 6. CONCLUSIONS	62
REFERENCES CITED.....	63
APPENDIX 1. Field Notes	67
APPENDIX 2. ICP/IC Analyses.....	76
APPENDIX 3. X-Ray Diffraction Patterns	80
APPENDIX 4. Raw Point Count Data.....	83
APPENDIX 5. Sample Spreadsheet Used to Calculate Mineral Formulas from Oxide Weight percent Data	91
APPENDIX 6. PHREEQC Input Files	93
APPENDIX 7. Published Mineral Dissolution Rates	126
CD with electronic files of thesis and data	Back Cover

LIST OF FIGURES

		Page
Figure 1	Schematic showing sinks and sources of dissolved ions in stream water...	4
Figure 2	Shaded relief map of study area (modified from Guler, 2002).....	13
Figure 3	Satellite image of study area showing canyons used for data collection....	14
Figure 4	Major mineral percentages for each of the study canyons.....	18
Figure 5	Variations in sodium content of igneous plumes in study area.....	20
Figure 6	Groundwater, spring, and surface water samples from in and around Indian Wells Valley plotted on a Ca/Mg activity diagram	20
Figure 7	Locations of water samples (A34-A51) and alluvium samples (A60-A64).....	22
Figure 8	Conceptual model of discharge through alluvium	34
Figure 9	Conceptual model of flow of water down the study canyons	35
Figure 10	Schoeller diagram plot of all surface water samples collected in 2002 field season.....	36
Figure 11	Piper diagram plot of all surface water samples collected in 2002 field session	37
Figure 12	Sample locations of data used in preliminary modeling overlaid on DEM of study area	39
Figure 13	TDS and PCO ₂ from previously collected samples, numbers are sample locations (see Figure 12).....	40
Figure 14	Mg/Si and PCO ₂ from previously collected samples, numbers are sample locations (see Figure 12).....	40
Figure 15	TDS and CO ₂ consumed from modeling of previously collected samples, numbers are sample locations (see Figure 12).....	41
Figure 16	TDS and Co ₂ consumed from 2002 field samples	42

Figure 17	Initial calculated plagioclase dissolution rates.....	44
Figure 18	Initial calculated Hornblende dissolution rates.....	45
Figure 19	Sensitivity of Paces equation to variables.....	46
Figure 20	Comparison between published field derived rates and rates calculated for this study from base of canyon samples.....	47
Figure 21	Comparison between published lab derived rates and rates calculated for this study from base of canyon samples.....	47
Figure 22	Calculated rates using sodium as mass balance constraint from base of canyon samples	48
Figure 23	Calculated biotite rates using fluoride as the mass balance constraint from base of canyon samples	48
Figure 24	Correlation between plagioclase dissolution rates and PCO_2	50
Figure 25	Correlation between AFS dissolution rates and PCO_2	52
Figure 26	Correlation between hornblende dissolution rates and PCO_2	52
Figure 27	Correlation between biotite dissolution rates and PCO_2	54
Figure 28	Uncertainty in calculated rates related to analytical uncertainty	54
Figure 29	Plagioclase rates for all samples that fit hydrologic model	56
Figure 30	Alkali-feldspar rates for all samples that fit hydrologic model	56
Figure 31	Hornblende rates for all samples that fit hydrologic model.....	57
Figure 32	Biotite rates for all samples that fit hydrologic model.....	57
Figure 33	Topographic map showing two branches of 5-Mile Canyon and sample locations.....	59
Figure 34	Calculated rates from this study plotted with aCO_3^{2-}	61

LIST OF TABLES

	Page
Table 1	Volumetric percent of minerals in alluvium from point count data.....19
Table 2	Results of charge balance analysis on water samples24
Table 3	060 peak positions for identification of smectites phase (Moore and Reynolds, 1997)25
Table 4	Mineral formulas determined by electron microprobe analysis.....27
Table 5	Definitions of variable used in Paces (1983) mass balance equations.....30
Table 6	Comparison of residence time calculations43
Table 7	Uncertainty in plagioclase rate associated with sodium flux distribution for 9-Mile Canyon.....51

ACKNOWLEDGEMENTS

Partial support of this project was provided by The Geological Society of America (student research grant number: 7234-02). Financial assistance provided from August 2000 to May 2002 by the Department of Geology and Geological Engineering, Colorado School of Mines is gratefully acknowledged.

I would like to thank the members of my thesis committee: Professors Humphrey and Romberger for their time and interest in this study. I would especially like to thank my advisor, Dr. Geoff Thyne, for his time, patience, and enthusiasm throughout this study.

Dr. Duane Hrcir (Mesa State College) and Dr. John Drexler (University of Colorado, Boulder) are gratefully acknowledged for their time and expertise in sample analysis. I would like to thank Charles and Candace Pierce for their support during a six-week field session.

Finally, I would like to thank my family and friends for their support and understanding.

Chapter 1 - Introduction

Measurements show that the atmospheric concentration of carbon dioxide (CO₂) has increased from 290 ppm to more than 360 ppm since 1890, primarily due to human activities such as the burning of fossil fuels (Robinson et al., 1998). The chemical weathering of silicate minerals is a natural sink for atmospheric CO₂ (Volk, 1987), but is not rapid enough to balance current anthropogenic inputs to the atmosphere, and these elevated levels of CO₂ may be contributing to global warming (Robinson et al., 1998). Recently, proposals have called for the sequestration of CO₂ by injection into depleted natural gas reservoirs and deep saline aquifers where it will react with reservoir rocks (Stevens and Gale, 2000). This process is an extension of enhanced oil recovery techniques presently used by many oil companies. Quantification of potential sequestration and the effects of injecting large amounts of CO₂ into the ground will require knowledge of mineral dissolution rates at the elevated CO₂ levels. This relationship has proven to be a source of significant uncertainty when trying to model this process. Laboratory rates have been determined for plagioclase dissolution in the presence of elevated CO₂ (Lagache, 1964), but field weathering rates are generally 2-4 orders of magnitude slower than lab measured rates (White et al., 2001) making the application of laboratory rates to field conditions questionable.

In addition to modeling CO₂ sequestration, many researchers have worked on creating paleoclimate and paleotemperature models (Berner et al., 1983; Suchet and Probst, 1993; Berner, 1995). These models require weathering reaction rates of silicate minerals that are CO₂ dependent. The major difference between models is the variability in PCO₂ dependence of silicate weathering rates. Most models are based on reaction rates proportional to PCO₂^{0.3}, a relationship developed by Lagache (1965) through high temperature feldspar dissolution experiments (Brady and Carroll, 1994).

The effect of CO₂ on mineral dissolution rates has been attributed to the lowering of pH in the presence of high concentrations of CO₂. Acceleration of silicate dissolution

rates due to low pH generally occurs under acidic conditions, pH less than 4-5 (Berg and Banwart, 2000). Under acidic conditions, the dissolution rate is proportional to a fractional power of the hydrogen ion activity ($a_{H^+}^n$) where n is between 0 and 1 (Lasaga, 1995). In neutral pH conditions the pH dependence is minimal and can be ignored. Values of pH in the study area for this research range from 6.8 to 8, indicating that the presence of excess CO₂ is not depressing stream water pH enough to cause a significant increase in dissolution rates.

Purpose

The purpose of this study was to calculate mineral dissolution rates from field-collected data and determine whether a relationship between field-derived mineral dissolution rates and CO₂ concentrations can be defined. Using inverse modeling and mass balance methods, dissolution rates can be calculated from data collected in an area of elevated PCO₂ and define a relationship between these rates and PCO₂. In order to evaluate the assumption that there is no relationship between CO₂ and dissolution rate at near-neutral pH, a method to determine dissolution rates for individual minerals was developed. Previous studies applying mass balance equations to calculate weathering rates have relied on the assumption that the entire flux of one ion is due to the dissolution of a single mineral. In most studies, plagioclase dissolution is calculated using sodium flux data. As a first approximation these calculations are correct if no other sources of sodium, such as hornblende ((Ca,Na)₂₋₃(Mg,Fe,Al)₅Si₆(Si,Al)₂O₂₂(OH)₂), are present in the rocks and the alkali-feldspar ((K,Na)AlSi₃O₈) is pure orthoclase (KAlSi₃O₈). If hornblende is present, or if the alkali-feldspar (AFS) is a solid solution between orthoclase and albite (NaAlSi₃O₈), there are multiple sources of sodium. Electron microprobe, x-ray diffraction, and petrographic analyses were used to distribute the flux of ions between different mineral phases, thereby allowing relative individual mineral dissolution rates to be calculated with a lower degree of uncertainty.

Concepts of Mass Balance Modeling

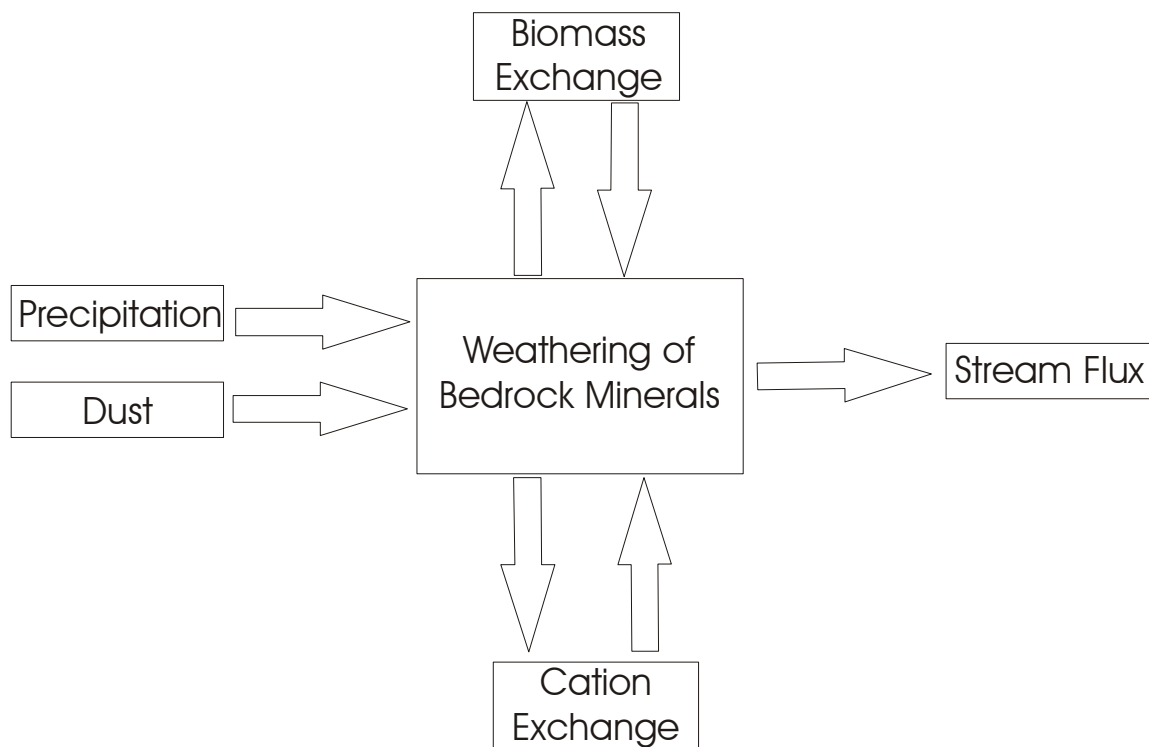
Mass balance calculations are the basis for inverse models in geochemical modeling software. Mass balance equations provide a budgeting system to keep track of fluxes of solutes into and out of a system. For instance, inverse models calculate all mathematically possible solutions when reacting water with the chemical composition of precipitation with bedrock minerals to produce water with the chemical composition of catchment outflow.

Drever's (1997) discussion of mass balance methods is summarized here. Sources and sink of solutes within a catchment are assigned and their fluxes measured; the sum of the sources must equal the sum of the sinks. Equation 1.1 illustrates a very simple mass balance model. Figure 1 is a schematic diagram showing sources and sinks of dissolved constituents found in stream waters and illustrates the concept in equation 1.1.

$$\begin{aligned} \text{solute in outflow} = & \text{solute from atmosphere} + \text{solute from weathering} \\ & \pm \text{solute from change in biomass} \pm \text{change in exchange pool} \end{aligned} \quad (1.1)$$

This simple concept is difficult to implement due the importance of identifying and quantifying all contributions to each flux measured. The resulting model often has uncertainties associated with measurement and analysis of both physical and chemical parameters. Time is not considered in a mass balance model. It is assumed that changes in water storage and biomass effects are averaged out over an annual cycle; therefore, most models are constructed for a time-scale greater than one year. Calculation of the solutes in outflow requires measurement of the total volume of water leaving the catchment and the chemical composition of that water. Stream gauging is the most common method of determining discharge volume, assuming that minimal amounts of water are leaving the catchment through groundwater flow (Drever, 1997). Solute input into the system from the atmosphere includes precipitation (rain and snow), condensation from mist or fog, and dry deposition (dust). Solute release from weathering is difficult to

Figure 1. Schematic showing sinks and sources of dissolved ions in stream water.



quantify. Most mass balance models are set up to calculate this term in the equation as an approximation of mineral dissolution rates. This approach requires assignment of values to solutes from change in both biomass and exchange pool or assuming these values to be negligible and dropping them from the equation. The uncertainty with this approach is minimized when constraining the mass balance equations with an element that behaves conservatively within the catchment, most commonly sodium. An element is conservative when the concentration is not decreased by removal from the system, either by precipitation or biomass activity.

Previous Mineral Dissolution Studies

Many researchers have addressed the difficulty of calculating weathering rates from field data. Starting with Garrels and MacKenzie (1967), the mass-balance approach has been the most widely used and become the most accepted. A number of researchers have demonstrated the use of variations on Garrels and MacKenzie's (1967) mass-balance methods to calculate weathering, cation denudation, and soil formation rates in the field (Plummer and Back, 1980; Paces, 1983; Velbel, 1985; Taylor and Velbel, 1991; Velbel, 1992; Furman et al., 1998). The mass-balance method has also been used to determine the effect that acid deposition has on field weathering rates (Mast et al., 1990).

Garrels and MacKenzie (1967) studied the composition of spring waters in the Sierra Nevada Mountain range of California. These springs lie northwest of this study area, in the northern Sierra Nevada. Based on previous work by Feth et al. (1964), a mass-balance model was constructed to back-react spring water with kaolinite ($\text{Al}_2\text{Si}_2\text{O}_5(\text{OH})_4$) and produce the original bedrock minerals. Ion flux from snow and rain precipitation was removed from average ephemeral spring water composition. Sodium, calcium, bicarbonate, and silica were removed from the water to react with kaolinite and produce plagioclase until sodium was exhausted. The remaining water was reacted with kaolinite to produce biotite ($\text{K}(\text{Mg},\text{Fe})_3(\text{AlSi}_3\text{O}_{10})(\text{OH})_2$) by removing the required magnesium, potassium, bicarbonate, and silica. Potassium, bicarbonate, and silica remaining were used to produce alkali feldspar. A slight excess of silica remained after the calculations had been performed. The results from these reactions were interpreted to show that the system is closed and that CO_2 is an important component. Silica mass balance showed that dissolution of quartz (SiO_2) is minor and adds an insignificant amount of dissolved silica to solution. It was also shown that plagioclase dissolution accounts for approximately 80% of the dissolved constituents in the water. Although hornblende is found in these rocks, Garrels and MacKenzie (1967) attributed all sodium in solution to the weathering of plagioclase and did not include hornblende in their mass-

balance calculations. The same procedure was followed starting with an average perennial spring composition resulting in a considerable amount of excess calcium and magnesium. It was assumed that these waters have deeper circulation paths and the excess calcium was a result of dissolution of calcium carbonate along the flow path. Excess magnesium was accounted for by converting kaolinite to montmorillonite. The models were unable to produce results that concluded that an equilibrium state had been reached between the minerals and the waters.

Paces (1983) developed an equation to calculate rate constants for dissolution from data collected in the field. Rate constants can be calculated using equation (1.2).

$$k = m_w - F\tau / n\hat{s}\tau = Q_r/n\hat{s}Hp \quad (1.2)$$

k = rate constant in mol mineral/m²/yr

m_w = concentration of chemical species in runoff in m/m³

F = net input of a chemical species from precipitation in mol/m³/yr

n = fraction of rock surface occupied by dissolving minerals

\hat{s} = specific wetted surface of rock saturated with water in m²/m³

τ = residence time of water in the catchment in yrs

Using equation 1.2 and data collected in two catchments in Czechoslovakia, Paces (1983) calculated a rate constant on the order of 10⁻¹⁴ for oligoclase (Ab₉₀-Ab₇₀) using sodium flux data. This value is 2 orders of magnitude lower than those calculated in the laboratory for the same study. The difference in these values was attributed to the fresh experimental surfaces of oligoclase for the lab-derived rates. Biological uptake in the calculations was ignored under the assumption of steady-state conditions where the amount of sodium taken up by plants equals the amount of sodium released by decaying plant matter.

Velbel (1985) used a system of geochemical mass balance equations developed by Plummer and Back (1980) to determine weathering rates of rock-forming silicate

minerals in the Nantahala Mountains in southwest North Carolina. Stream chemistry and saprolite composition were used to constrain the mass balance model. Weathering rates were calculated based on the flux of material leaving the system dissolved in stream water, uptake of calcium, magnesium, and potassium by the biomass, and weathering products identified in the saprolites. Major minerals found in the metamorphic rocks of the region are quartz, muscovite and biotite micas, plagioclase feldspar, and almandine garnet. Other accessory minerals were present, but not found to influence the chemistry of the soils and therefore not considered in the weathering calculations. Velbel (1985) found that the formation of local saprolite was primarily from the weathering of biotite mica, almandine garnet, and sodic plagioclase feldspar. Weathering products were determined through petrographic analysis and the combination of these data with empirical mineral compositions constrained the weathering reactions used in the mass balance model.

Calculated rates indicated that there was relatively more plagioclase and biotite weathering from one rock type compared to others, possibly related to a larger percentage of biotite and plagioclase in that rock type. Calculated garnet weathering rates were independent of rock type. In order to compare his field measured rates to previous laboratory measured rates, the rates were normalized to an estimated particle size of 1 mm in diameter and the modal percentages of each mineral. In any normalization of field weathering rates, the reactive mineral surface area is a major source of error, but as Velbel (1985) pointed out, estimated weathering rates will not vary by more than one order of magnitude due to the linear relationship between surface area normalized rate, particle size and modal percent since it is highly unlikely that any of these parameters will be off by an order of magnitude. The rates calculated by Velbel's (1985) mass balance model ranged from 2.3×10^{-9} to 8.64×10^{-10} moles/m²/sec for plagioclase, 3.8×10^{-12} for almandine, and 1.2×10^{-13} for biotite. When normalized to reactive surface area, the rates for almandine and plagioclase are no more than one or two orders of magnitude slower than laboratory rates.

Taylor and Velbel (1991) examined the effect of botanical uptake terms on weathering rates determined by mass balance methods. They noted that Cleaves et al. (1970) calculated weathering rates based on Na and Mg, two elements that are the least likely to be affected by botanical processes and that these rates produced more K and Ca than could be accounted for in the mass balance. Their study calculated weathering rates both with a system that included botanical uptake as an unknown and one where botanical processes were assumed to be steady state. While plagioclase rates were generally similar between the two methods, the rates of garnet weathering were up to 46% higher in the calculation where a botanical exchange term was included and rates of biotite were up to 248% higher. Based on these data, it can be assumed that a weathering rate calculated without accounting for botanical processes is a minimum estimate.

Velbel (1992) continued his work in the southern Blue Ridge by calculating amphibole, biotite, and plagioclase weathering rates in a canyon near his previous studies. Unlike the prior study areas, bedrock in this canyon contains amphibole. This study concluded that the mass-balance of alkali and alkaline earth elements in the watershed could be explained by weathering of plagioclase, hornblende, biotite, and calcite. Final weathering rates were increased to allow for uptake of ions by plants based on his previous studies in nearby watersheds. Weathering rates calculated for plagioclase, hornblende, biotite, and calcite were 393, 115, 407, and 1270 moles of mineral per hectare per year, respectively. Calcite is present in the watershed as a minor phase in the bedrock and also as residual lime from agriculture activities in the 1940's. If the weathering rates for plagioclase and hornblende are normalized by modal percentages of the minerals in bedrock, plagioclase and hornblende appear to weather at almost exactly the same rate per unit modal abundance.

Boeglin and Probst (1998) calculated weathering rates in the Niger basin in west Africa based on a mass balance model. Their model requires knowledge of the amount of silica in the parent material and saprolite, as well as the flux of silica exiting the basin via stream flow. Equation 1.3 was used to calculate a chemical weathering rate (WR_{ch}).

$$WR_{ch} = F_{SiO_2} / (S_o - S_s) \quad (1.3)$$

F_{SiO_2} = specific flux of dissolved silica in kg/km²/yr

S_o = Average silica content of the parent material in kg/m³

S_s = Average silica content of the saprolite in kg/m³

A weathering rate (rate of saprolite formation) of 4.4 m/Myr was calculated based on silica data. This is a minimum estimate because it was noted that if it were assumed that quartz is not dissolving, the weathering rate would increase because the silica is coming from other silicate minerals.

Furman and others (1998) calculated long-term weathering rates for three watersheds in northern Virginia, using the NETPATH mass balance model. The three watersheds studied were lithologically different. NETPATH was used to model the weathering processes, including the amount of mineral required and the weathering product produced. Models were chosen or rejected based on geologic observations in the field and chemical analysis. A system of linear equations was used to calculate the proportions of primary minerals involved in the weathering reactions. X-ray diffraction was used to determine the nature of weathering products found in soil profiles. Chemical weathering rates were calculated by multiplying total stream flow output (precipitation volume multiplied by the average yield of the watershed) by molar concentration of mineral species per liter of stream water. This calculation resulted in the total number of moles lost to the watershed on an annual basis. Dividing this number by the area of the watershed resulted in a mineral-weathering rate reported in moles/hectare/year. Weathering rates of individual cations equal the product of mineral-weathering rate and cation proportion determined from the chemical formula. Results showed that plagioclase was the dominant mineral undergoing chemical weathering and that kaolinite was the only weathering product produced. The rate of plagioclase weathering ranged from 597 to 706 moles/ha/year; these values overlap the range calculated for one of the watersheds studied by Taylor and Velbel (1991).

Previous PCO₂-Dependent Rate Studies

The effect of carbon dioxide on dissolution rates has been evaluated in the lab and relationships have been observed and developed for individual minerals. Wildman and Whittig (1968) examined the dissolution of serpentine in high PCO₂ solutions to explain the occurrence of iron-rich montmorillonites. Results showed that both magnesium and silica dissolution rates from serpentine increased with increasing PCO₂, but magnesium rates increased more than silica rates. This resulted in higher Mg/Si ratios in waters with higher PCO₂.

Brady and Carroll (1994) performed laboratory experiments using anorthite and augite as proxies for Ca and Mg silicates. Experiments were carried out at PCO₂ concentrations equal to 10^{-3.5} and 1 atmosphere, both experiments were buffered to a pH of 4 using HCl. These experiments were repeated at 25°, 35°, and 60° C. Results showed no direct dissolution rate dependence on CO₂, but did show a dependence on temperature. Based on these results, Brady and Carroll (1994) attributed any apparent increase in silicate dissolution rates related to CO₂ to increased production of corrosive organic acids due accelerated plant activity with the addition of CO₂.

Berg and Banwart (2000) performed laboratory studies on the dissolution of anorthite to examine the relationship between dissolution rate and aqueous inorganic carbon. Data showed that aluminum release was increased in the presence of high PCO₂. Aluminum release is the rate-limiting step in the dissolution of plagioclase under natural conditions; therefore, an increase in aluminum release corresponds to an increase in the overall dissolution rate of plagioclase. Research to date has explained an increase in rate related to increased PCO₂ through complexation of aluminum with carbonate ion (Berg and Banwart, 2000). According to Le Chatlier's Principle, as the aluminum ion concentration in the water is reduced more plagioclase is allowed to dissolve. The relationship developed between aluminum release rates and inorganic carbon is expressed in equation 1.4.

$$\text{Rate} = k[\text{CO}_3^{2-}]^{0.24} \quad (1.4)$$

k = rate at atmospheric PCO_2

This rate law shows a potential relationship between dissolution rate and PCO_2 . The study concluded that the dependence is most significant in field conditions where the pH is neutral to near basic and PCO_2 is elevated.

Chapter 2 – Description of Study Area

Location

Indian Wells Valley is located in Inyo and Kern Counties of Southern California on the east side of the Sierra Nevada range (fig. 2). Two towns have developed in Indian Wells Valley around the China Lake Naval Weapons Facility, Inyokern and Ridgecrest, California. Five canyons along the west side of Indian Wells Valley have been chosen for study based on availability of surface water, ease of access, and preliminary geochemical analyses. From north to south the canyons are Fivemile, Ninemile, Noname, Sand, and Short (figs. 2 and 3). These canyons can be found on USGS Little Lake and Ninemile Canyon quadrangles. They are also found on the Ridgecrest California 1:100,000-scale map from the USGS.

Physiography

The study area lies within the Sierra Nevada Mountains. The escarpment along which the study canyons have formed marks the boundary between the Basin and Range and the Sierra Nevada physiographic provinces. The canyons originate high in the Sierra Nevada just east of the Kern Plateau. Relief along the canyons is approximately 1300 meters with the mouths of the canyons at approximately 580 meters above mean sea level and the Kern Plateau just over 2100 meters above mean sea level. Gradients in the canyons are steep, ranging from 5.5% to 8.4%. Stream discharge down the canyons is intermittent throughout most of the year. During spring runoff surface flow can be found in the canyons, but during base flow conditions surface water is only found where springs discharge water or the water table intersects the ground surface. Large alluvial fans extend from the mouths of the canyons onto the relatively flat valley floor. China Lake, a

Figure 2. Shaded relief map of study area (modified from Guler, 2002).

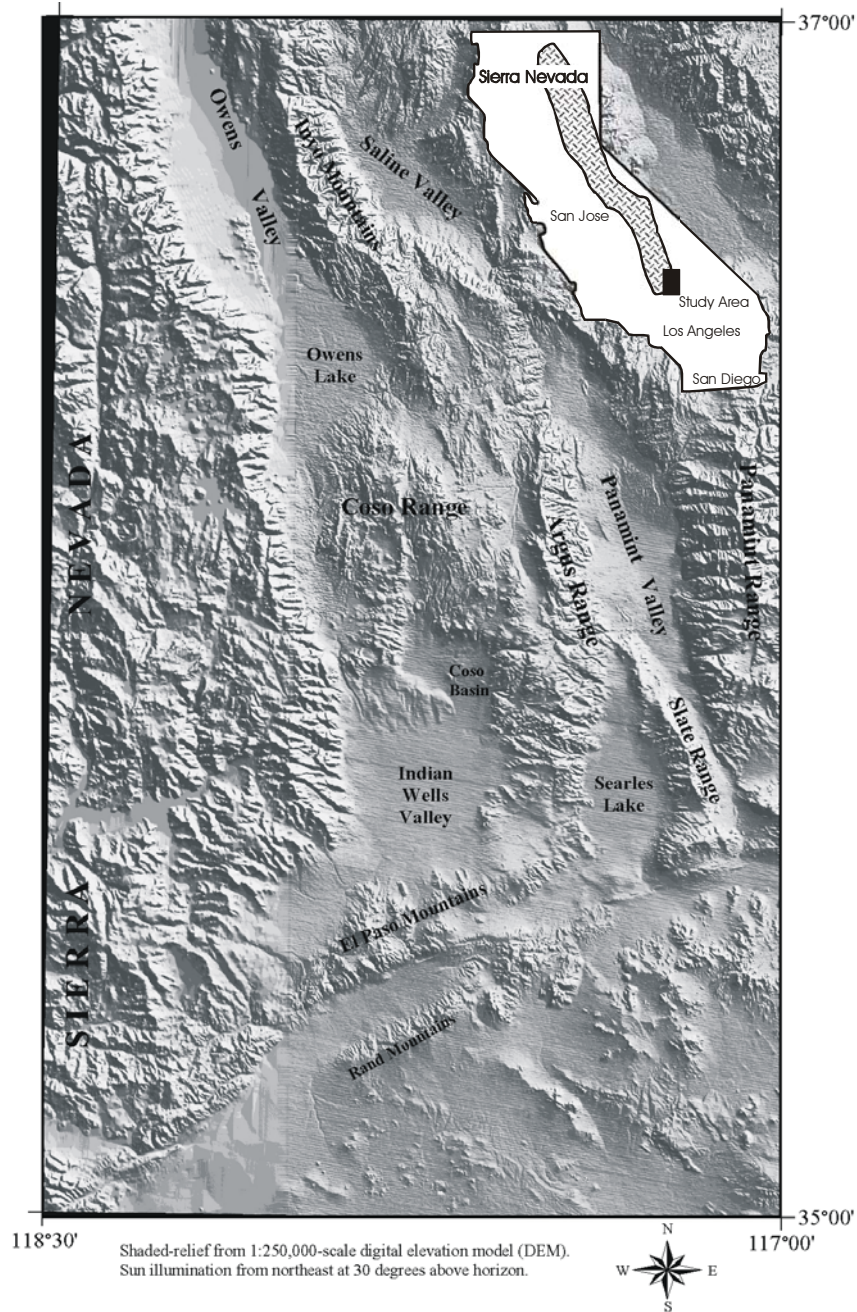
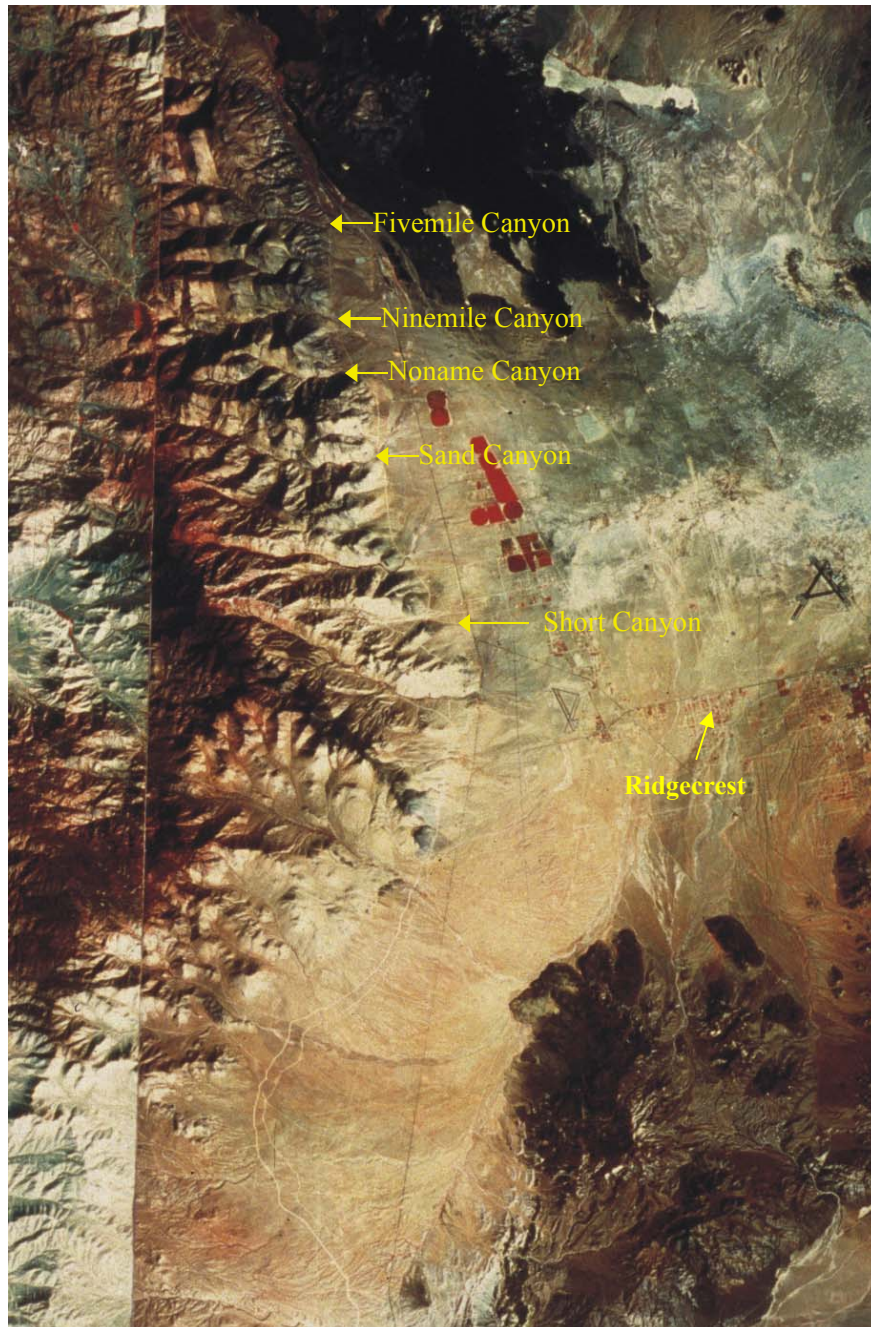


Figure 3. Satellite Image of Study Area showing canyons used for data collection



dry playa, occupies the northeastern part of the valley. The Los Angeles Water District pipeline runs north-south and transects the canyons near the valley floor. Access is available by pipeline roads and other dirt roads east of the pipeline. Area beyond the pipeline has been designated as the Owen's Peak Wilderness Area by the BLM, and access is only available by foot or horseback.

Climate

The study canyons lie in a transition zone between two climate types. Indian Wells Valley lies in the rain shadow of the Sierra Nevada, resulting in a mid-latitude desert climate (Robertson, 1991). The mean annual winter temperature reported in Ridgecrest (fig. 3) is about 3° C, while it is 28°C in the summer. An average of 10-15 cm of precipitation falls each year, mainly during winter and spring (Berenbrock and Martin, 1991). Precipitation in the summer occurs as afternoon thunderstorms. These events can be violent, causing flash flooding in the area. Evaporation averages 200 cm per year from surface-water impoundments in Indian Wells Valley (Farnsworth et al., 1982).

Alpine climate conditions are found at the canyons headwaters. Most precipitation that falls in the high Sierra Nevada occurs as snow (90-95%), varying from 50.8 to 140 cm annually (Guler, 2002). Temperature conditions at the canyons headwaters are not well known. Climate in the Emerald Lake watershed, located to the northwest of the study area in Sequoia National Park, is assumed to be representative of high alpine conditions in the southern Sierra Nevada. Monthly average air temperatures were reported for November 1985 to September 1986 and they ranged from -6°C in December to 10°C in August (Guler 2002).

Vegetation

Where surface water is found, riparian vegetation occurs, including California sycamore (*Platanus racemosa*), black cottonwood (*Populus trichocarpa*), willows, grasses, and rushes (Carver, 1969, Diggles et al., 1989). Joshua trees (*Yucca brevifolia*),

yucca (*yucca elephantipes*), Nevada saltbrush (*Atriplex canescens*), rabbitbrush (*Chrysothamnus sp.*) and other desert plants characterize the canyon sides and areas between surface water.

Vegetation in the high alpine areas is mainly alpine meadow with scattered pinon pine (*Pinus monophylla*), juniper (*Juniperus sp.*), and digger pine (*P. sabiniana*).

Regional Geologic Setting and History

Indian Wells Valley has been described as a half-graben resulting from extensional movement along the north-trending Sierra Nevada fault zone. Normal movement along this fault during Pliocene time has resulted in approximately 760 meters of displacement (Christensen, 1966; Duffold and Smith, 1978). The valley floor is underlain by 760 meters of alluvium that serves as the local aquifer. Because temperatures and evaporation are so high, it is assumed that most recharge to the local aquifer is from precipitation that falls at higher altitudes on the east side of the Sierra Nevada. Studies of the geochemical signatures of the groundwater also indicate high altitude recharge (Thyne et al., 1999; Guler, 2002). The headwaters of the study canyons are located in this recharge area. Bedrock underlying the alluvium consists of pre-Tertiary igneous and metamorphic rocks and sedimentary rocks of the Tertiary Ricardo Group (Loomis and Burbank, 1988). Seismic activity is common around the Indian Wells Valley and an average of 5000 seismic events occur annually (Zellmer, 1988; Monastero et al., 2002). A series of basalt flows lie to the north of the Indian Wells Valley in the Coso Range. Volcanic activity began in this range about 4 million years ago and has occurred as recently as late Pleistocene (Duffold and Smith, 1978). Geothermal activity associated with the Coso volcanic complex has resulted in the development of the Coso geothermal energy field by personnel at China Lake Naval Weapons Center. This geothermal activity produces CO₂ that migrates through fractures in the bedrock and is the source of CO₂ in the canyons of the study area. Variation of CO₂ concentration between canyons is due to natural variation from the geothermal activity. This CO₂ flux

appears to have changed with time. Large calcium carbonate deposits in the study area appear to be related to the abandonment of springs similar to the “grotto” of Noname Canyon. The “grotto” is an area where water flowing through the alluvium has undercut the bank where a side canyon confluences with the main drainage. As this water discharges calcium carbonate is precipitated on grass blades, rocks, roots, and other surfaces.

Study Area Mineralogy

In the study area, the Sierra Nevada Range is a complex assortment of Mesozoic plutons that range in composition from gabbroic to granitic (Duffold and Smith, 1978). Quartz, alkali feldspar, and plagioclase are the major minerals with accessory hornblende, biotite, and sphene. Plagioclase feldspar has a range of compositions between oligoclase (An_{26}) to andesine (An_{40}), with andesine being the dominant composition (Feth et al., 1964). No previous detailed mineralogical studies have been published for the area. A trend in the mineralogy of the alluvium is seen from north to south between the canyons. Plagioclase in the northern canyons is more calcic and the alluvium contains higher percentages of hornblende and biotite than Short and Sand Canyons (see fig. 3). Field investigations revealed a higher occurrence of mafic dikes and intrusions in the northern canyons. Table 1 and Figure 4 show the volumetric percentages of major minerals in each canyon determined by point count analysis for this study. Figure 5 is a plot of the sodium content of both plagioclase and hornblende determined by electron microprobe analysis for this study. Trace amounts of olivine, sphene, muscovite, and other opaque minerals (ilmenite?) are present in each canyon. Electron microprobe analyses showed the presence of fluoride in the chemical structure of biotite. Biotite is assumed to be the only source of fluoride in the system. Work by Guler and Thyne (2003) identified a mixture of Ca and Mg saponite as the primary weathering products. These clays appear to be buffering the calcium and magnesium concentrations in the

stream water (fig. 6). Drever (1988) suggested that cation exchange is responsible for a similar plot of data from Norton (1974) from the Rio Tanama system in Puerto Rico.

General chemical characteristics of the stream waters in the study area have been summarized by Thyne et al. (1999) and are attributed to the chemical weathering of typical Sierran rocks (Guler and Thyne, 2003). These waters are dominated by $\text{Na}^+ > \text{Ca}^{2+}$ and HCO_3^- . High concentrations of HCO_3^- are a result of high amounts of aqueous CO_2 reacting with bedrock. Stream waters to the north and south of the study area have the same chemical signatures as streams in the study area with overall lower TDS. Stream waters are not in equilibrium with respect to the minerals from the bedrock, it is assumed that the system is far from equilibrium due to the short residence time of groundwater in the system. As minerals dissolve the water becomes more saturated with respect to these minerals and if the water were to remain in the system eventually the water would become saturated with respect to each of the reacting minerals and mineral dissolution would no longer occur. As the water moves through the system it removes ions that are the result of mineral dissolution and therefore the groundwater does not reach a point of saturation with respect to the any of the reacting minerals. The groundwater-mineral system can be defined as a non-equilibrium system.

Figure 4. Major mineral percentages for each of the study canyons.

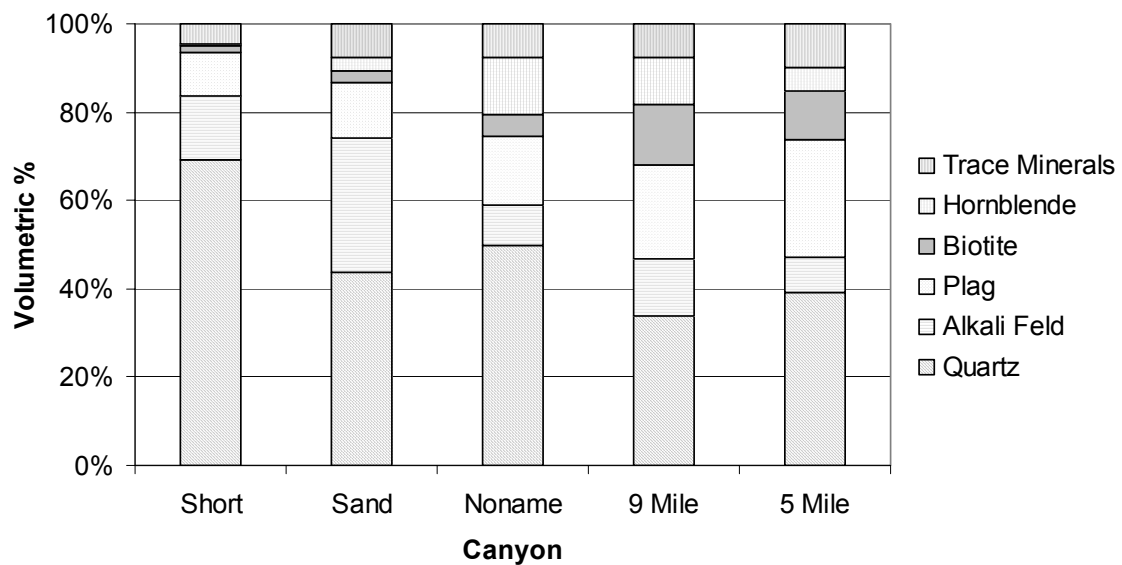
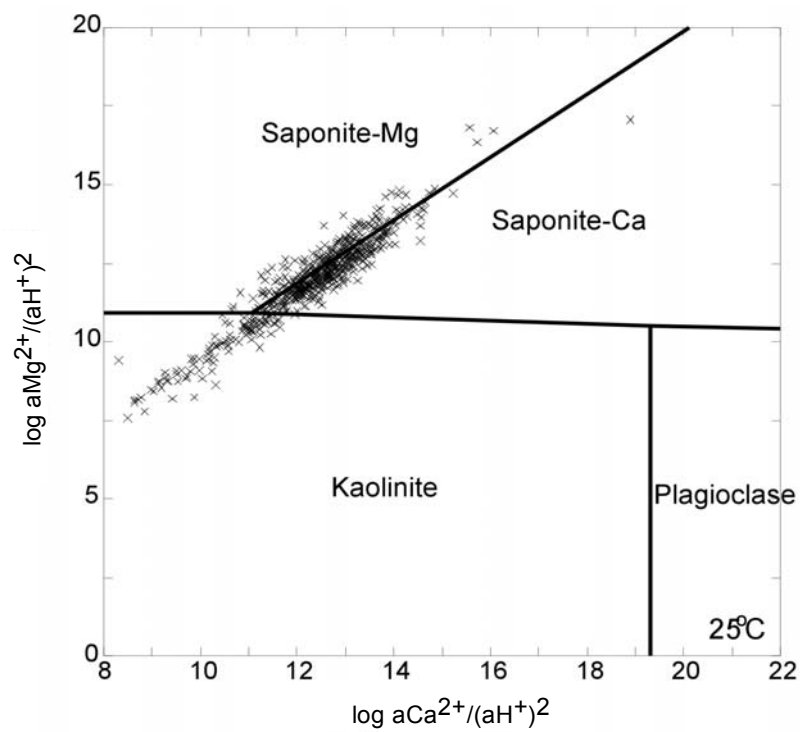


Table 1. Volumetric % of minerals in alluvium from point count data.

	Short	Sand	Noname	9 Mile	5 Mile
Quartz	69.3	43.8	49.8	33.8	39.4
Alkali Feld	14.7	30.2	9.3	13.1	7.9
Plag	9.7	12.8	15.6	21.1	26.4
Muscovite	1.3	1.6	0.0	0.4	0.7
Olivine	1.7	3.5	5.5	4.4	3.6
Biotite	1.7	2.7	4.8	13.8	11.2
Hornblende	0.3	2.7	13.1	10.5	5.4
Sphene	0.7	0.4	0.3	0.4	0.0
Opaque	0.3	1.9	1.4	2.5	0.4
Unknown	0.3	0.4	0.3	0.0	4.3
Rock Frag	0.3	0.0	0.0	0	0.7

Figure 5. Variations in sodium content of plumes in study area.

Figure 6. Groundwater, spring, and surface water samples from in and around Indian Wells Valley plotted on a Ca/Mg activity diagram (Guler, 2002).



Chapter 3 – Research Methods

Field Methods

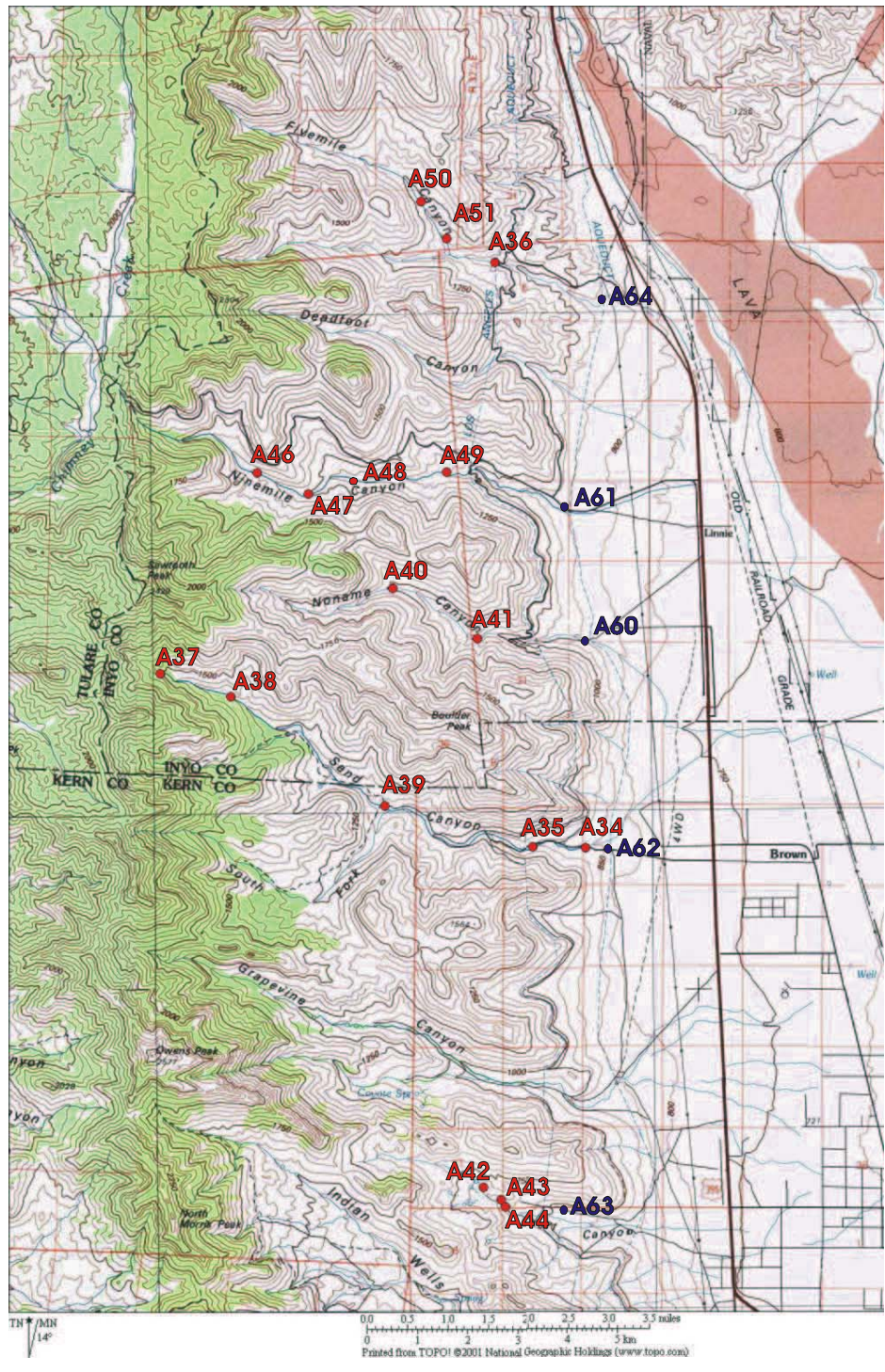
One six-week field session to make field observations and collect water and bedrock/alluvium samples occurred in May and June 2002. During fieldwork, the presence of mafic dikes, large quantities of altered material from in-situ weathering, faulting, location of springs and running surface water, and other geologic or hydrologic conditions found to be pertinent were recorded (see Appendix 1 for field notes). Bedrock samples were collected throughout the field area and alluvium samples were collected at the mouth of each canyon before the canyon opened up into the valley (fig. 7).

Water samples were collected where spring and surface waters were found in each canyon (fig. 7). At each of these sample sites the following data was collected in the field (see Appendix 2 for results):

1. Temperature – Measured directly in sample source in degrees celcius.
2. pH – Measured with a standard pH probe directly in sample source.
3. Conductivity – Measured directly in sample source in μ seimens/second.
4. TDS – Measured directly in sample source in mg/L.

Samples for alkalinity titrations were collected in a 30 mL HDPE bottle. Water was filtered through a Fisher Brand 0.45-micron syringe filter and no headspace was allowed in the sample container. Parafilm was wrapped around the mouth of the sample container before the lid was replaced. Alkalinity titrations were performed within 5 hours of sample collection after returning from the field area. Before performing alkalinity

Figure 7. Locations of water samples (A34-A51) and alluvium samples (A60-A64)



titrations samples were opened to the atmosphere and pH was monitored until stable. This allowed for slight degassing of CO₂ from the sample. The change in pH was recorded to apply a correction factor to the alkalinity calculation. Samples were titrated with a Hach digital titration kit and pH probe using 1.6N H₂SO₄ to an endpoint pH of less than 4. A titration curve was plotted and the break point picked to calculate alkalinity. Henry's Law constants used in alkalinity calculations were calculated for each sample at the temperature measured in the stream. Alkalinity is reported as mg/L bicarbonate (Appendix 2).

Samples for chemical analysis were filtered through Fisher Brand 0.45-micron syringe filters in the field and collected in 30 mL HDPE bottles. Bottles were acidified to pH less than 2 with nitric acid for cation analysis. Samples were stored in refrigeration until analyzed.

Chemical analyses

Samples were analyzed for cation concentrations using a Perkin-Elmer ICP-OES at Mesa State College in Grand Junction, Colorado. Each element was run in 3 replicates for each sample and the average, standard deviation, and relative standard deviation (RSD) reported. Values for RSD were mostly under 5%, but some elements with very low concentrations (Rb, Zn) had RSD values up to 16% with one occurrence of Zn up to 142%. Appendix 2 contains raw data from ICP analyses including wavelength of analyses for each element.

Anion analyses were performed by ion-chromatography (IC) at University of Colorado, Boulder. Raw data from these analyses are contained in Appendix 2.

Charge balance was calculated in an Excel spreadsheet for each water sample to check for analytical error. Table 2 shows the results of charge balance calculations.

Table 2. Results of charge balance analysis on water samples (locations on fig. 7).

Sample Number	Description	Charge Balance, %
A34	Sand - first crossing	0.98
A35	Sand - picnic area	1.21
A36	5 mile - upper aquiduct	1.00
A37	sand upper spring	0.43
A38	Sand -	0.52
A39	Sand - Road to Rodecker Flat	0.74
A40	Noname - spring near confluence at top of canyon	0.59
A41	noname-grotto	1.86
A43	Short - above falls	0.85
A44	Short - below falls	0.75
A46	9 mile - 3/4 way up canyon - standing water	1.03
A47	9 mile - upstream of mine	1.08
A48	9 mile - downstream of mine	2.16
A49	9 mile - 1/4 mile from aquiduct	2.44
A50	5 mile - spring	0.69
A51	5 mile - spring	0.87

X-Ray Diffraction

Clay mineralogy of the alluvium was determined by X-ray diffraction (XRD) analysis of material collected at Colorado School of Mines. Alluvium samples were sieved through a number 200 mesh screen. Sieved material was suspended in water and a small amount of Calgon (water softener) as an anti-flocculent. Each sample was centrifuged at 1000 rpm for 2 ½ minutes to separate the <2-micron fraction for analysis. This material was used to prepare an orientated sample on a glass slide by vacuum filtration through a 0.45-micron filter. The orientated sample was air-dried and scanned at 2 degrees 2θ per minute from 3 to 35 degrees to determine the presence of expandable clay minerals. A random powder mount was prepared from the filtered material of samples that showed smectites in the oriented clay analysis for smectite determination by 060 reflection analysis (Brindley and Brown, 1980). To prepare random sample mounts,

filtered material was placed on a glass slide and a small amount of powdered quartz was added as an internal standard. Acetone was used to provide adhesion of the clay material to the slide. Diffraction scans for 060 reflections were performed from 58 to 63 degrees at a scan rate of 0.40 degrees 2θ per minute. Table 3 lists peak positions for di- and tri-octahedral smectites (Moore and Reynolds, 1997).

Extra material from the sieving process was used to perform a whole rock analysis for each canyon. Whole rock scans were performed at 2 degrees 2θ per minute from 5 to 60 degrees. Appendix 3 contains diffraction patterns for each sample.

Table 3. 060 peak positions for identification of smectites phase (Moore and Reynolds, 1997).

Mineral	d(060)	2-theta
Kaolinite	1.49	62.31
Montmorillonite	1.492-1.504	62.22-61.67
Illite (Muscovite)	1.499	61.9
Glauconite	1.511	61.35
Saponite	1.52	60.95
Nontronite	1.521	60.91
Hectorite	1.53	60.51
Serpentines	1.531-1.538	60.47-60.16
Biotite	1.538	60.16
Chlorites	1.538-1.549	61.16-59.69
Sepiolite	1.540-1.550	60.07-59.65
Vermiculite	1.541	60.03
Berthierine	1.555	59.44
Palygorskite	1.56	59.23

Petrographic Analyses

Polished thin sections were made for each canyon sample by creating a thin section billet with blue epoxy and alluvium material. A point count analysis was performed on each thin section by identifying a minimum of 300 grains. During this analysis alteration states of the grains were also recorded and documented as less than

50% or greater than 50% weathered. These data helped define the study area mineralogy (see Chapter 2) and to determine relative weathering rates of each mineral and to examine the compositional evolution of the alluvium. Appendix 4 contains the raw data resulting from point count analysis.

Electron Microprobe Analyses

Thin sections used in petrographic analyses were carbon coated and analyzed by electron microprobe at University of Colorado, Boulder. Weight percent oxides were determined quantitatively for plagioclase, alkali feldspar, hornblende, and biotite. At least 8 grains of each mineral were analyzed and an average composition calculated for each mineral in all five samples. Excel spreadsheets created by Preston and Still (2001) were used to calculate mineral chemical formulas from the electron microprobe data, listed in Table 4 (sample spreadsheet in Appendix 5, all spreadsheets and raw data in electronic files).

Geochemical Analyses

Samples from previous studies in the area have been classified using traditional plotting techniques and statistical methodologies (Thyne et al., 1999; Guler, 2002). Graphical techniques were used to classify water samples collected during the field session. The Mg/Si ratio was calculated for all stream water samples for comparison to PCO_2 values.

Inverse Modeling

Data from both previous studies and sampling from this study were used to create inverse models with the geochemical modeling software PHREEQC. Models were created for this system with four assumptions. (1) The majority of the discharge from the canyons is occurring through alluvium filling the valley. Water budgets have been calculated for each of the canyons (Thyne and Gillespie, 1997). Some evidence indicates

Table 4. Mineral formulas determined by electron microprobe analysis

	Short Canyon	Sand Canyon	Noname Canyon
Plagioclase	$\text{Na}_{0.83}\text{Ca}_{0.16}\text{K}_{0.01}\text{Sr}_{0.01}\text{Al}_{1.19}\text{Si}_{2.81}\text{O}_8$	$\text{Na}_{0.70}\text{Ca}_{0.29}\text{K}_{0.01}\text{Sr}_{0.01}\text{Al}_{1.29}\text{Si}_{2.70}\text{O}_8$	$\text{Na}_{0.60}\text{Ca}_{0.16}\text{K}_{0.01}\text{Sr}_{0.01}\text{Al}_{1.36}\text{Si}_{2.61}\text{O}_8$
AFS	$\text{K}_{0.93}\text{Na}_{0.07}\text{Sr}_{0.01}\text{Al}_{1.01}\text{Si}_{2.98}\text{O}_8$	$\text{K}_{0.93}\text{Na}_{0.08}\text{Sr}_{0.01}\text{Al}_{1.01}\text{Si}_{2.98}\text{O}_8$	$\text{K}_{0.94}\text{Na}_{0.08}\text{Sr}_{0.01}\text{Al}_{1.02}\text{Si}_{2.98}\text{O}_8$
Biotite	$\text{K}_{0.71}\text{Fe}_{0.95}\text{Mg}_{0.98}\text{Mn}_{0.03}\text{Ca}_{0.02}\text{Ti}_{0.10}\text{Na}_{0.01}\text{Al}_{1.57}\text{Si}_{3.05}\text{F}_{0.07}\text{O}_{10}(\text{OH})_2$	$\text{K}_{0.74}\text{Fe}_{1.27}\text{Mg}_{1.17}\text{Mn}_{0.02}\text{Ca}_{0.03}\text{Ti}_{0.12}\text{Na}_{0.01}\text{Al}_{1.37}\text{Si}_{2.92}\text{F}_{0.02}\text{Cl}_{0.01}\text{O}_{10}(\text{OH})_2$	$\text{K}_{0.64}\text{Fe}_{0.96}\text{Mg}_{0.978}\text{Mn}_{0.02}\text{Ca}_{0.10}\text{Ti}_{0.10}\text{Na}_{0.01}\text{Al}_{1.57}\text{Si}_{2.64}\text{F}_{0.02}\text{Cl}_{0.01}\text{O}_{10}(\text{OH})_2$
Hornblende		$\text{Ca}_{1.71}\text{Na}_{0.30}\text{K}_{0.15}\text{Fe}_{2.34}\text{Mg}_{2.19}\text{Mn}_{0.07}\text{Ti}_{0.07}\text{Al}_{1.50}\text{Si}_{6.84}\text{O}_{22}(\text{OH})_2$	$\text{Ca}_{1.65}\text{Na}_{0.27}\text{K}_{0.09}\text{Fe}_{1.69}\text{Mg}_{2.74}\text{Mn}_{0.03}\text{Ti}_{0.13}\text{Al}_{1.58}\text{Si}_{6.83}\text{O}_{22}(\text{OH})_2$

	9-Mile Canyon	5-Mile Canyon
Plagioclase	$\text{Na}_{0.61}\text{Ca}_{0.38}\text{K}_{0.01}\text{Sr}_{0.01}\text{Al}_{1.38}\text{Si}_{2.64}\text{O}_8$	$\text{Na}_{0.64}\text{Ca}_{0.36}\text{K}_{0.01}\text{Sr}_{0.01}\text{Al}_{1.34}\text{Si}_{2.64}\text{O}_8$
AFS	$\text{K}_{0.92}\text{Na}_{0.09}\text{Sr}_{0.01}\text{Al}_{1.01}\text{Si}_{2.98}\text{O}_8$	$\text{K}_{0.94}\text{Na}_{0.08}\text{Sr}_{0.01}\text{Al}_{0.93}\text{Si}_{3.05}\text{O}_8$
Biotite	$\text{K}_{0.74}\text{Fe}_{1.29}\text{Mg}_{1.26}\text{Mn}_{0.02}\text{Ca}_{0.04}\text{Ti}_{0.10}\text{Na}_{0.01}\text{Al}_{1.33}\text{Si}_{2.91}\text{F}_{0.07}\text{Cl}_{0.01}\text{O}_{10}(\text{OH})_2$	$\text{K}_{0.72}\text{Fe}_{1.14}\text{Mg}_{1.27}\text{Mn}_{0.02}\text{Ca}_{0.03}\text{Ti}_{0.10}\text{Na}_{0.01}\text{Al}_{1.34}\text{Si}_{2.99}\text{F}_{0.07}\text{Cl}_{0.01}\text{O}_{10}(\text{OH})_2$
Hornblende	$\text{Ca}_{1.70}\text{Na}_{0.35}\text{K}_{0.20}\text{Fe}_{2.26}\text{Mg}_{2.24}\text{Mn}_{0.06}\text{Ti}_{0.14}\text{Al}_{1.54}\text{Si}_{6.76}\text{O}_{22}(\text{OH})_2$	$\text{Ca}_{1.68}\text{Na}_{0.35}\text{K}_{0.19}\text{Fe}_{2.22}\text{Mg}_{2.27}\text{Mn}_{0.08}\text{Ti}_{0.13}\text{Al}_{1.50}\text{Si}_{6.81}\text{O}_{22}(\text{OH})_2$

that a small amount of discharge from 5-Mile canyon may be diverted through a large fracture system, but calculated discharge values generally agree with calculated groundwater flux values into the Indian Wells Valley aquifer within the study area (Thyne et al., 1999).

(2) There is limited biological uptake of nutrients and that uptake is of the same magnitude in each canyon. Because the study area lies in a desert climate the amount of vegetation in the canyons is minimal. Most vegetation occurs where springs form at the surface, and a significant difference in the amount of vegetation in each canyon was not observed. Because final analysis of the data only requires that relative rates between canyons have low uncertainty; calculating dissolution rates without consideration of exchange with the biologic pool does not significantly affect the results.

(3) Dust input to the system has been measured and can be accounted for in the mass balance model. Owens Lake to the north of the study area is a major source of dust for the entire region. Investigations by Rehis (1995, 1997) have quantified the amount and chemical composition of dust that is transported through the area. According to these studies dust from Owen's Lake does not contribute to the regional dust flux beyond 30-50 km south of the playa. Therefore, the influence of Owen's Lake dust does not reach Indian Wells Valley (Rehis, 1997). Dust input was estimated based on chloride concentration of snow samples and approximately 20% of the total annual flux of sodium is due to dry deposition; this input has been included in the models.

(4) Feldspar dissolution is congruent. Most weathering studies assume that congruent dissolution is the main mechanism of feldspar dissolution in a natural environment (Mast et al., 1990). Dissolution of feldspar crystals has been observed to be incongruent in laboratory studies immediately after a fresh surface is exposed, but becomes congruent after minutes to days (Wollast and Chou, 1985). Berg and Banwart (1994) suggest that anorthite dissolution becomes stoichiometric after 2-5 years. Alluvium in the canyons does not undergo rapid physical weathering to remove material

and expose fresh surfaces; therefore the assumption that congruent dissolution of feldspar controls stream water chemistry is considered to be valid.

Data were organized in an Excel spreadsheet and copied into PHREEQC using the solution spread command. Appendix 6 contains data and input files used for inverse modeling in this study. Chloride is the default anion used to charge balance waters, but charge balance was performed on the waters using bicarbonate due to low concentrations of chloride. Each inverse model was set up to react average snowmelt chemistry with a combination of user defined and end-member mineral compositions previously reported by Feth and others (1964). CO₂ was added as a reactant to simulate a system open to excess CO₂. Biotite, plagioclase, hornblende, and the saponite phases were user defined as the PHREEQC database either did not contain data for the mineral or the chemical composition of the mineral was changed to reflect actual bedrock mineralogy. Biotite, plagioclase, hornblende, K-feldspar, and CO₂ were constrained to dissolution; amorphous silica, kaolinite, calcite, Ca-saponite, and Mg-saponite were constrained to precipitation. Halite and gypsum were added to account for dust input from Owen's Lake but were not constrained to either precipitation or dissolution; the dissolution and precipitation of each phase is purely dependent upon the mass balance of elements. Numerical uncertainty in all models was set to 5%.

Mass Balance Equations

Paces (1983) developed a series of equations based on mass balance principles to calculate mineral dissolution rates based on field-measured parameters. The form of this equation used is expressed in equation 3.1. Definitions of the variables as they were used or calculated for this study are listed in Table 5, and methods used to calculate each variable are discussed below if additional steps were taken beyond the definition in Table 2. Data collected during field activities are used in calculations of these variables.

Table 5. Definitions of variable used in Paces (1983) mass balance equations.

Variable	Units	Definition
k	mol/m ² sec	Linear rate constant of dissolution of mineral
m_w	mole/m ³	Concentration of a chemical species in runoff
m	mole/m ²	concentration of a chemical species due to net input from the surrounding of a water-rock system
n		volumetric percent of mineral from detailed point count of alluvium
ŝ	m ² /m ³	specific wetted surface of rock saturated with water
τ	years	residence time of subsurface water in catchment
S	m ²	total surface of pores and joints saturated with ground water in a catchment
W	m ³	total volume of ground water in the catchment (V _t -V)
λ		mass fraction of minerals in rock releasing a chemical species
s	m ² /kg	specific surface area of a mineral or rock
σ	kg/m ³	density of rock without pores, assumed to be 2.65 g/cm ³
V	m ³	total volume of rock without pores within the aquifer of the catchment
V_t	m ³	total volume of aquifer

$$k = \left[\frac{M_{\min}}{n\hat{s}\tau} \right] \left[\frac{1}{3.14 * 10^7} \right] \quad (3.1)$$

Concentration of a species in runoff is measured directly, but most ions are added to stream water through the dissolution of more than one mineral. Equations 3.2 through 3.9 demonstrate the distribution of a species in runoff whose concentration is the result of the dissolution of two or more minerals with different relative dissolution rates.

Concentrations calculated from distribution of chemical elements are defined as M_{\min} for this study. M_{\min} is equal to the total concentration of an ion in the discharge of a catchment (M_w) minus the concentration of the ion added to the catchment through both precipitation (M_{ppt}) and dry deposition (M_{dust}), multiplied by a distribution percent to separate the concentration of the ion from different minerals.

$$M_{\min} = [M_w - \bar{M}] \text{dist \%} \quad (3.2)$$

These concentrations are converted to ion fluxes by multiplying M_{\min} by the total volume of water in the catchment. This variable is included in the specific wetted area calculation discussed with equation 3.9.

Inputs to the system from precipitation and dry deposition must be accounted for when calculating the flux of an ion from mineral dissolution. These two fluxes are added together and subtracted from the total flux before distribution of the ion between minerals is calculated.

$$\bar{M} = M_{ppt} + M_{dust} \quad (3.3)$$

Input of ions through precipitation was calculated by multiplying an average concentration in Sierra Nevada snow by the annual precipitation.

$$M_{ppt} = [X]_{ppt} * \text{annual precipitation} \quad (3.4)$$

Rehis (1997) demonstrated the importance of dry deposition from Owen's Lake material in the southeastern region of the Sierra Nevada. A correction for dust is only applied when sodium is used as the mass balance constraint. The addition of sodium through dry deposition of halite is estimated by calculating the percentage of additional sodium in Short Canyon (22%). It is assumed that the amount of dry halite deposition in Short Canyon is equal to the annual flux of chloride in Short Canyon. Short Canyon alluvium contains a negligible amount of biotite and no hornblende; therefore, the majority of the chloride is added to the system through airborne halite. The calculated

percentage of additional sodium in Short Canyon was applied to the remainder of the canyons as an estimate of the flux of sodium resulting from dry deposition.

$$M_{dust} [Na] = [Cl^-]_{ppt} * \text{annual precipitation} \quad (3.5)$$

After ion flux from mineral dissolution is calculated it is necessary to distribute this flux and assign percentages to specific mineral dissolution. Distribution takes into account the relative dissolution rates of each mineral contributing to the total flux of the species of interest and the mole fraction of each mineral phase. An alteration rate relative to plagioclase for each mineral was determined through detailed petrographic analyses by comparing the volumetric percentage of each mineral altered. This relative alteration rate was converted to a relative dissolution rate through equations 3.6 and 3.7. Electron microprobe analysis data determined the mineral phases contributing to the flux of the ion of interest.

$$\left[\frac{\text{Vol \% of wx min}}{\text{Vol \% of wx plag}} \right] \left[\frac{\text{Vol \% total min}}{\text{Vol \% total plag}} \right] = \text{relative \% altered grains} \quad (3.6)$$

$$\left[\text{Relative \% altered grains} \right] \left[\frac{\text{molar vol. Plag}}{\text{molar vol. Hornblende}} \right] = \text{relative rate of dissolution} \quad (3.7)$$

This relative rate of dissolution was used in equation 3.8 to perform the final distribution of the flux of an ion where $\chi_{[X]}$ equals the mole fraction of the ion in each mineral determined through electron microprobe analyses.

$$Dist\% = \frac{\text{relative rate} * \chi_{[x]}}{\sum_1^n \text{relative rate} * \chi_{[x]}} \quad (3.8)$$

The variable \hat{s} is a measure of the specific wetted surface of each mineral and is related to the specific surface area, density, mass fraction, and volumetric percent of the mineral and the volume of water and alluvium in the catchment by equation 3.9.

$$\hat{s} = \frac{\lambda s \sigma V}{nW} \quad (3.9)$$

The volume of alluvium (V) and water (W) in each canyon was calculated based on the conceptual model illustrated in Figures 8 and 9. Each canyon is filled with alluvium that sits directly on top of bedrock. Recharge to the canyon occurs at the headwaters and the majority of flow moves through the saturated lower part of the alluvium. Water surfaces due to irregularities in the alluvium/bedrock contact and in areas where surface water is present it can be assumed that the alluvium is saturated from the bedrock contact to the surface. By measuring the slopes of each canyon wall and projecting the walls down below the surface of the alluvium to where they meet, the depth to bedrock at these locations can be calculated and a cross-sectional area of wetted alluvium estimated. This was calculated at each location where surface water was observed and the average cross-sectional area was applied to entire length of the canyon to calculate the total volume of wetted alluvium (V_t) where V used in the mass balance equation equals $V_t - W$. The total volume of groundwater (W) was calculated assuming 35% porosity.

The specific surface area (s) was calculated geometrically using a value of 0.5 mm for the average radius of grains in the alluvium, an average density of 2.65 g/cm³ and a porosity of 35%. The mass of 0.65 m³ of rock was calculated (1m³- pore space) in

kilograms and divided into the surface area of the total number of grains in 1 m³ of alluvium. Dividing the volume of one grain into the total volume of alluvium and multiplying that by the surface area of one grain calculated the total surface area.

Point count analyses were performed to determine n , the volumetric percent of the minerals in alluvium. A value for λ was calculated for each mineral using equation 3.10, using sodium as an example.

$$\lambda = \frac{2Na_2O\%}{100\%} \left[\frac{\text{molecular weight of mineral}}{\text{molecular weight of } Na_2O} \right] \quad (3.10)$$

After calculation of k in mol/m²/year, the rate was converted to mol/m²/sec to compare with literature rates.

Figure 8. Conceptual model of discharge through alluvium.

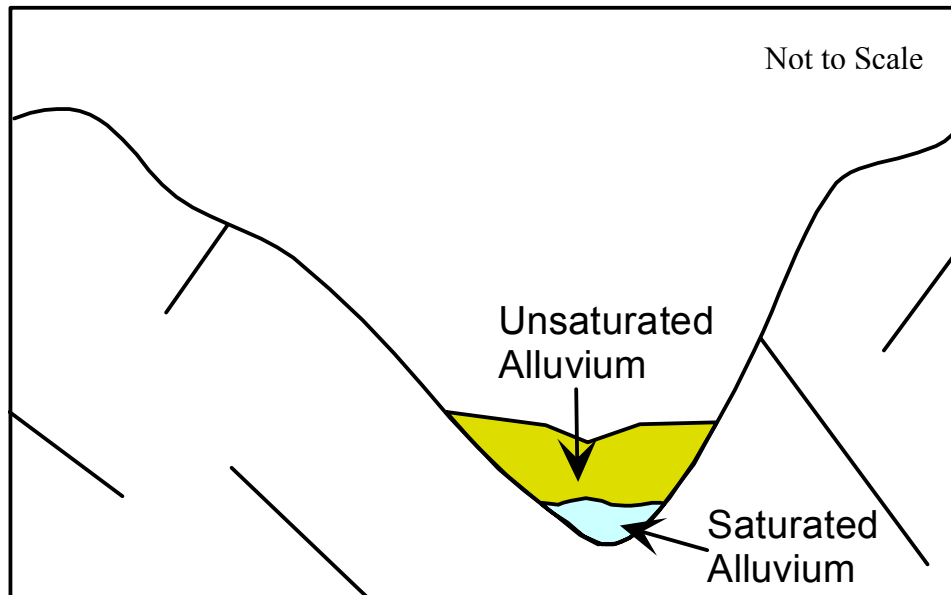
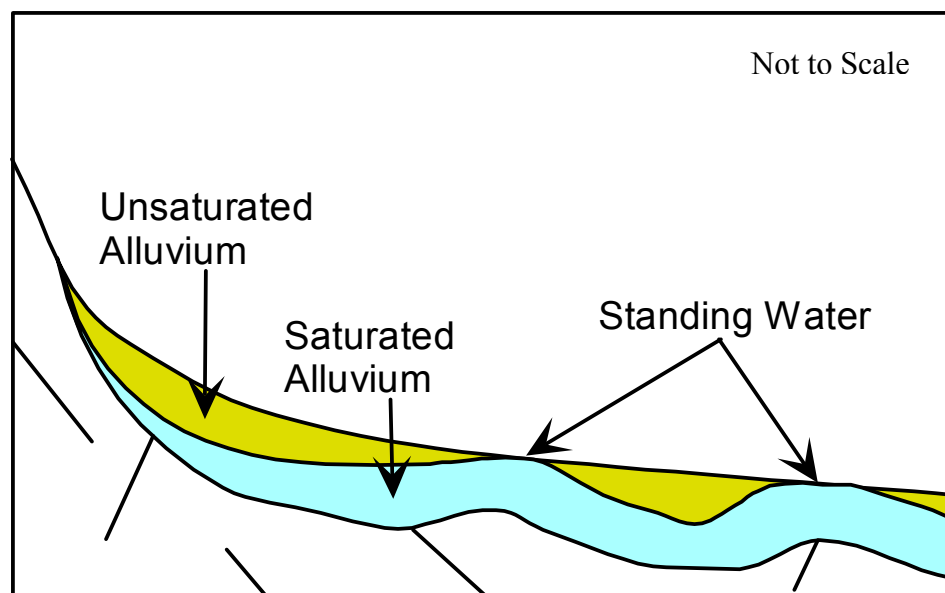


Figure 9. Conceptual model of flow of water down the study canyons.



Chapter 4 - Preliminary Modeling

Preliminary Observations

Chemical data from surface water samples collected during the 2002 field session were plotted using graphical techniques (figs. 10 and 11). The similarity of the patterns of the lines in Figure 10 indicates that in general the waters are chemically similar. One sample from 9-Mile Canyon shows an increase in Mg relative to Ca. This difference may be due to a slight change in composition of the smectites since Ca and Mg concentrations appear to be controlled by the clays. Figure 11 is a plot of the same samples on a Piper diagram. No distinct groups of different water chemistries can be delineated from either of these plots. The waters are $\text{Na}^+/\text{Ca}^{2+} - \text{HCO}_3^-$ waters, the same classification reported by Guler and Thyne (2003).

Figure 10. Schoeller diagram plot of all surface water samples collected in 2002 field session.

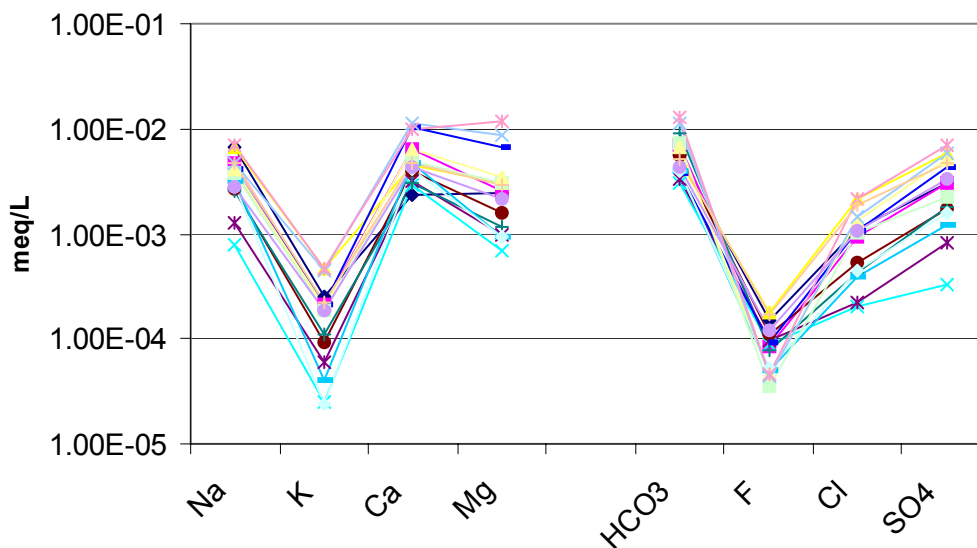
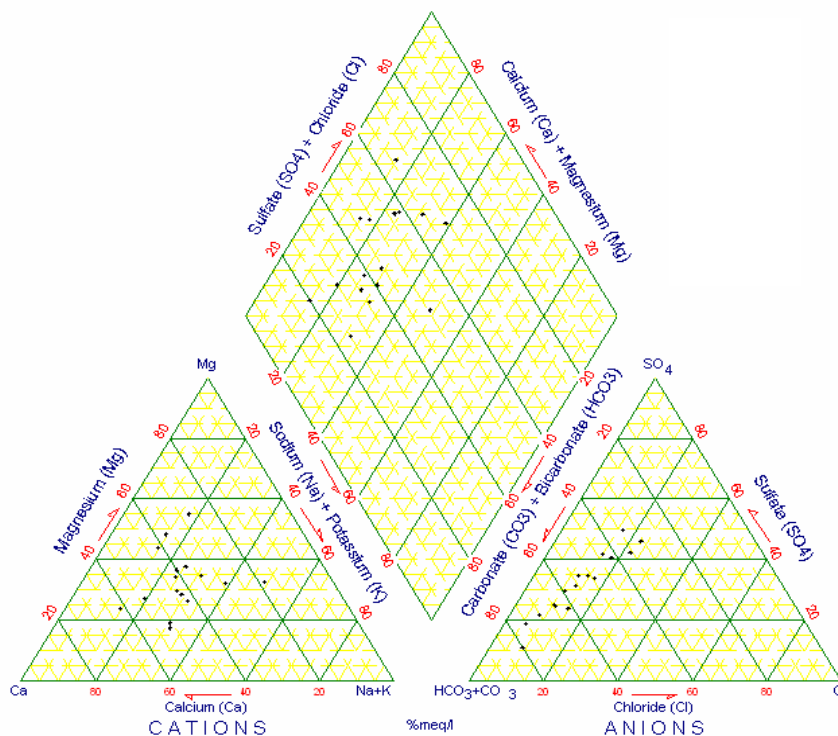


Figure 11. Piper diagram plot of all surface water samples collected in 2002 field session.



Preliminary data analysis and geochemical modeling were conducted to evaluate the relationship between dissolution rates and PCO_2 . Previously collected and published data were used in these analyses (Thyne et al., 1999; Bauer, 2001). Because structure, topographic gradient, precipitation amounts and lithology do not change dramatically between the study canyons, it is not expected that the chemical characteristics of the streams in these canyons change dramatically. However, data show that not only do stream chemistries differ but the total dissolved solid (TDS) measurements are also highly variable along a north-south transect. Calculated PCO_2 values from alkalinity measurements range from atmospheric (360 ppm) to 78 times atmospheric concentrations along the same transect. Sample locations range from north of Indian Wells Valley in

Little Lake Canyon to south of Indian Wells Valley in Bird Spring Canyon (fig. 12).

Variability in TDS appears to be directly related to calculated PCO_2 (fig. 13).

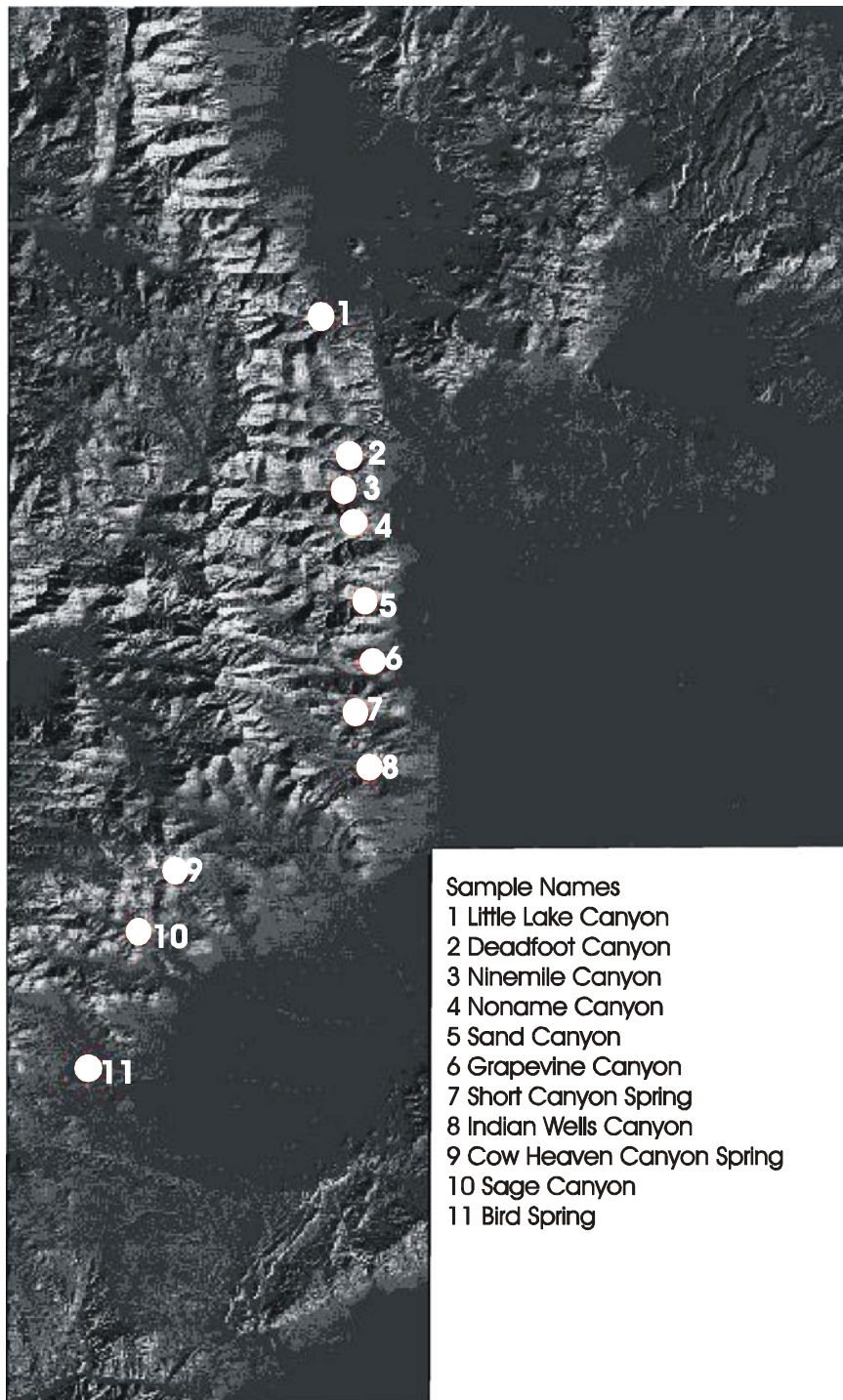
It is important to note that samples used to create Figure 13 were not taken with the intent of using them to define an area of elevated CO_2 . Due to levels of CO_2 higher than atmospheric in the area, rapid degassing occurs upon collection of water samples. Sample collection should be performed such that degassing is minimized. It cannot be assured that this procedure was followed for any previous sampling activities. In addition, the data are for both spring and surface water samples with variable spatial distribution along the length of the canyons. In spite of these uncertainties, there is a good correlation between TDS and calculated PCO_2 except in some southern canyons where water samples originated from springs or were taken near the head of the canyon and the water was unable to react with alluvium for any significant period of time.

It has also been shown that the Mg/Si ratio of stream waters increases as PCO_2 of the water increases (Wildman et al., 1968). Figure 14 is a plot of PCO_2 vs. Mg/Si along the north south transect. It is interesting to note that the area with high Mg/Si ratios between Noname and Deadfoot Canyons corresponds to an area of mature geomorphologic features identified through satellite imagery and field observations. These features contain large amounts of unconsolidated material formed by in-situ weathering, indicating a higher apparent rate of weathering than canyons to the north or south.

Geochemical Modeling with PHREEQC

Preliminary inverse models were created using the geochemical modeling software PHREEQC (Parkhurst and Appelo, 1999). These models reacted average snowmelt composition with typical Sierra Nevada bedrock mineralogy (Garrels and MacKenzie, 1967) to produce observed stream chemistries (Guler and Thyne, 2003). All

Figure 12. Sample locations of data used in preliminary modeling overlaid on digital elevation map of study area.



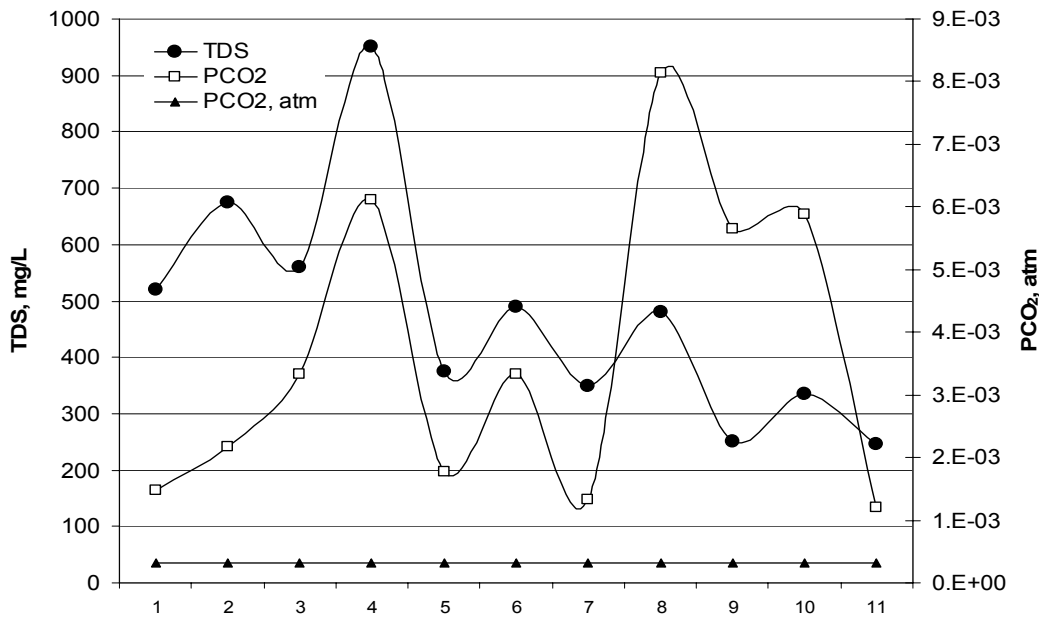
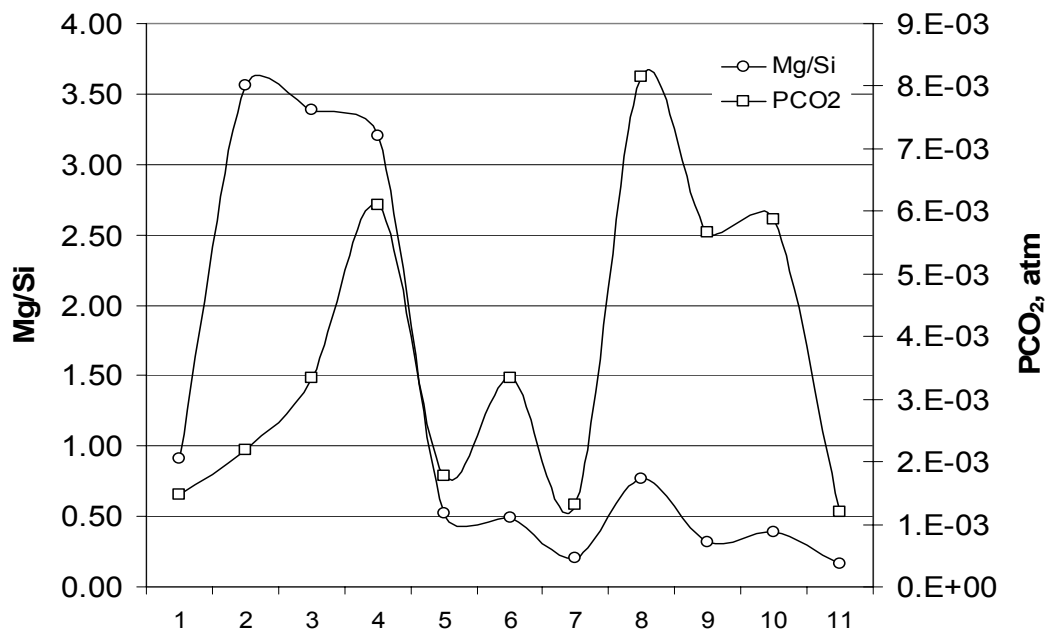


Figure 14. Mg/Si and PCO₂ from previously collected samples, numbers are sample
ion between Mg/Si and P



of the possible models consumed CO_2 . A model was chosen for each canyon based on the sum of squared residuals and field observations. A plot of measured TDS vs. moles of CO_2 consumed in the model (fig. 15) indicates a strong correlation between PCO_2 and TDS when combined with trends in Figures 13 and 14. If TDS is used as a measure of mineral dissolution rates, these trends suggest that elevated PCO_2 increases mineral dissolution rates.

Additional samples were collected in June 2002 and their chemical properties determined. Alkalinity was measured in the field and to reduce previous uncertainty associated with calculated PCO_2 values related to sampling and titration procedures additional inverse models were created using these samples. Results from these models show the same relationships seen previously with a higher correlation between CO_2 consumed and measured TDS (fig. 16). Pearson correlation coefficients between TDS and CO_2 consumed were calculated for each data set. The correlation coefficient is 0.66 for previously collected samples and 0.94 for the 2002 field samples.

Figure 15. TDS and CO_2 consumed from modeling of previously collected samples, numbers on x-axis are sample locations (see fig. 12).

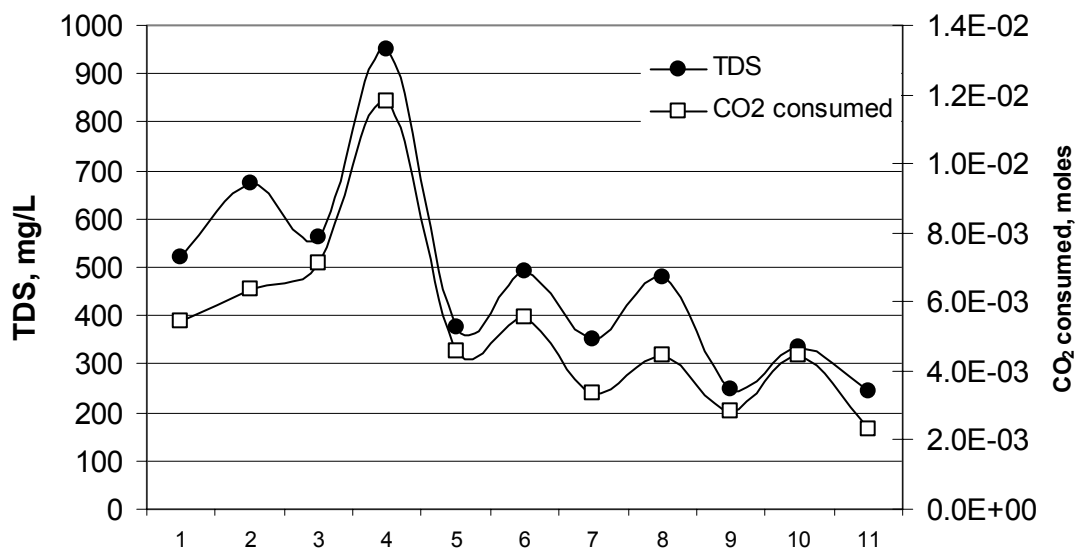
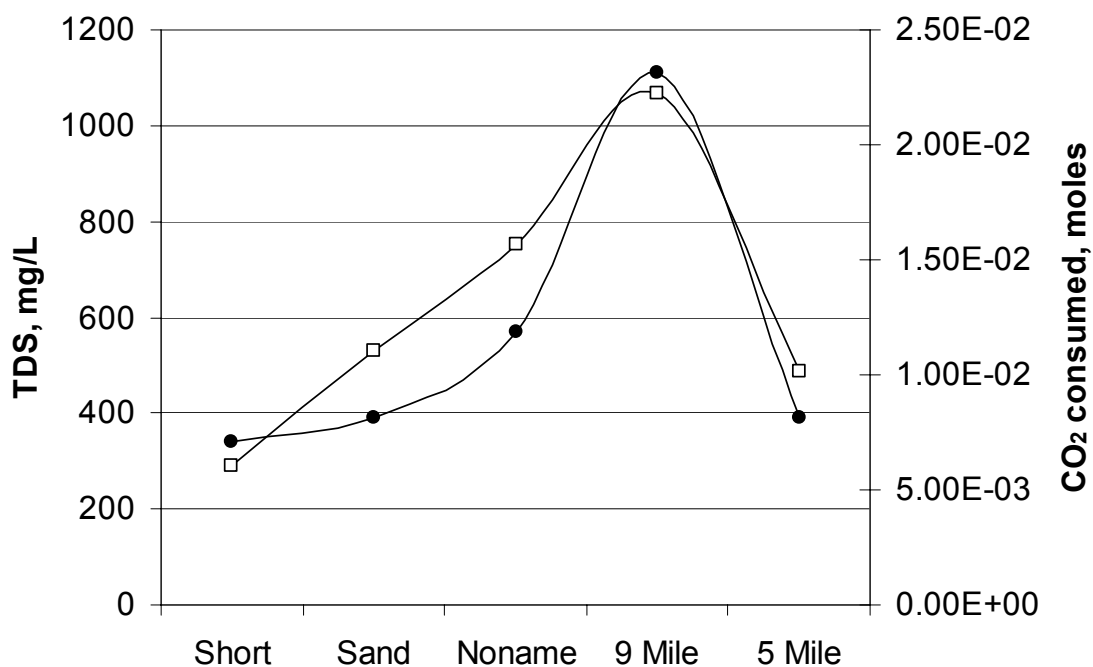


Figure 16. TDS and CO₂ consumed from 2002 samples

Dissolution Rate Calculations

The revision of Paces (1983) method as described in Chapter 3 was applied to the 2002 field data to calculate individual mineral dissolution rates. Sodium flux data were used to calculate rates for plagioclase and hornblende by initially assuming identical relative rates. Typical hornblende composition and plagioclase composition from the literature (Garrels and Mackenzie, 1967) were used in these calculations. Results showed no correlation between dissolution rates and PCO_2 (figs. 17 and 18). Each variable in Paces equation was changed by one order of magnitude at a time to determine the sensitivity (fig. 19). Variables with the highest sensitivity were residence time and ion concentration in stream runoff (mineral chemistry and relative rates). Techniques to determine relative rates and parent mineral/weathering product compositions (Chapter 3)

were used to reduce uncertainty in the calculated rates and a second calculation of residence time was performed for each canyon using a version of Darcy's Law (equation 3.12) where v_x is the average linear velocity, k is the hydraulic gradient estimated from literature values, n_e is the effective porosity estimated from literature values, and dh/dl is the hydraulic gradient estimated from the topographic gradient.

$$v_x = \frac{k}{n_e} \frac{dh}{dl} \quad (3.12)$$

In all canyons the residence time calculated from Darcy's Law was no more than a factor of two away from the residence time calculated by recharge mass balance (see Table 6). Final rate calculations were made using average linear velocity to estimate residence time.

Table 6. Comparison of residence time calculations.

Canyon	Recharge Mass Balance	Darcy's Law
Short	1.06	0.65
Sand	1.2	1.4
Noname	1.4	0.98
9-Mile	0.94	1.64
5-Mile	0.81	1.59

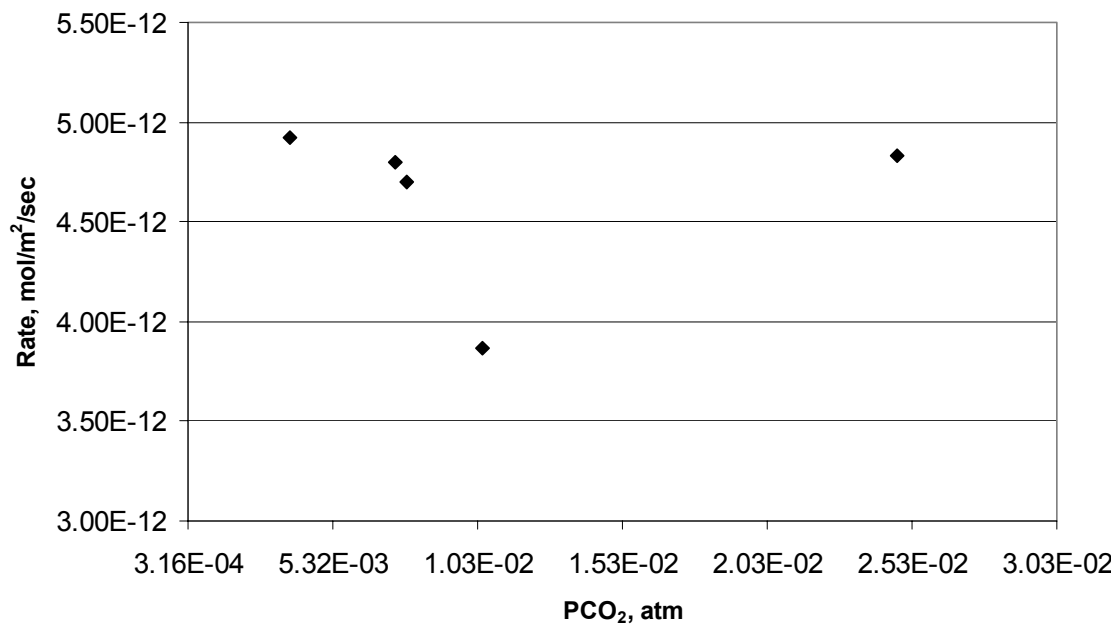


Figure 18. Initial calculated Hornblende dissolution rates.

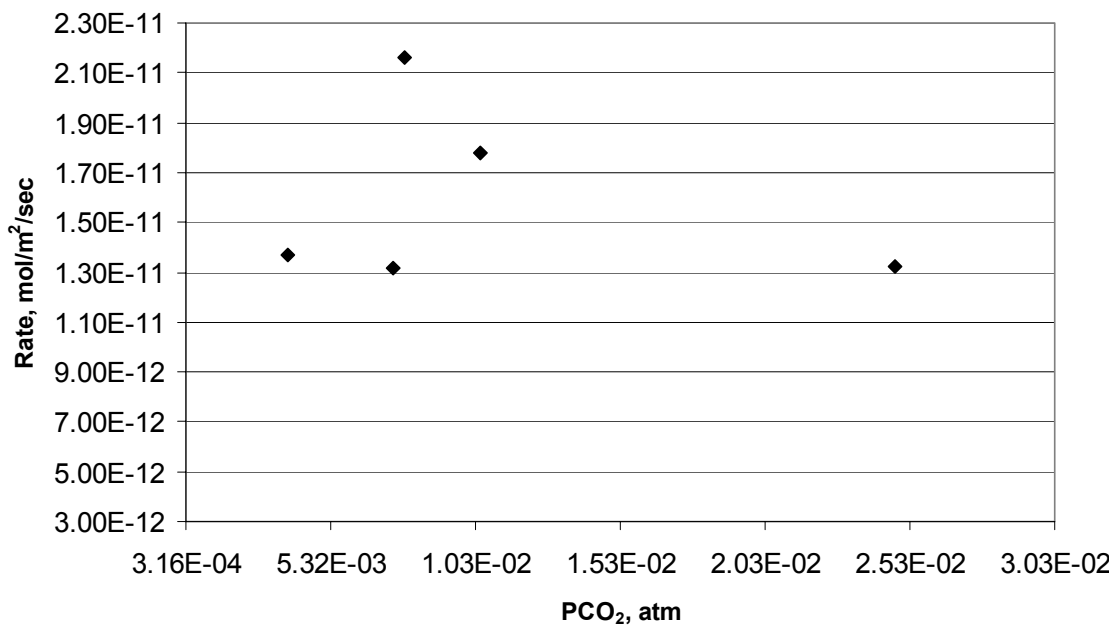
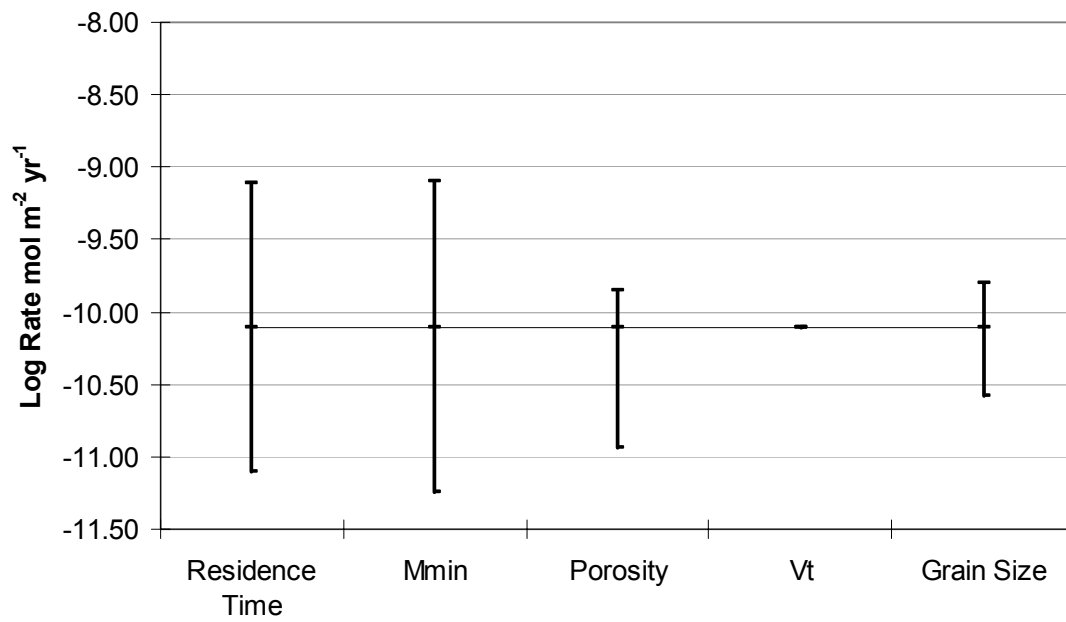


Figure 19. Sensitivity of Paces equation to variables.



Chapter 5 - Results and Discussion

General Discussion

Observations made during petrographic and electron microprobe analyses indicated that the weathering mechanism is alteration to clays and iron oxides and not complete dissolution and re-precipitation. Rates calculated are referred to as mineral dissolution or weathering rates but are probably more correctly defined as rates of release of sodium (fluoride in the case of biotite).

In general, reported field-calculated weathering rates are 1 to 2 orders of magnitude slower than laboratory rates (White et al., 2001). All of the field dissolution rates calculated at the base of each canyon in this study lie in the range of published field dissolution rates, but are greater than the median value of published rates (fig. 20). In Figure 20, the value plotted for literature rates is the median value, while the lines show the range of published rates. Figure 21 plots field dissolution rates from this study versus the range of literature laboratory rates. All rates are below the median value except for plagioclase rates, which cluster around the median value of lab rates and the biotite dissolution rate for 5-Mile canyon, which falls right at the median value. Rates faster than published field literature rates were expected due to elevated CO_2 in the area. Plagioclase rates from field data that are near the published laboratory rates were not expected. This shows that elevated CO_2 appears to increase dissolution rates in the field to near laboratory rates. A table listing sources of rates is included in Appendix 7.

Figure 22 shows plagioclase, AFS, and hornblende rates calculated using sodium as the mass balance constraint. The variation in PCO_2 is reflected in the dissolution rates. In general, canyons with higher PCO_2 have higher rates for all minerals. For instance, calculated rates for Sand and Noname Canyons are very similar; these canyons also have very similar PCO_2 values. Trends in PCO_2 are also seen in the dissolution rates. Nine-Mile Canyon has the highest PCO_2 as well as the highest calculated rates for each

Figure 20. Comparison between published field derived rates and rates calculated for this study from base of canyon samples.

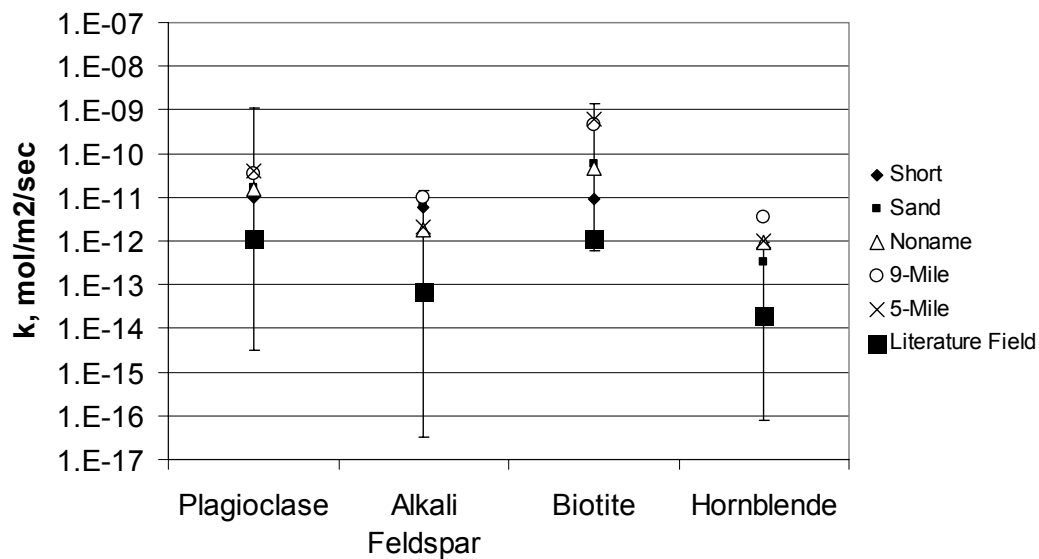


Figure 21. Comparison of published lab derived rates and field rates calculated for this study from base of canyon samples.

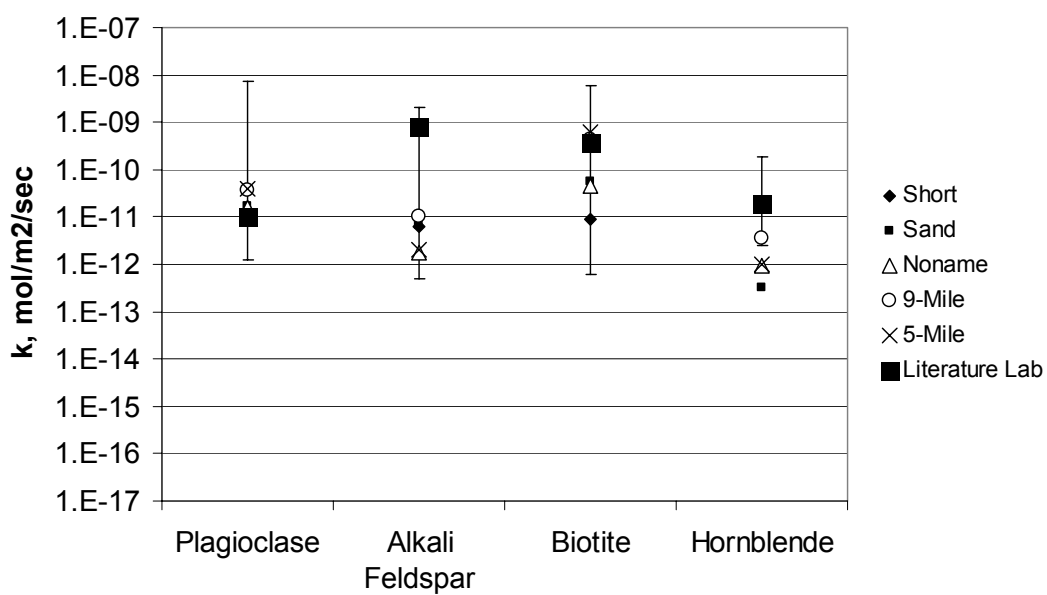


Figure 22. Calculated rates using sodium as mass balance constraint from base of canyon samples.

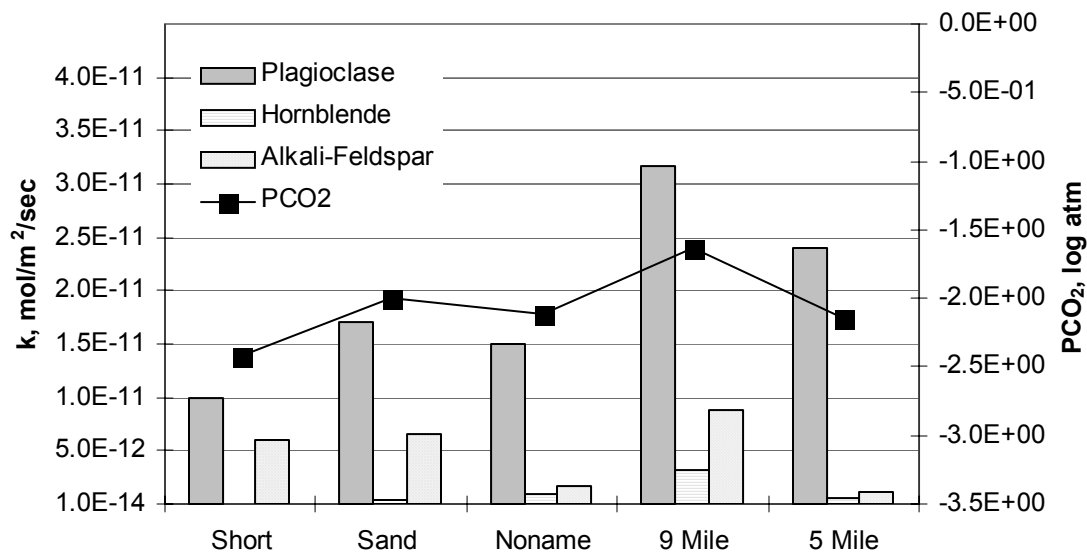
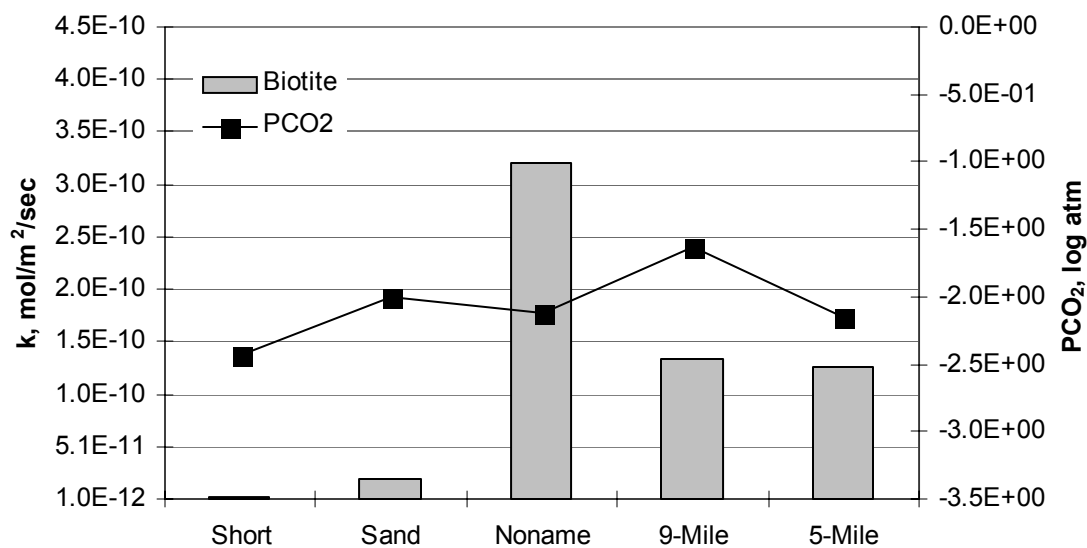


Figure 23. Calculated biotite rates using fluoride as the mass balance constraint from base of canyon samples.



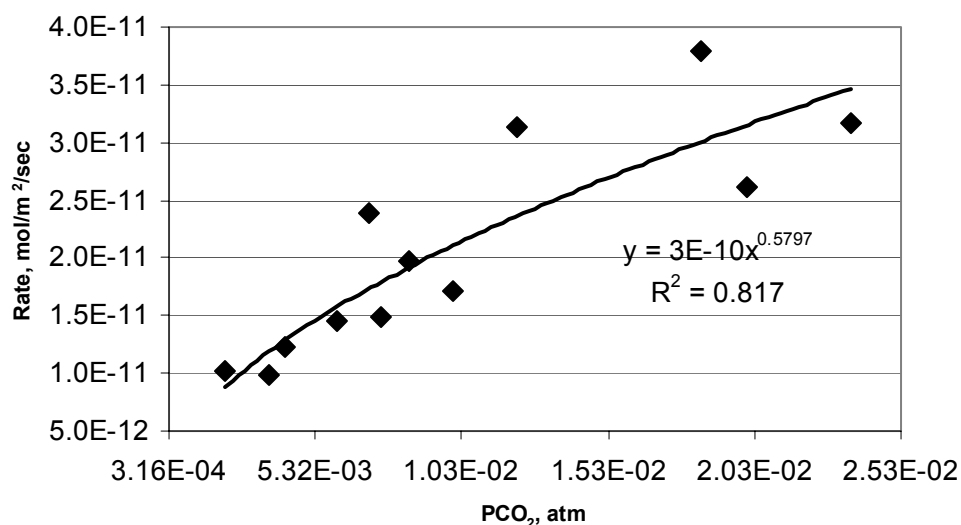
mineral. However, the PCO_2 values for 5-Mile, Noname, and Sand canyons are very similar but the plagioclase rate is slightly higher in 5-Mile.

Biotite rates calculated using fluorine as the mass balance constraint are shown in Figure 23; note the change in scale on the y-axis in this Figure. Biotite rates are within one order of magnitude of plagioclase rates. In Short Canyon, the biotite rate is one order of magnitude lower than the plagioclase rate, but in the other canyons biotite is dissolving at a faster rate than plagioclase. In Short, Sand, and 5-Mile Canyons, 100% of the biotite identified in thin section was at least 50% weathered as indicated by the replacement of sheets of biotite by iron oxide, while in 9-Mile and Noname Canyons more than half of the biotite was at least 50% weathered, indicating an extremely fast dissolution rate. However, in contrast to plagioclase trends in biotite dissolution rates are not as well correlated with PCO_2 . Biotite dissolution is the highest in Noname Canyon, but 9-Mile has the highest PCO_2 .

Plagioclase

The percentage of sodium assigned to plagioclase weathering after subtraction of dust and precipitation input ranged from 91% in 9-Mile Canyon to 98% in 5-Mile Canyon. Calculated field dissolution rates of plagioclase ranged from 9.9×10^{-12} mol/m²/sec in Short Canyon to 3.8×10^{-11} mol/m²/sec in 9-Mile Canyon. Figure 24 shows a relationship between calculated plagioclase dissolution rate and PCO_2 . The correlation is good ($R^2=0.817$) and shows that plagioclase dissolution rate is proportional to $\text{PCO}_2^{0.58}$. This relationship is similar to the relationship defined using data from Lagache (1965) where dissolution rate is proportional to $\text{PCO}_2^{0.3}$.

Rates calculated for plagioclase have the least amount of uncertainty associated with them compared to rates calculated for other minerals because almost all of the calculated flux of sodium is assigned to plagioclase dissolution. As the percentage of sodium assigned decreases, the uncertainty in the rate increases because of the linear relationship between M_{min} and k (equation 5.1).

Figure 24. Correlation between plagioclase dissolution rates and PCO₂.

$$k = \left[\frac{M_{\min}}{n\hat{s}\tau} \right] \left[\frac{1}{3.14 * 10^7} \right] \quad (5.1)$$

The percent increase or decrease in rates is directly related to the percent increase or decrease in M_{\min} . For example, in 9-Mile Canyon, assigning 100% of the sodium flux to plagioclase results in a 9.7% increase in M_{\min} and the corresponding rates are 9.7% higher than with 91% of the sodium flux assigned to plagioclase dissolution (Table 7).

Alkali-Feldspar

Calculated field dissolution rates of alkali-feldspar (AFS) range from 6.1×10^{-13} to 1.1×10^{-11} mol/m²/sec and are 0.2 to 1.2 orders of magnitude slower than plagioclase dissolution rates. Figure 25 shows the correlation between AFS dissolution rates and PCO₂. The correlation coefficient ($R^2=0.08$) indicates a poor correlation, so the dissolution rate does not appear to be very dependent upon PCO₂.

Hornblende

Hornblende make up less than 1% of the alluvium composition in Short Canyon, therefore it was not included in the distribution of sodium flux and a dissolution rate was not calculated. Rates for the remaining four canyons ranged from 2×10^{-13} to 3.8×10^{-12} mol/m²/sec. Hornblende dissolution rates are 1 to 1.7 orders of magnitude lower than plagioclase rates. Figure 26 shows the correlation between hornblende dissolution rates and PCO₂. The statistics of this regression show a correlation between PCO₂ and dissolution rate ($R^2=0.6$). The circled data point is calculated from the sample farthest up 5-Mile Canyon. A recalculation of the correlation without this point results in an $R^2=0.74$ and a rate proportional to PCO₂^{1.4}.

Biotite

The only source of fluoride to the stream waters was assumed to be the dissolution of biotite. Electron microprobe analysis confirmed the presence of fluoride in the biotite crystal in trace amounts. Rates were calculated for the dissolution of biotite using fluoride as the mass balance constraint with 100% of the fluoride flux as M_{\min} . Calculated biotite dissolution rates range from 3.2×10^{-12} to 3.2×10^{-10} mol/m²/sec. Figure 27 shows the correlation between PCO₂ and biotite dissolution rates. Statistics show a weak correlation ($R^2=0.3$). Malstrom and others (1996) found no effect of CO₂ on biotite

Table 7. Uncertainty in plagioclase rate associated with sodium flux distribution for 9-Mile Canyon

k	k(100%)	% change k	Mmin	Mmin(100%)	% change flux
3.16E-11	3.47E-11	-9.73	2.60E-01	5.06E+00	-9.73
3.13E-11	3.44E-11	-9.73	1.80E-01	3.49E+00	-9.73
3.79E-11	4.16E-11	-9.73	1.55E-01	3.01E+00	-9.73
5.28E-11	5.80E-11	-9.73	1.41E-01	2.75E+00	-9.73

dissolution in a laboratory setting for pH values between 7 and 8.5. Due to the uncertainty associated with biotite rates calculated in this study, a definite conclusion cannot be drawn on the CO₂ dependence of biotite dissolution.

Figure 25. Correlation between AFS dissolution rates and PCO₂.

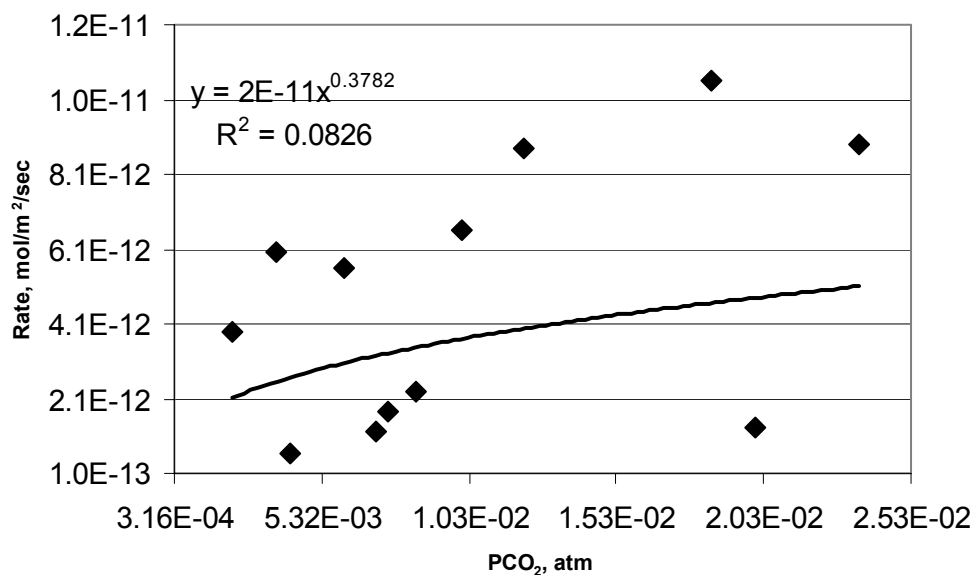
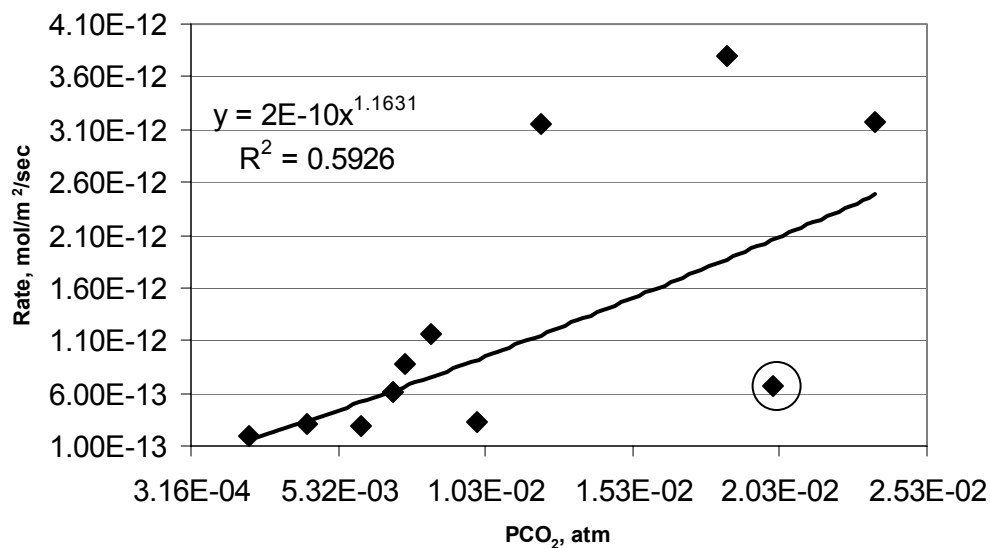


Figure 26. Correlation between hornblende dissolution rates and PCO₂.



Uncertainty in Calculation of Rates

Rates calculated for hornblende and alkali-feldspar are more sensitive to the percentage of sodium assigned to the dissolution of these minerals than plagioclase because the relative flux associated with the changes in percentages is large. For example, sodium percentages attributed to alkali-feldspar weathering in Short Canyon is 5%. An increase from 5 to 10% of the total sodium flux corresponds to an increase of over 100% in M_{\min} and therefore an increase in dissolution rate of over 100%. All of the fluoride in solution is attributed to the dissolution of biotite. Uncertainty arises in the calculation of biotite rates from the analytical error of measuring small amounts of analytes in solution and in the small amount of fluoride in the crystal structure of biotite. Uncertainty also arises in hornblende and alkali-feldspar rates due to the small amount of sodium contained in the crystal structures of these minerals as well. Rate calculation includes the oxide weight percent of the constraining ion (λ). Smaller weight percent results in larger potential uncertainty. Weight percent is proportional to λ and λ is inversely proportional to k . Increasing weight percent by a factor of 2 increases λ by a factor of 2 and results in a decrease in dissolution rate by approximately a factor of 2. Rates have been calculated for hornblende, alkali-feldspar, and biotite, but the uncertainty in these calculations prevents any relationships between dissolution rate and PCO_2 from being established that are as reliable as that between plagioclase weathering and PCO_2 .

When developing relationships between dissolution rate and PCO_2 , the uncertainty in relative rates is small, because each rate was calculated using the same procedure for all the samples. The rate calculations and field observations show that hydrologic and geologic conditions do not appear to introduce a high degree of uncertainty. Analytical procedures are also a source of uncertainty in the rates. A 2% error was assumed for each analytical method and error was calculated for each and error bars plotted in Figure 28. Uncertainty resulting from analytical data is very small. Alkali-

feldspar rates have the highest uncertainty related to analytical data due to the small percentage of sodium assigned to AFS dissolution.

Uncertainty in the rates calculated in this study arises from the assumptions. The

Figure 27. Correlation between biotite dissolution rates and PCO_2 .

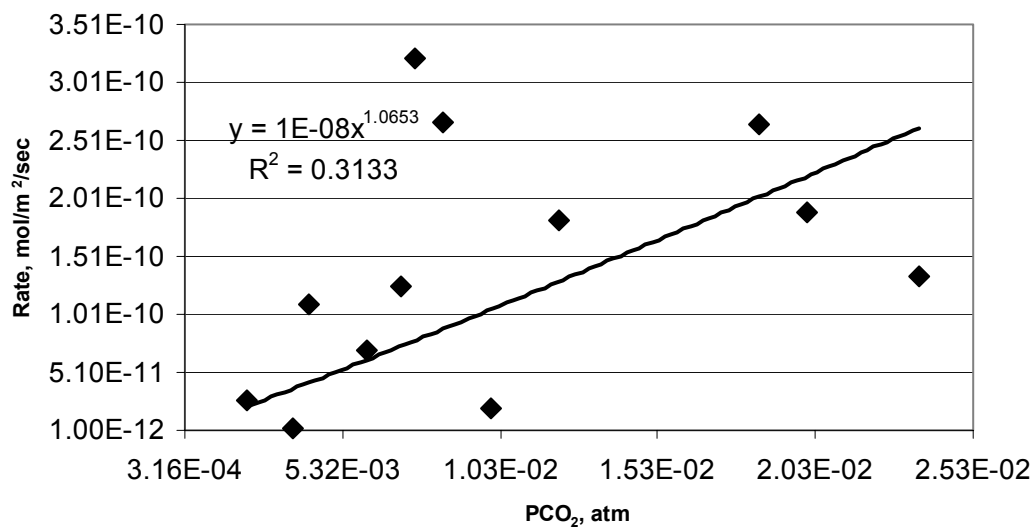
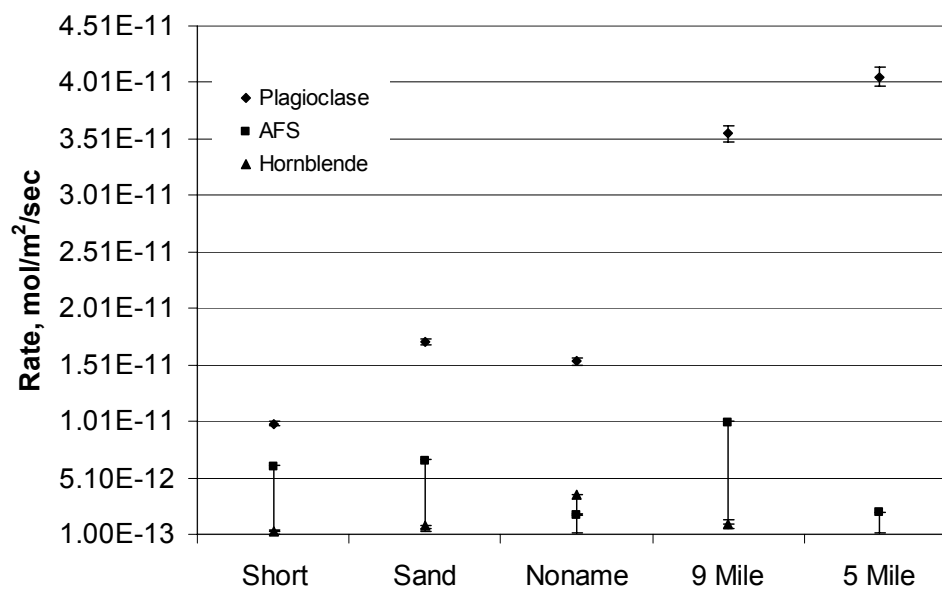


Figure 28. Uncertainty in calculated rates related to analytical uncertainty.



largest sources of uncertainty lay in the residence time and specific surface area calculations. Residence time used in the calculations most likely represents a minimum value because assumed values of porosity and hydraulic conductivity were on the high end of the range of possible values for sandy-gravel alluvium. It is unlikely that these values are more than one order of magnitude in error based on the agreement between two separate methods of calculating this variable (see Chapter 4). Specific surface area was calculated using a geometric method assuming an average grain diameter of 0.5 cm for each canyon. Large differences in grain size between canyons were not observed in thin section analysis. BET surface area measurements are generally one order of magnitude higher than geometric surface area calculations (Sverdrup and Warfvinge, 1988; White, 1995); therefore, the linear relationship between surface area and dissolution rate results in up to an order of magnitude of uncertainty in absolute rates due to the specific surface area assumptions.

Multiple samples were taken along the flow path of each canyon where hydrologic conditions permitted. Rates were calculated for all the samples that met the hydrologic criteria of the model for the canyons (see Chapter 3). Samples taken from springs high in the canyons were not used in these calculations due to their inconsistencies with the hydrologic model of the canyons. Water discharging at these springs was not flowing through alluvium, but most likely through fracture systems connected to the high altitude recharge area. This leaves great uncertainty in the residence time, volume, and specific surface area values. If the hydrologic and geologic model of the canyons is fundamentally correct, calculated rates along the flow path should have very little variation. These rates are shown in Figures 29 through 32. Rates calculated in all canyons show very little variation along the flow path. Five-Mile Canyon shows the greatest amount of variation in plagioclase rates ranging from 1.2×10^{-11} to 2.6×10^{-11} mol/m²/sec. The variation is by a factor of two. In 5-Mile Canyon there are two main branches (fig. 33) that feed into the mouth of the canyon. Observations and samples were only taken in the northern branch and it is possible that the mineralogy of

Figure 29. Plagioclase rates for all samples that fit hydrologic model.

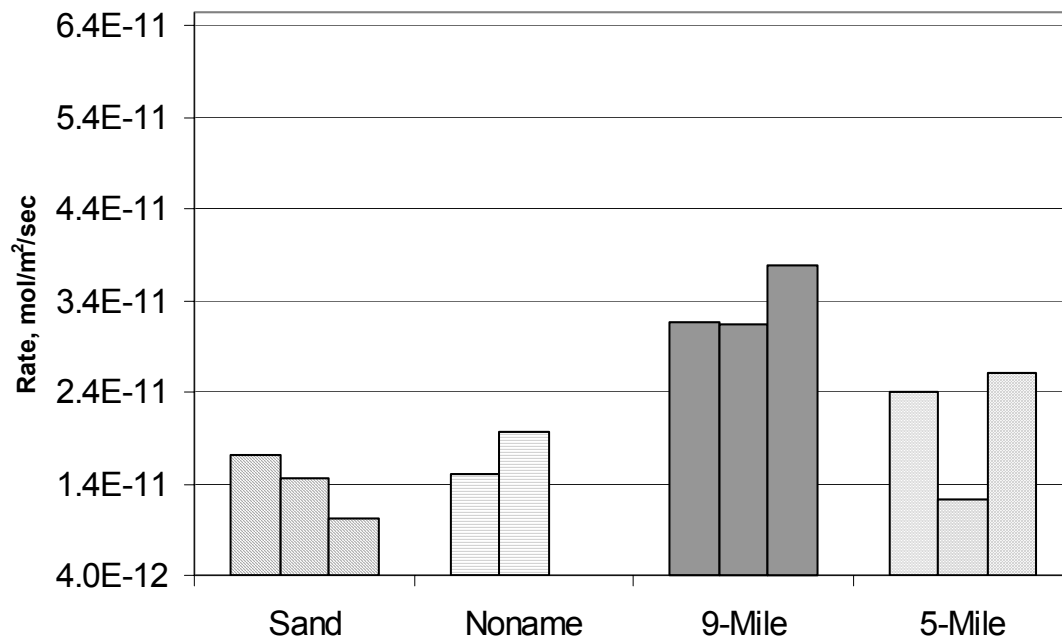


Figure 30. Alkali-feldspar rates for all samples that fit hydrologic model.

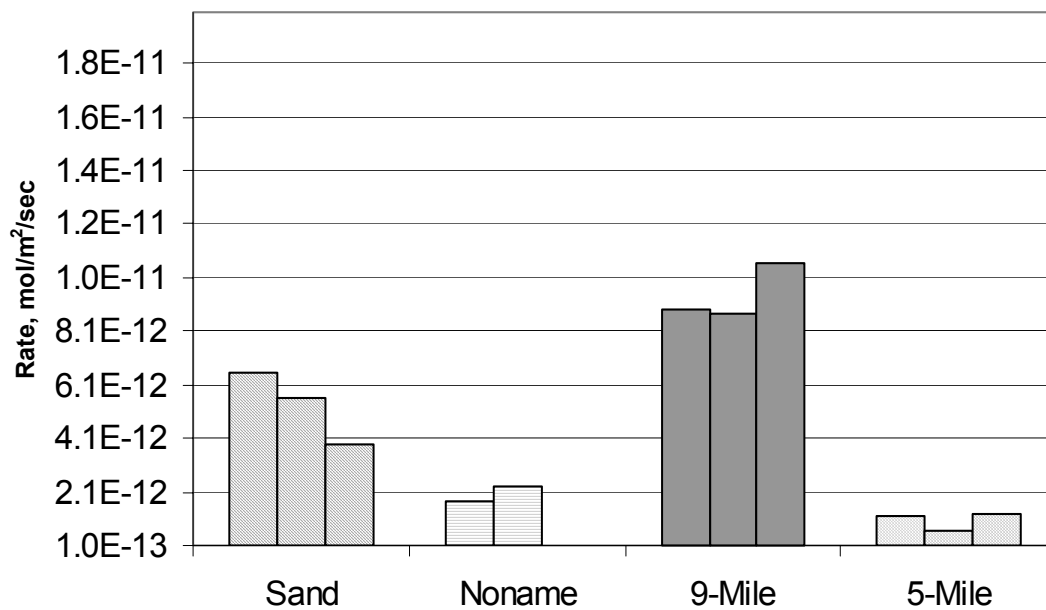


Figure 31. Hornblende rates for all samples that fit hydrologic model.

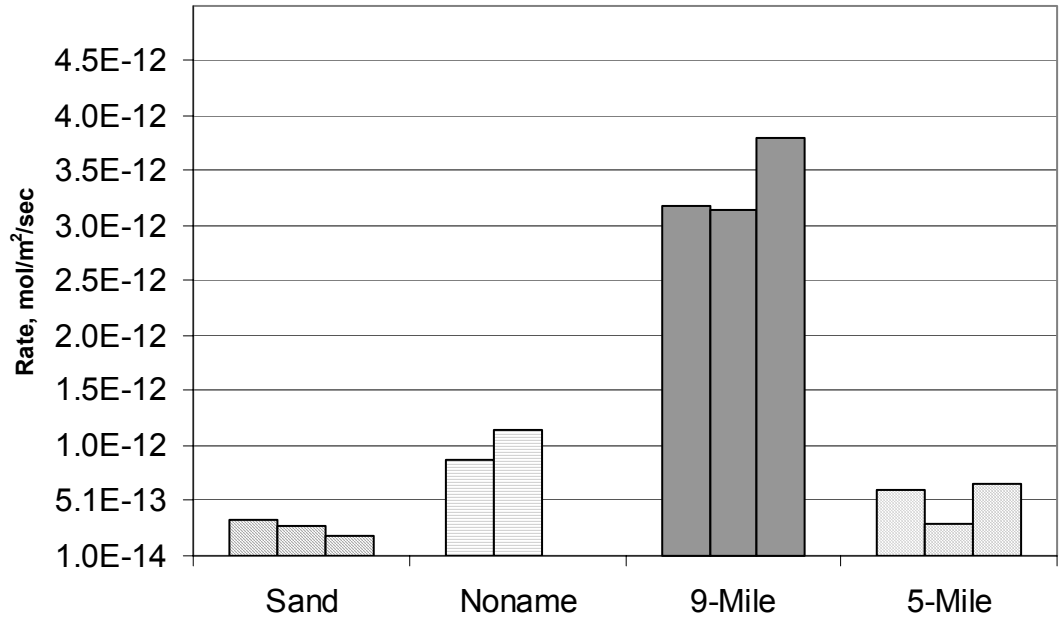
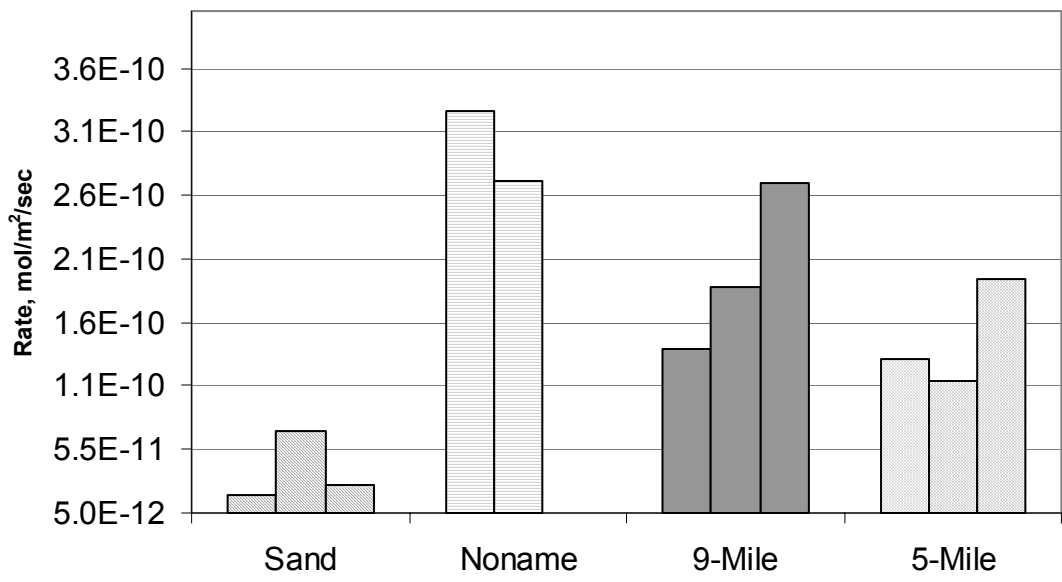


Figure 32. Biotite rates calculated for all samples that fit hydrologic model.



the canyon in the southern branch is different, resulting in different water chemistry and hydrologic/geologic conditions in the canyon that are slightly different than the defined model conditions resulting in a system that is more complex than was assumed in the calculation. Despite these variations, dissolution rates calculated in 5-Mile Canyon were included in the correlation between rates and PCO_2 that still show a strong PCO_2 dependence.

Rate Dependence on PCO_2

All calculated plagioclase rates are plotted versus PCO_2 in Figure 34. This Figure shows a correlation between PCO_2 and dissolution rate. Other possible causes of the variation are temperature and pH effects arising from variation between the canyons. Brady and Carroll (1994) report a relationship between plagioclase dissolution rate increase and temperature increase expressed in equation 5.2.

$$\ln\left(\frac{R}{R_0}\right) = \frac{\Delta T}{13.7} \quad (5.2)$$

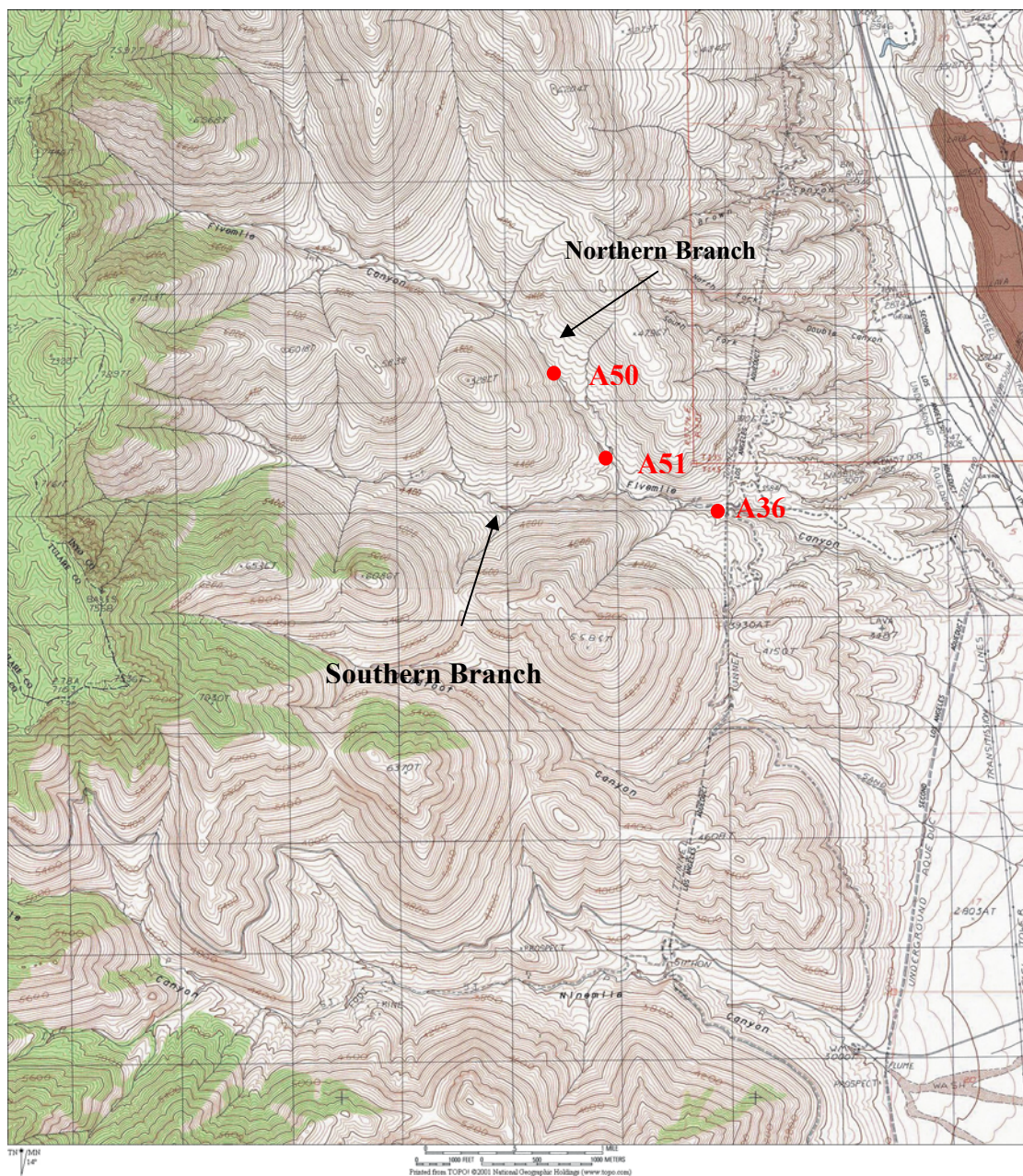
Where: R = weathering rate at atmospheric PCO_2

R_0 = weathering rate at elevated PCO_2

T = temperature in degrees Celsius

According to this relationship a temperature variation of greater than 28°C would be needed to create the variations in calculated weathering rates of plagioclase. Because measured temperatures range from 17° to 22.4°C , the variation seen in dissolution rates cannot be attributed to a temperature effect.

Figure 33. Topographic map showing two branches of 5-Mile Canyon and sample locations.



Stream waters in the study area are neutral to slightly basic with measured pH ranging from 6.8 to 8. It is well documented that proton accelerated weathering is not an important mechanism of rate increase in this pH range (Berg and Banwart, 2000).

A PCO_2 dependence of mineral dissolution rates has been derived from data of high temperature feldspar dissolution laboratory experiments performed by Lagache in 1965 (Brady and Carroll, 1994). This relationship defines mineral dissolution rates proportional to $\text{PCO}_2^{0.3}$. Results from this study show that this relationship is similar to that derived from the field data for the effect of PCO_2 on dissolution rates.

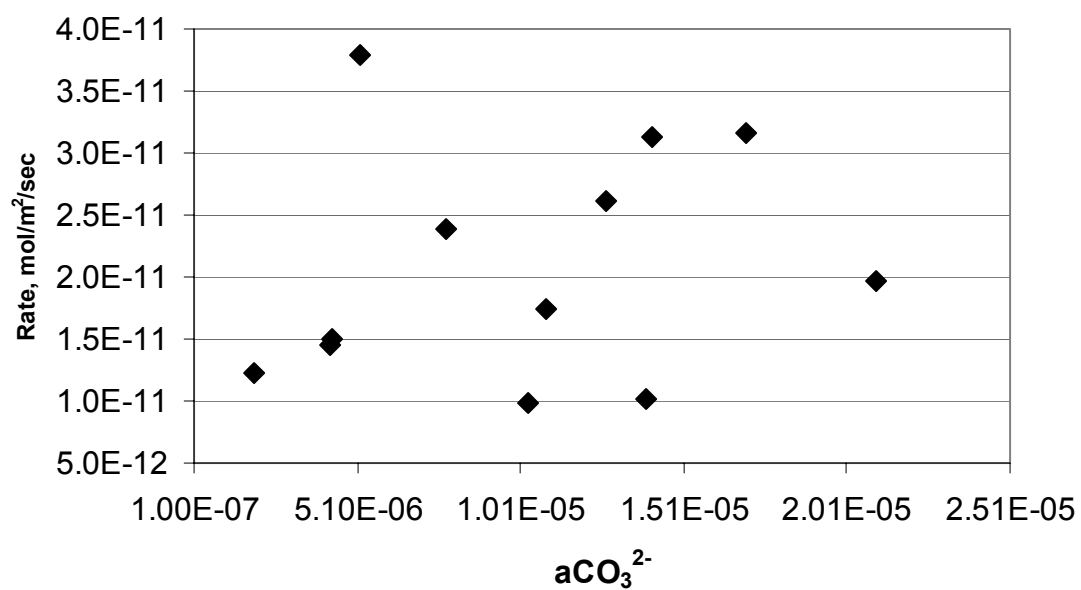
Mechanism of Increased Rate

Berg and Banwart (2000) performed laboratory dissolution experiments of anorthite at PCO_2 values of 9.7×10^{-2} and 9.7×10^{-3} atm over a range of hydrogen ion concentrations. Their study concluded that the release of aluminum is the rate-controlling step in the dissolution of plagioclase. Increasing the concentration of inorganic carbon (CO_3^{2-}) results in an increase of aluminum release and therefore an increase in the dissolution rate of plagioclase. They found that in acidic conditions ($\text{pH} < 4$), the main mechanism for an increase in dissolution rate is a proton effect, but in neutral to near-basic environments with elevated PCO_2 , carbonate-promoted weathering is expected to be the most significant mechanism of increased dissolution. They also showed an initial increase in carbonate-promoted rate with more alkaline pH that plateaus, indicating a maximum effect of CO_2 increased weathering that is reached at pH 9. They concluded that carbonate-promoted weathering has the potential to increase weathering by a factor of five. Figure 35 shows the relationship between PCO_2 and rate from Berg and Banwart (2000). Data from the present study do not indicate that the increase in dissolution rate can be attributed to aCO_3^{2-} (fig. 34).

Trends seen in calculated dissolution rates in this study cannot be explained using proton-mediated weathering. Although an increase in PCO_2 will decrease pH, in this study it was not sufficient to lower the pH below 4. In order for a natural system to have

a pH of 4 due to increases in PCO_2 , the PCO_2 in equilibrium with the system would have to be near 0.5 atm, much larger than any PCO_2 measured in the study area.

Figure 34. Calculated rates from this study plotted with $a\text{CO}_3^{2-}$.



Chapter 6 – Conclusions

- The study area is an area of elevated PCO_2 where the effects of PCO_2 on silicate dissolution rates can be examined in a natural system.
- Canyons used to calculate weathering rates have similar geologic and hydrologic characteristics, except for PCO_2 , and these small differences between canyons can be accounted for in the dissolution rate calculations.
- Dissolution rates calculated for plagioclase, hornblende, AFS, and biotite are different between canyons. Plagioclase dissolution rates have low uncertainty and the differences in rates appear to be correlated to PCO_2 .
- Other workers have developed PCO_2 -dependent rates based on high temperature laboratory dissolution of feldspar where dissolution rate is proportional to $\text{PCO}_2^{0.3}$ (Brady and Carrol, 1994). Data from this study supports that dissolution rates have a similar dependency upon PCO_2 with dissolution rates proportional to $\text{PCO}_2^{0.58}$.
- The mechanism of this increase is unclear but increasing rate due to proton-mediated dissolution does not appear to be the cause, because stream waters in the study area have neutral to slightly basic pH values. Berg and Banwart (2000) have suggested that aCO_3^{2-} is related to increased dissolution rates at pH values near neutral, but a good correlation between dissolution rate and aCO_3^{2-} could not be demonstrated.

REFERENCES CITED

- Bauer, C.M., 2001, The hydrogeology of Rose Valley and Little Lake Ranch, Inyo County, California [Master's Thesis], California State University, Bakersfield
- Berenbrock, Charles, and Martin, Peter, 1991, The ground-water flow system in Indian Wells Valley, Kern, Inyo, and San Bernardino Counties, California: U.S. Geological Survey Water-Resources Investigations Report 89-4191, 81 p.
- Berg, A., Banwart, S., 2000, Carbon dioxide mediated dissolution of Ca-feldspar: implications for silicate weathering: *Chemical Geology*, v. 163, pp. 25-42.
- Berner, R.A., Lasaga, A.C., Garrels, R.M., 1983, The carbonate-silicate geochemical cycle and its effect on atmospheric carbon dioxide over the past 100 million years: *American Journal of Science*, v. 283, pp. 641-683.
- Berner, R.A., 1995, Chemical weathering and its effect on atmospheric CO₂ and climate *in* Chemical weathering rates of silicate minerals: Mineralogical Society of America, Washington D.C., pp. 565-583.
- Boeglin, J.L., Probst, J.L., 1998, Physical and chemical weathering rates and CO₂ consumption in a tropical lateritic environment: the upper Niger Basin: *Chemical Geology*, v. 148, no. 3-4, pp. 137-156.
- Brady, P.V., Carroll, S.A., 1994, Direct effects of CO₂ and temperature on silicate weathering: Possible implications for climate control: *Geochimica et Cosmochimica Acta*, v. 58, no. 8, pp. 1853-1856.
- Brindley, G.W., Brown, 1980, Crystal structures of clay minerals and their X-ray identification: Mineralogical Society, London, pp.495.
- Carver, G.A., 1969, Quaternary tectonism and surface faulting in the Owens Lake basin, California [Master's Thesis]: University of Nevada, Reno.
- Christensen, M.N., 1966, Late Cenozoic crustal movements in the Sierra Nevada of California: *Geological Society of America Bulletin*, v. 77, no. 2, pp. 163-182.
- Cleaves, E.T., Godfrey, A.E., Bricker, O.P., 1970, Geochemical balance of a small watershed and its geomorphic implications: *geological Society of America Bulletin*, v. 81, no. 10, pp. 3015-3032.
- Diggles, M.F., Jachens, R.C., and Peters, T.J., 1989, Mineral resources of the Rockhouse Wilderness study area, Kern and Tulare Counties, California: U.S. Geological Survey Bulletin 1705-E, 20p.
- Drever, J.I., 1988, *The Geochemistry of Natural Waters*, Prentice-Hall, Upper Saddle River, NJ.
- Drever, J.I., 1997, *The Geochemistry of Natural Waters: Surface and Groundwater Environments* (third edition), Prentice-Hall, Upper Saddle River, NJ, 436 p.

- Duffold, W.A., and Smith, G.I., 1978, Pleistocene history of volcanism and the Owens River near Little Lake, California: *Journal Research, U.S. Geological Survey*, v. 6, no. 3, pp. 395-408.
- Farnsworth, R.K., Thompson, E.S., Peck, E.L., 1982, Evaporation atlas for the contiguous forty-eight United States: U.S. Department of Commerce, National Oceanic and Atmospheric Administration Technical Report NWS33.
- Feth, J.H., Roberson, C.E., and Polzer, W.L., 1964, Sources of mineral constituents in water from granitic rocks, Sierra Nevada, California and Nevada: U.S. geological Survey Water-Supply Paper 1535-I, 70 p.
- Furman, T., Thompson, P., Hatchl, B., 1998, Primary mineral weathering in the central Appalachians: A mass balance approach: *Geochimica et Cosmochimica Acta*, v. 62, no. 17, pp. 2889-2904.
- Garrels, R.M., and MacKenzie, F.T., 1967, Origin of the chemical compositions of some springs and lakes, *in* Equilibrium concepts in natural waters: American Cancer Society, Washington, D.C., pp. 222-242.
- Guler, C., 2002, Hydrogeochemical evaluation of the groundwater resources of Indian Wells-Owens Valley area, southeastern California [Ph.D. Dissertation]: Colorado School of Mines.
- Guler, C., Thyne, G., In Press, Groundwater flowpath delineation in Indian Wells Valley, California, using major-ion chemistry, cluster analysis, and geographic information system: Evidence for an interbasin flow path: *GSA Bulletin*.
- Lagache, M., 1964, Sur les conditions de formation de la boehmite, de la kaolinite et de la muscovite, par alteration de l'albite a 200 degrees C, en presence de CO₂: *Compte Rendus Hebdomadaires des Seances de l'Academie des Sciences*, v. 258, no. 13, pp. 3515-3517.
- Lagache, M., 1965, Contribution a l'etude de l'alternation des feldspaths dans l'eau, entre 100 et 200oC, sous diverses pressions de CO₂, et application a la synthese des mineralux argileux: *Bulletin de la Societe Francaise de Mineralogie et de Cristallographie*, v. 88, no. 2, pp. 223-253.
- Lasaga, A.C., 1995, Chemical weathering rates of silicate minerals: an overview *in* Chemical Weathering rates of silicate minerals: American Mineralogical Society, Washington D.C., pp. 1-21.
- Loomis, D.P., Burbank, D.W., 1988, The stratigraphic evolution of the El Paso Basin, Southern California; implications for the Miocene development of the Garlock Fault and uplift of the sierra Nevada: *Geological Society of America Bulletin*, v. 100, no. 1, pp. 12-28.
- Malmstrom, M., Banwart, S., Lewenhagen, J., Duro, L., Bruno, J., 1996, The dissolution of biotite and chlorite at 25 degrees C in the near-neutral pH region: *Journal of Contaminant Hydrology*, v. 1, No. 1-4, pp. 201-213.

- Mast, M.A., Drever, J.I., Baron, J., 1990, Chemical weathering in the Loch Vale Watershed, Rocky Mountain National Park, Colorado: *Water Resources Research*, v. 26, no. 12, pp. 2971-2978.
- Monastero, F.C., Walker, J.D., Katzenstein, A.M., Sabin, A.E., 2002, Neogene evolution of the Indian Wells Valley, east-central California: Geologic evolution of the Mohave Desert and southwestern Basin and Range, *Geological Society of America Memoir*, v. 195, pp. 199-228.
- Norton, D., 1974, Chemical mass transfer in the Rio Tanama system, west-central Puerto Rico: *Geochimica et Cosmochimica Acta*, v. 38, no. 2, pp. 267-277.
- Paces, T., 1983, Rate constants of dissolution derived from the measurements of mass balance in hydrological catchments: *Geochimica et Cosmochimica Acta*, v. 47, pp. 1855-1863.
- Paces, T., 1987, Steady-state kinetics and equilibrium between ground water and granitic rock: *Geochimica et Cosmochimica Acta*, v. 37, p. 2641-2663.
- Parkhurst, D.L., Appelo, C.A.J., 1999, User's guide to PHREEQC-A computer program for speciation, reaction-path, advective-transport, and inverse geochemical calculations: U.S. Geological Survey Water –Resources Investigations report 95-4227, 143 p.
- Plummer, L.N., Back, W., 1980, The mass balance approach: Application to interpreting the chemical evolution of hydrologic systems: *American Journal of Science*, v. 280, pp. 130-142.
- Preston, J., Still, J., 2001, <http://www.abdn.ac.uk/geology/profiles/analysis/software/>
- Rehis, M., Goodmacher, J.C., Harden, J.W., McFadden, L.D., Rockwell, T.K., Shroba, R.R., Sowers, J.M., Taylor E.M., 1995, Quaternary soils and dust deposition in southern Nevada and California: *GSA Bulletin*, v. 170, n. 9, pp. 1003-1022.
- Rehis, M.C., 1997, Dust deposition downwind of Owens (dry) Lake, 1991-1994: Preliminary findings. *Journal of Geophysical Research*, v. 102, no. D22, pp. 25,999-26,008.
- Robertson, F.N., 1991, Geochemistry of ground water in alluvial basins of Arizona and adjacent parts of Nevada, New Mexico, and California: U.S. Geological Survey Professional Paper, Report: P 1406-C, pp. C1-C90.
- Robinson, A.B., Baliunas, S.L., Soon, W. and Robinson, Z.W. 1998. Environmental effects of increased atmospheric carbon dioxide. Oregon Institute of Science and Medicine (<http://www.oism.org/pproject/s33p36.htm>).
- Stevens, S.H., Gale, J., 2000, Geologic CO₂ sequestration may benefit upstream industry: *Oil & Gas Journal*, pp. 40-44.
- Suchet, P.A., Probst, J.L., 1993, Modelling of atmospheric CO₂ consumption by chemical weathering of rocks: Application to the Garonne, Congo and Amazon basins: *Chemical Geology*, v. 107, pp. 205-210.

- Sverdrup, H., Warfvinge, P., 1988, Weathering of primary silicate minerals in the natural soil environment in relation to a chemical weathering model: *Water, Air, and Soil Pollution*, v. 38, pp. 387-408.
- Taylor, A.B., Velbel, M.A., 1991, Geochemical mass balances and weathering rates in forested watersheds of the southern Blue Ridge II. Effects fo botanical uptake terms: *Geoderma*, v. 51, p. 29-50.
- Thyne , G., Gillespie, J., 1997, Indian Wells Valley Hydrogeology: Technical report for the NAWS-Geothermal Projects Office China Lakes Naval Weapons Center, China Lake CA.
- Thyne, G.D., Gillespie, J.M., and Ostdick, J.R., 1999, Evidence for interbasin flow through bedrock in the southeastern Sierra Nevada: *Geological Society of America Bulletin*, v. 11, no. 11, ppl 1600-1616.
- Velbel, M.A. 1985, Geochemical mass balances and weathering rates in forested watersheds of the southern Blue Ridge: *American Journal of Science*, v. 285, pp. 904-930.
- Velbel, M.A., 1992, Geochemcial mass balances and weathering rates in forested watersheds of the southern Blue Ridge. III. Cation budgets and the weathering rate of amphibole: *American Journal of Science*, v. 292, pp. 58-78.
- Volk, T., 1987, Feedbacks between weathering and atmospheric CO₂ over the last 100 million years: *American Journal of Science*, v. 287. pp. 763-779.
- White, A., 1995, Chemical weathering rates of silicate minerals in soils *in* *Chemical weathering rates of silicate minerals*: Mineralogical Society of America, Washington D.C., pp. 407-458.
- White, A., Bullen, T., Schulz, M., Blum, A., Huntington, T., Peters, N., 2001, Differential rates of feldspar weathering in granitic regoliths: *Geochimica et Cosmochimica Acta*, v. 65, no. 6, pp. 847-869.
- Wildman, W.E., Whittig, L.D., 1968, Serpentine rock dissolution as a function of carbon dioxide pressure in aqueous solution: *The American Mineralogist*, v. 53, pp. 1252-1263.
- Wollast, R., Chou, L., 1985, Kinetic study of the dissolution of albite with a continuous flow-through fluidized bed reactor *in* *The chemistry of weathering*: D. Reidel Publishing Company, Boston, pp. 75-96.
- Zellmer, J.T., 1988, Engineering and environmental geology of the Indian Wells Valley area, southeastern California: *Bulletin of the Association of Engineering Geologists*, v. 25, no. 4, pp. 437-457.

Appendix 1: Field Notes

5/12/02

Chuck and Candace Pierce

Son and daughter in law – Mike and Rhonda

Rhonda's dad Tim worked at the Yellow Aster Mine

Rhonda's mother Jane works for water district and has access to data

Ninemile Canyon – Fault running length of canyon, check chemistry, Chuck says it has the highest TDS.

Possibly no water to sample, drought

Into Ridgecrest tomorrow for maps, water, etc.

Small canyons formed by leaks in aqueduct – CO₂ gathers and kills birds

Coso was pumping CO₂ back into the ground

5/13/02

To Ridgecrest for maps, food, etc.

Went to Tungsten mine with Chuck and drove around the rest of the canyons

Definitely a change in weathering between north and south no water in canyon bottoms – Noname to 2nd aqueduct

Cottonwoods and grass are green

Weathering appears to be most advanced in fractures

4 tons of CO₂ per day from 4 wells at Coso

Tritium indicates flow from recharge to valley <50 years through fractures

Zellmer 1988

Population of IWV approx 30,000 in 1988, most in Ridgecrest

Good regional fault map

Roquemore and Zellmer 1987 – geologic mapping

5/14/02 Noname Canyon

A1 – standing water in streambed, 30 meters upstream streambed is dry.

Outcrop on north side – fairly grusified

Granodiorite – lots of biotite, cut by granite pegmatite – mostly
 Quartz – differential weathering pattern, dike vs. host
 50 meters from A1 North bank
 granite outcrop with granodiorite intrusion, granodiorite obviously weathers faster

A2 – Same granite as A1 – no granodiorite

A3 – granite – a little different, contains a mineral with feathery habit
 Sampled – coarse quartz
 Possibly metamorphosed, lots of ??????
 Some large pieces of granodiorite with epidote along fracture faces, possibly
 rolled down from above pegmatites

A4 – granodiorite with pegmatite and other granite dikes (?????)
 Possibly metamorphosed in areas granodiorite intruded into granite, chill margins
 Float between A3 and A4 contains lots of mafics – green epidote
 Possibly lots of hornblende?

A5 – granodiorite 20 meters from A3

A6 – no running water from mouth to here, turn around to Bakersfield by 1:30

A7 – stop here for day

A8 – standing water – highly vegetated

California State University, Bakersfield – Dirk Baron 2:00 p.m.

Jan Gillispie

Elizabeth Powers – see her for supplies

Dirk is only running trace metals, not cations

Borrowed all equipment needed

TDS, conductivity, pH, temperature meters

Mercuric chloride for isotope sampling

Nitric acid for anion sampling

Hach digital titrator for alkalinity, magnetic stirrer

Did not get battery for Geopump, will filter using syringe filters from
 Duane.

1:00 meeting at water district office 5/14/02, Norma and Ridgecrest

Navy, water district, Kern County conservation district, Kern County water agency,
 Tetrattech

Kern County water agency monitors stream gauges in Sand and Grapevine Canyons

Donna (?) says there is water in Sand, further up canyon outdoor classroom for 5th
 graders.

Tom Hasselbacher monitors gauges

Saturday Jane will be a water resource office – Norma just down from Inyokern Blvd.
Call Friday to set up time.

A9 – Outcrop along road to aqueduct sampled very light granite – in contact with weathered granodiorite

Appears to be a lot more mafic rock in float on south side of Noname

5/14/02

Walmart – Sharpies, ziplocks etc.

Went to water district, meeting next week, not today.

Called Geoff and left message

5/15/02

Sand Canyon – running water

A10 – North side of canyon, side canyon developed along lithologic change, fault?

Granite on west, granodiorite on east (more weathered)

Above looks like granite dikes cut across diorite, picture granite dike sticking up, granodiorite on either side weathered down.

Side canyons appear to be developing in more mafic rock

A11 – sample of in place diorite, hopefully less weathered.

A12 – spring? Picture

A13 – roadcut – date of road?

Slickenlines on granite

Trend N60E

Plunge 14W

Sampled weathered granite

5/17/02 Deadfoot Canyon

A14 – “Outcrop” of weathered diorite on south bank

A15 – Outcrop of weathered diorite all along north bank – granitic dikes

Starting to get green vegetation in stream bed, no visible water

A16 – picture – south bank – diorite

Metamorphosed right at contact with granite dike. Rock in stream bed is less

weathered than rock above it (?) exposure time?

No granite outcrop from foot to second aqueduct road

A17 – white crust on rock in stream bed, sample

A18 – granodiorite outcrop on north bank, green fine grained rock
Hydrothermal alteration? Sampled both

A19 – first standing water

5/20/02 Grapevine Canyon

A20 – weathered granodiorite with granite dikes in roadcut – very gussified, sampled
joint and fracture filling

A21 – sample of granodiorite may be able to look at weathering progression

A22 – granite with pink, intrusions? Fracture filling? Hydrothermal alteration?
Sample and picture

Between Ninemile and Noname

A23 – Fault, reverse - picture
Strike 221 degrees
Dip 70W

A24 – fault zone, fault gauge?
Pictures

A25 – Fault?

A26 – faulted piece of granite (219, 52W) within diorite
Hornblende crystals, sampled

A27 – grapevine, phyllite/slate, sampled

A28 – back to granite

5/21/02

A29 – up Ninemile, snow sample off bush branches
Lat/long: 35 51.784 N/118 00.540 W 6300 feet elevation

A30 – upper aqueduct road between Ninemile and Deadfoot
Sample fracture fill, looks very mafic again with granite dikes, one small granitic
intrusion

A31 – first appearance of granite along this road, very weathered sample and photo

A32 – running water at second aqueduct

5/22/02

BLM office

Grapevine owners:

Ed Koch

Standards – don't live there

Chamberlains

Visitor Center

Book of Sand Canyon plants, horse trails up most of Ninemile Canyon.

5/23/02

Sand Canyon

A33 – this site was wet but not running on 5/15

Lat/long: 35 46.553N 117 54.004 W 2787' elev

Cond – 106 microseimen /cm

Low battery on TDS meter

Went into town for a battery, came back at 12:30 and there was no longer water here

A34 – surface water just above culvert

Lat/long: 35 46.536N 117 54.060W 2776' elev

T = 27.7C

Cond = 1.05 mS/cm

TDS= 0.52 g/L

pH = 8.25

CO₂ titration = 130 drops (0.2) = 26 mg/L as CO₂

A35 – Sand Canyon – next to picnic area

Lat/long: 35 46.534/117 54.758

5/29/02 Sand Canyon

A37 - spring near head of sand

Lat/long: 35 48.418W/117 59.734N 5028' elev

T 20.32

Cond 0.38 mS/cm

TDS 0.21 g/L

pH 7.935

7 drops NaOH for CO₂

A38 – stream in sand

Lat/long: 35 48.170N/117 58.785W 4392' elev

T 19.5

Cond 0.50 mS/cm
TDS 0.25 g/L
pH 7.535
24 digits NaOH for CO₂

5/29/02

A39 – Road to Rodecker Flat
T = 20.8 degrees C
pH 7.824
Cond 0.76 mS/cm
TDS 0.35 g/L
Lat/long: 35 46.991 N/ 117 56.714W 3563' elev

5/31/02

A40
Lat/long: 35 49.353N/ 117 56.639W 4075' elev
Cond 0.24 mS/cm
TDS 0.12 g/L
T 17.8 degrees C
pH 7.802
NaOH 20 drops

A41 Noname grotto
Lat/long: 35 48.792N 117 55.499W
Cond 1.44 ms/cm
TDS 0.57 g/L
pH 7.492
T 20.2 degrees C
NaOH 59 drops

6/14/02 Short Canyon

no water at headwaters
greenery indicating springs

a couple of areas above A42 with water but banks were too steep to climb into and get a sample

A42 small pool of standing water, impossible to filter due to turbidity

Cond 0.42 mS/cm
TDS 0.20 g/L
T 16.9 degrees C
pH 6.417
Lat/long: 35 42.838N/ 117 55.433W 3829' elev

A43 – along trail just above cliff at parking area with fire ring
TDS 0.33 g/L
Cond 0.68 mS/cm
NaOH 62 drops
pH 6.682
T 17.2 degrees C
Lat/long: 35 42.713N/117 55.195W 3687' elev

A44 Short-just above picnic area, water running over rock
TDS 0.34 g/L
Cond 0.68 mS/cm
T 22.4 degrees C
pH 7.843
Lat/long: 35 42.634N/117 55.138W 3503' elev
NaOH 24 drops

6/5/02 9-mile

A45 limestone in float along road

A46 small puddle of standing water
Cond 1100 mS/cm
TDS 550 g/L
T 16.9 degrees C
pH 7.167
Lat/long: 35 50.605N/117 58.444W 4381' elev

A41 up stream of mine, flowing water
pH 7.327
T 17.4 degrees C
Cond 1330 mS/cm
TDS 650 g/L
Lat/long: 35 50.366N/117 57.760W

A48 running water

Lat/long: 35 50.522N/117 57.125W 3814' elev
T 23.3 degrees C
Cond 890 mS/cm
TDS 940 g/L
pH 7.781

A49
pH 7.543
TDS 1110 mg/L
Cond 2220 uS/cm
Lat/long: 35 50.609N/117 55.918W 3467' elev

6/11/02
A50-5 Mile
Directly from spring tried to sample flowing water
T 15.1 degrees C
TDS 0.45 g/L
Cond 0.91 mS/cm
pH 7.087
Lat/long: 35 53.562N/ 117 56.272W

A51
pH 7.831
Cond 1.21 mS/cm
TDS 0.61 g/L
T 15 degrees C
Lat/long: 35 53.142N/117 55.914W

*** Sample locations shown on topographic map in electronic files (samples.jpg)

Appendix 2: ICP/IC Analyses

Element	wavelength	Sample: A43		Sample: A48		Sample: A34		Sample: A41		Sample: A37	
		Conc, mg/l	Std Dev	Conc, mg/l	Std Dev	Conc, mg/l	Std Dev	Conc, mg/l	Std Dev	Conc, mg/l	Std Dev
Li	670.784	0.062	0.0007	0.059	0.0009	0.36	0.004	0.169	0.0028	0.067	0.0003
Na	330.237	73.3	0.11	110.5	0.004	156.8	0.031	93.5	0.008	18.2	0.0133
K	766.49	1.58	0.009	17.5	0.02	9.84	0.078	8.29	0.094	0.967	0.0072
Rb	780.023	0.056	0.0081	0.065	0.0034	0.058	0.0032	0.07	0.0021	0.048	0.0038
Sr	421.552	0.411	0.001	0.4	0.0001	0.543	0.0024	0.036	0.0002	0.259	0.0016
Ca	317.933	92.9	1.07	223.25	0.077	46	0.57	205.25	0.095	58.5	0.04
Mg	285.213	11.6	0.03	107.25	0.018	30.1	0.14	79.75	0.014	8.35	0.028
Ti	334.94	-0.007	0	-0.016	0.0002	-0.003	0.0001	-0.013	0.0002	-0.004	0
Mn	257.61	0.135	0.0027	0.221	0.0018	0.002	0	0.002	0	0.001	0
Fe	238.204	0.782	0.0184	0.024	0.0001	0.012	0.0001	0.009	0	0.008	0.0001
Zn	206.2	-0.002	0.003	-0.002	0.0001	-0.003	0.0004	0	0.0003	-0.001	0.0003
Al	396.153	-0.049	0.001	-0.066	0.0007	-0.04	0.0011	-0.059	0.0006	-0.045	0.0005
Si	251.611	20.2	0.23	21.7	0.06	20	0.14	21.9	0.15	8.3	0.018

Element	wavelength	Sample: A36		Sample: A44		Sample: A35		Sample: A39		Sample: snow	
		Conc, mg/l	Std Dev	Conc, mg/l	Std Dev	Conc, mg/l	Std Dev	Conc, mg/l	Std Dev	Conc, mg/l	Std Dev
Li	670.784	0.022	0.0001	0.067	0.0008	0.279	0.001	0.118	0.0009	0.016	0.0001
Na	330.237	154.2	0.11	65.7	0.006	110.25	0.013	61.9	0.051	0.361	0.0076
K	766.49	17.9	0.05	0.948	0.012	8.31	0.095	3.55	0.028	0.253	0.0018
Rb	780.023	0.052	0.0059	0.073	0.003	0.051	0.0043	0.053	0.0085	0.038	0.0114
Sr	421.552	0.406	0.0008	0.415	0.0013	0.375	0.001	0.511	0.002	0.006	0.0001
Ca	317.933	92.2	0.73	83.5	0.89	128	0.062	77.9	0.43	0.527	0.0072
Mg	285.213	37.5	0.11	11.6	0.02	31.25	0.004	19.5	0.11	0.103	0.0075
Ti	334.94	-0.007	0	-0.006	0.0001	-0.008	0.0001	-0.006	0.0001	0.003	0
Mn	257.61	0.002	0	0.002	0	0.022	0.0002	0.006	0	0.006	0
Fe	238.204	0.008	0.0001	0.02	0.0002	0.009	0.0001	0.022	0.0001	0.028	0.0006
Zn	206.2	-0.002	0.0001	-0.002	0.0001	-0.001	0.0003	-0.002	0.0001	0.004	0.0001
Al	396.153	-0.05	0.0004	-0.047	0.0009	-0.053	0.0001	-0.048	0.0004	0.017	0.0003
Si	251.611	10.8	0.09	22	0.08	18.6	0.09	17.1	0.04	0.025	0.0004

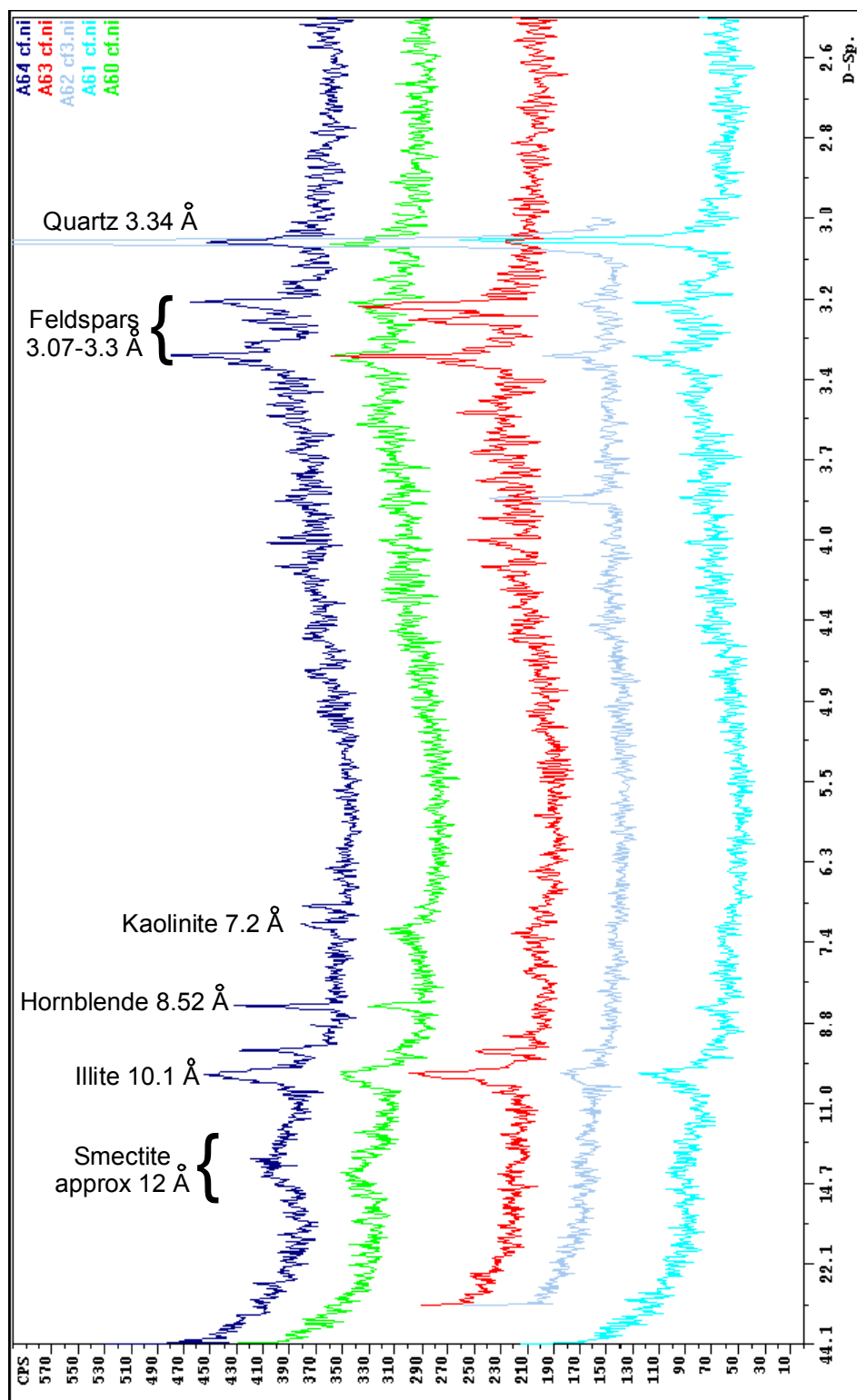
Element	wavelength	Sample: A49		Sample: A50		Sample: A40		Sample: A51		Sample: A47	
		Conc, mg/l	Std Dev	Conc, mg/l	Std Dev	Conc, mg/l	Std Dev	Conc, mg/l	Std Dev	Conc, mg/l	Std Dev
Li	670.784	0.151	0.001	0.019	0	0.035	0.0003	0.021	0	0.018	0
Na	330.237	160	0.069	63.5	0.036	59	0.06	109.4	0.016	95.3	0.064
K	766.49	18.4	0.05	7.16	0.05	4.38	0.038	8.52	0.086	7.97	0.004
Rb	780.023	0.057	0.0082	0.046	0.003	0.052	0.0048	0.056	0.0118	0.061	0.0107
Sr	421.552	0.5	0.0001	0.277	0.0004	0.205	0.0005	0.37	0.0025	0.527	0.0018
Ca	317.933	198.75	0.09	86.2	0.47	61.3	0.82	95.2	1.24	128	2.1
Mg	285.213	146.25	0.037	26.2	0.13	14.1	0.05	35.1	0.11	43	0.24
Ti	334.94	-0.012	0.0001	-0.006	0.0001	-0.004	0	-0.007	0.0001	-0.01	0
Mn	257.61	0.595	0.0067	0.311	0.0058	0.008	0.0001	0.006	0.0001	0.077	0.001
Fe	238.204	0.047	0.0005	0.012	0.0002	0.013	0.0001	0.011	0.0001	0.021	0.0188
Zn	206.2	-0.002	0.0003	-0.002	0.0003	-0.002	0.0001	-0.002	0.0004	-0.002	0.0002
Al	396.153	-0.062	0.0007	-0.05	0.0005	-0.044	0.001	-0.052	0.0005	-0.053	0.0001
Si	251.611	21.9	0.17	9.18	0.021	11.3	0.07	12.3	0.05	12.4	0.12

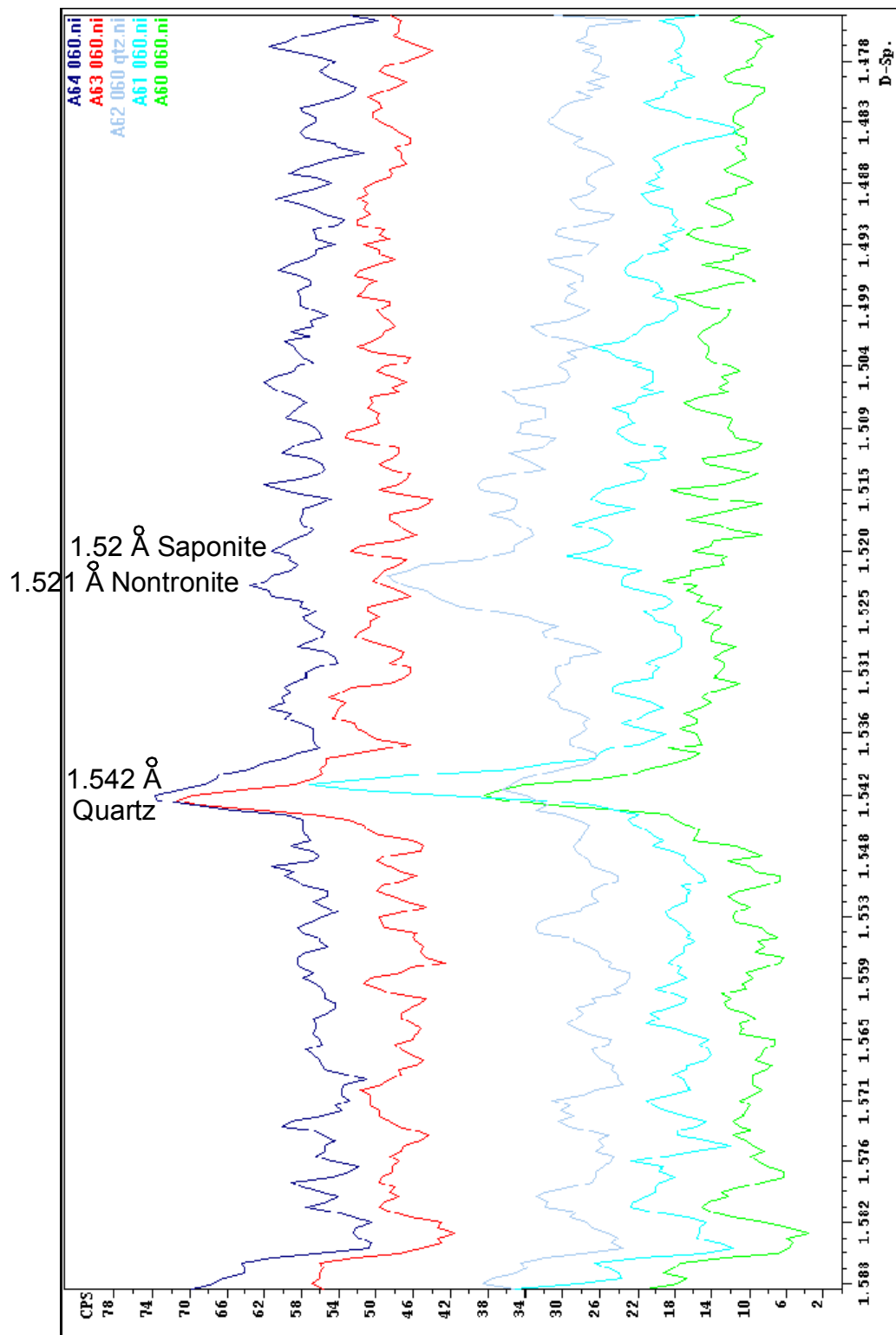
Element	wavelength	Sample: A46		Sample: A38	
		Conc, mg/l	Std Dev	Conc, mg/l	Std Dev
Li	670.784	0.018	0	0.056	0.0003
Na	330.237	87.1	0.036	29.8	0.005
K	766.49	7.3	0.051	2.38	0.021
Rb	780.023	0.06	0.0041	0.061	0.0083
Sr	421.552	0.423	0.0019	0.307	0.0002
Ca	317.933	99.8	1.22	63.7	0.8
Mg	285.213	37.2	0.1	11.9	0.04
Ti	334.94	-0.008	0	-0.005	0.0001
Mn	257.61	0.002	0	0.003	0
Fe	238.204	0.009	0.0001	0.008	0.0001
Zn	206.2	-0.002	0.0001	-0.003	0.0002
Al	396.153	-0.05	0.0003	-0.046	0.0011
Si	251.611	11.5	0.14	11.4	0.15

Raw Data from IC Analyses

<u>Sample:</u>	<u>F-</u>	<u>Cl-</u>	<u>Br-</u>	<u>SO42-</u>
SNOW	0.014	0.76	0	0.611
A34	2.81	39.9	0.099	148.7
A35	1.64	33.89	0.111	147.7
A36	3.33	76.7	0.255	278.9
A37	1.69	7.21	0.054	16.1
A38	1.85	7.86	0.046	39.5
A39	2.12	18.75	0.06	83.7
A40	1.48	14.82	0.098	85.6
A41	1.78	37.45	0.204	208.8
A43	0.95	13.74	0.162	58.4
A44	0.98	15.48	0.133	76.1
A46	0.67	35.98	0.214	107.6
A47	0.86	47.51	0.275	242
A48	0.83	52.44	0.342	276.7
A49	0.88	77.44	0.369	339.4
A50	2.31	38.18	0.135	158.1
A51	3.25	65.77	0.335	228.5

Appendix 3: X-Ray Diffraction Patterns





Appendix 4: Raw Point Count Data

Short Canyon Alluvium						
Category						
Original Grain		Altered Grain	<50%	>50%	Matrix	
Quartz	208	Quartz			Clay	8
Alkali Feld	44	Alkali Feld	15	3	Calcite/Siderite?	
Plag	21	Plag	8	10	grain rim	0
Muscovite	4	Muscovite	0		free	0
Olivine	5	Olivine	1		FeOxide	2
Biotite	5	Biotite	0	5		
Hornblende	1	Hornblende	0	0		
Sphene	2	Sphene	2			
Opaque	1	Opaque				
Unknown	8	Unknown		7		
Rock Frag	1					
total count	310					

Sand Canyon Alluvium						
Category						
Original Grain		Altered Grain	<50%	>50%	Matrix	
Quartz	113	Quartz			Clay	1
Alkali Feld	78	Alkali Feld	8		Calcite/Siderite?	
Plag	27	Plag	8	5	grain rim	18
Muscovite	4	Muscovite			free	26
Olivine	9	Olivine			FeOxide	1
Biotite	7	Biotite	1	3		
Hornblende	7	Hornblende	1			
Sphene	1	Sphene	1			
Opaque	5	Opaque				
Unknown	7	Unknown	1	6		
Rock Frag						
total count	304					

Appendix 5: Sample Spreadsheet Used to Calculate Mineral Formulas from Oxide
Weight Percent Data.

FELDSPAR CALCULATION SHEET						
	Wt%	Mol Prop	At Prop O	No anions	Formula	
SiO ₂	63.544	1.058	2.115	22.515	Si	11.257
Al ₂ O ₃	22.710	0.223	0.668	7.112	Al	4.741
FeO	0.062	0.001	0.001	0.009	Fe(ii)	0.009
CaO	3.363	0.060	0.060	0.638	Ca	0.638
Na ₂ O	9.617	0.155	0.155	1.652	Na	3.303
K ₂ O	0.180	0.002	0.002	0.020	K	0.041
SrO	0.522	0.005	0.005	0.054	Ba	0.054
TOTAL	99.999		3.006		TOTAL	20.044
			No Oxyg	32		
			T2	10.644		
MOLECULAR WEIGHTS						
SiO ₂	60.08				An	16.03
Al ₂ O ₃	101.96				Ab	82.95
FeO	71.85				Or	1.02
CaO	56.08					
Na ₂ O	61.98					
K ₂ O	94.2					
SrO	103.62					

Appendix 6: PHREEQC Input Files

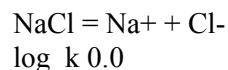
INPUT FILE FROM PREVIOUSLY TAKEN SAMPLES

SOLUTION_SPREAD

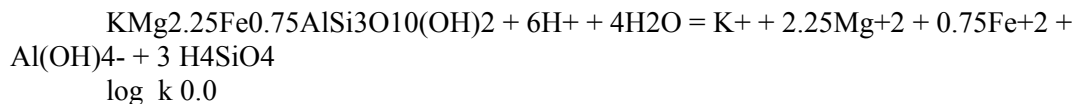
number	description	temp	pH	Na	K	Ca	Mg	C(4)	Cl	S(6)
	Si Al									
								as HCO3 charge		
1	snow 5.00	5.92	0.43	0.47	0.84	0.190	3.59	0.47	1.14	0.17
	0.01									
2	Tunawee Cyn sprg		16.6	8.13	27.0	4.5	77.1	18	342.9	8.6
	35.9 26.18	0.02								
3	Protugese bench sprg		20	7.73	17.8	3.37	61.5	10.47	248.7	5.1
	26.9 25	0.02								
4	LL Cyn sprg.	25.5		7.99	48.6	5.57	88.1	20.79	343.5	
	31.7 81.7	27.49		0.02						
5	LL Cyn 2	17.5	8.3	56	6.9	82.00	22.00	359	30.60	83.00
	28 0.02									
6	Deadfoot Cyn.	15.00	8.1	84	8.6	75.00	37.00	310	45.40	180.00
	12 0.02									
7	Ninemile Cyn	14.2	8.0	57	6.3	68.00	44.00	385	22.30	105.00
	15 0.02									
8	Noname Cyn	15.2	7.9	104	6.4	115.00	72.00	637	37.00	246.00
	26 0.02									
9	Sand Cyn	13.0	8.1	46	4.1	59.00	16.30	280	11.40	74.00
	36 0.02									
10	Grapevine Cyn	13.2	7.9	49	5.4	78.00	21.00	336	9.60	106.00
	49 0.02									
11	Short Cyn sprg	13.3	8.1	42	1.6	55.00	7.90	209	10.00	79.00
	44 0.02									
12	IWCyn strm	13.9	7.4	38	3.7	82.00	22.00	268	14.60	151.00
	33 0.02									
13	Cow Hvn Cyn sprg		16.9	7.5	24	1.6	43.00	8.40	204	7.70
	18.00 31	0.02								
14	Sage Cyn Crk	14.8	7.6	42	1.8	58.00	11.00	275	14.70	34.00
	33 0.02									
15	Bird sprg	19.0	8.0	43	1.3	36.00	2.90	118	20.60	55.80
	20 0.02									

SELECTED_OUTPUT

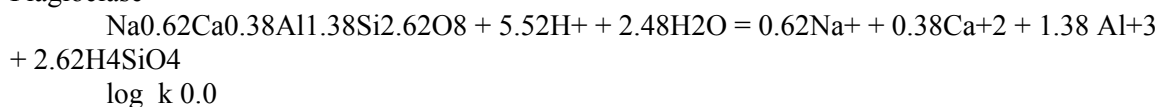
-file nasa.csv
 -inverse_modeling
 -saturation_indices CO2(g) Calcite
 PHASES
 Halite



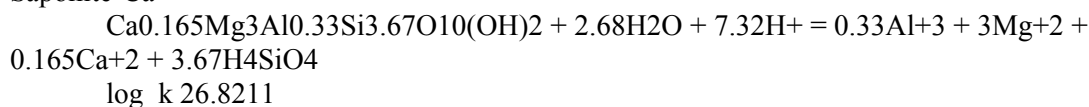
Biotite



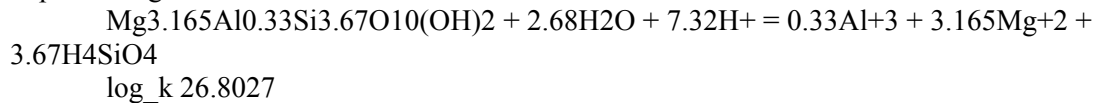
Plagioclase



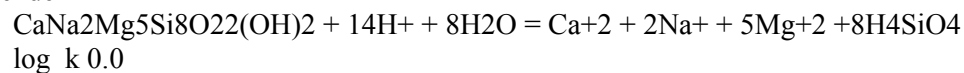
Saponite-Ca



Saponite-Mg



Hornblende



INVERSE_MODELING

-solutions 1 2

-uncertainty .05

-range

-phases

biotite dissolve
 calcite precip
 CO2(g) dissolve
 gypsum
 halite
 K-feldspar dissolve
 Plagioclase dissolve
 Saponite-Ca precip
 Saponite-Mg precip
 Kaolinite
 SiO2(a)precip
 hornblende dissolve

-minimal

END

INVERSE_MODELING

-solutions 1 3

-uncertainty .05

-range

```
-phases
    biotite dissolve
    calcite precip
    CO2(g) dissolve
    gypsum
    halite
    K-feldspar    dissolve
    Plagioclase  dissolve
    Saponite-Ca  precip
    Saponite-Mg  precip
    Kaolinite
    SiO2(a)precip
    hornblende   dissolve
-minimal
END
INVERSE_MODELING
-solutions 1 4
-uncertainty .05
-range
-phases
    biotite dissolve
    calcite precip
    CO2(g) dissolve
    gypsum
    halite
    K-feldspar    dissolve
    Plagioclase  dissolve
    Saponite-Ca  precip
    Saponite-Mg  precip
    Kaolinite
    SiO2(a)precip
    hornblende   dissolve
-minimal
END
INVERSE_MODELING
-solutions 1 5
-uncertainty .05
-range
-phases
    biotite dissolve
    calcite precip
    CO2(g) dissolve
    gypsum
    halite
    K-feldspar    dissolve
```

```

        Plagioclase    dissolve
        Saponite-Ca    precip
        Saponite-Mg    precip
        Kaolinite
        SiO2(a)precip
        hornblende     dissolve
-minimal
END
INVERSE_MODELING
-solutions 1 6
-uncertainty .05
-range
-phases
        biotite    dissolve
        calcite    precip
        CO2(g)    dissolve
        gypsum
        halite
        K-feldspar    dissolve
        Plagioclase    dissolve
        Saponite-Ca    precip
        Saponite-Mg    precip
        Kaolinite
        SiO2(a)precip
        hornblende     dissolve
-minimal
END
INVERSE_MODELING
-solutions 1 7
-uncertainty .05
-range
-phases
        biotite    dissolve
        calcite    precip
        CO2(g)    dissolve
        gypsum
        halite
        K-feldspar    dissolve
        Plagioclase    dissolve
        Saponite-Ca    precip
        Saponite-Mg    precip
        Kaolinite
        SiO2(a)precip
        hornblende     dissolve
-minimal

```

```

END
INVERSE_MODELING
-solutions 1 8
-uncertainty .05
-range
-phases
    biotite dissolve
    calcite precip
    CO2(g) dissolve
    gypsum
    halite
    K-feldspar    dissolve
    Plagioclase  dissolve
    Saponite-Ca  precip
    Saponite-Mg  precip
    Kaolinite
    SiO2(a)precip
    hornblende   dissolve
-minimal

```

```

END
INVERSE_MODELING
-solutions 1 9
-uncertainty .05
-range
-phases
    biotite dissolve
    calcite precip
    CO2(g) dissolve
    gypsum
    halite
    K-feldspar    dissolve
    Plagioclase  dissolve
    Saponite-Ca  precip
    Saponite-Mg  precip
    Kaolinite
    SiO2(a)precip
    hornblende   dissolve

```

```

-minimal
END
INVERSE_MODELING
-solutions 1 10
-uncertainty .05
-range
-phases
    biotite dissolve

```

```

    calcite
    CO2(g) dissolve
    gypsum
    halite
    K-feldspar    dissolve
    Plagioclase   dissolve
    Saponite-Ca   precip
    Saponite-Mg   precip
    Kaolinite
    SiO2(a)precip
    hornblende    dissolve
-minimal
END
INVERSE_MODELING
-solutions 1 11
-uncertainty .05
-range
-phases
    biotite    dissolve
    calcite    precip
    CO2(g)    dissolve
    gypsum
    halite
    K-feldspar    dissolve
    Plagioclase   dissolve
    Saponite-Ca   precip
    Saponite-Mg   precip
    Kaolinite
    SiO2(a)precip
    hornblende    dissolve
-minimal
END
INVERSE_MODELING
-solutions 1 12
-uncertainty .05
-range
-phases
    biotite    dissolve
    calcite    precip
    CO2(g)    dissolve
    gypsum
    halite
    K-feldspar    dissolve
    Plagioclase   dissolve
    Saponite-Ca   precip

```

```

        Saponite-Mg  precip
        Kaolinite
        SiO2(a)precip
        hornblende  dissolve
-minimal
END
INVERSE_MODELING
-solutions 1 13
-uncertainty .05
-range
-phases
        biotite  dissolve
        calcite  precip
        CO2(g)  dissolve
        gypsum
        halite
        K-feldspar  dissolve
        Plagioclase  dissolve
        Saponite-Ca  precip
        Saponite-Mg  precip
        Kaolinite
        SiO2(a)precip
        hornblende  dissolve
-minimal
END
INVERSE_MODELING
-solutions 1 14
-uncertainty .05
-range
-phases
        biotite  dissolve
        calcite  precip
        CO2(g)  dissolve
        gypsum
        halite
        K-feldspar  dissolve
        Plagioclase  dissolve
        Saponite-Ca  precip
        Saponite-Mg  precip
        Kaolinite
        SiO2(a)precip
        hornblende  dissolve
-minimal
END
INVERSE_MODELING

```

-solutions 1 15
-uncertainty .05
-range
-phases
 biotite dissolve
 calcite precip
 CO2(g) dissolve
 gypsum
 halite
 K-feldspar dissolve
 Plagioclase dissolve
 Saponite-Ca precip
 Saponite-Mg precip
 Kaolinite
 SiO2(a)precip
 hornblende dissolve
-minimal
END

INPUT FILE FROM 2002 FIELD SAMPLES

SOLUTION_SPREAD

units mg/l

number	sample	temp	pH	Na	K	Ca	Mg	Si	C(4) as HCO3 charge	Cl	S(6)
1	SNOW	5	5.92	0.026	0.253	0.527	0.103	0.025	3.59	0.76	0.611
2	A34	27.7	8.25	156.8	9.84	46	30.1	20	338.4	39.9	148.7
3	A35	19.5	7.63	110.25	8.31	128	31.25	18.6	420	33.89	147.7
4	A36	19.5	7.63	154.2	17.9	92.2	37.5	10.8	300	76.7	278.9
5	A37	20.2	7.935	18.2	0.967	58.5	8.35	8.3	188	7.21	16.1
6	A38	19.5	7.535	29.8	2.38	63.7	11.9	11.4	204	7.86	39.5
7	A39	20.8	7.824	61.9	3.55	77.9	19.5	17.1	344	18.75	83.7
8	A40	17.8	7.802	59	4.38	61.3	14.1	11.3	544	14.82	85.6
9	A41	20.2	7.492	93.5	8.29	205.25	79.75	21.9	228	37.45	208.8
10	A43	17.2	6.682	73.3	1.58	92.9	11.6	20.2	244	13.74	58.4
11	A44	22.4	7.843	65.7	0.948	83.5	11.6	22	244	15.48	76.1
12	A46	16.9	7.167	87.1	7.3	99.8	37.2	11.5	444	35.98	107.6
13	A47	17.4	7.327	95.3	7.97	128	43	12.4	400	47.51	242
14	A48	19.5	7.535	110.5	17.5	223.25	107.25	21.7	676	52.44	276.7
15	A49	17	7.543	160	18.4	198.75	146.25	21.9	800	77.44	339.4
16	A50	15.1	7.087	63.5	7.16	86.2	26.2	9.18	260	38.18	158.1
17	A51	15	7.831	109.4	8.52	95.2	35.1	12.3	308	65.77	228.5

SELECTED_OUTPUT

-file nofor.csv

-inverse_modeling

-saturation_indices CO2(g) Calcite

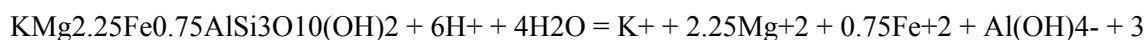
PHASES

Halite



log_k 0.0

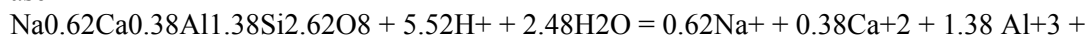
Biotite



H4SiO4

log_k 0.0

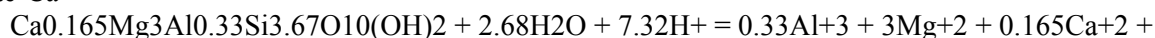
Plagioclase



2.62H4SiO4

log_k 0.0

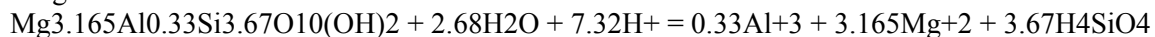
Saponite-Ca



3.67H4SiO4

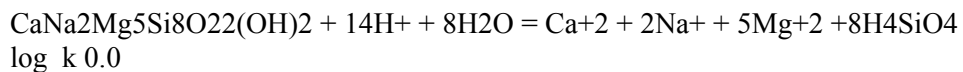
log_k 26.8211

Saponite-Mg



log_k 26.8027

Hornblende



INVERSE_MODELING

-solutions 1 2

-uncertainty .05

-range

-phases

biotite dissolve
 calcite precip
 CO2(g) dissolve
 gypsum
 halite
 K-feldspar dissolve
 Plagioclase dissolve
 Saponite-Ca precip
 Saponite-Mg precip
 Kaolinite
 SiO2(a)precip
 hornblende dissolve

-minimal

END

INVERSE_MODELING

-solutions 1 3

-uncertainty .05

-range

-phases

biotite dissolve
 calcite precip
 CO2(g) dissolve
 gypsum
 halite
 K-feldspar dissolve
 Plagioclase dissolve
 Saponite-Ca precip
 Saponite-Mg precip
 Kaolinite
 SiO2(a)precip
 hornblende dissolve

-minimal

END

INVERSE_MODELING

-solutions 1 4

-uncertainty .05

-range

-phases

biotite dissolve
 calcite precip
 CO2(g) dissolve
 gypsum

```

    halite
    K-feldspar    dissolve
    Plagioclase   dissolve
    Saponite-Ca   precip
    Saponite-Mg   precip
    Kaolinite
    SiO2(a)precip
    hornblende    dissolve
-minimal
END
INVERSE_MODELING
-solutions 1 5
-uncertainty .07
-range
-phases
    biotite    dissolve
    calcite    precip
    CO2(g)     dissolve
    gypsum
    halite
    K-feldspar    dissolve
    Plagioclase   dissolve
    Saponite-Ca   precip
    Saponite-Mg   precip
    Kaolinite
    SiO2(a)precip
    hornblende    dissolve
-minimal
END
INVERSE_MODELING
-solutions 1 6
-uncertainty .07
-range
-phases
    biotite    dissolve
    calcite    precip
    CO2(g)     dissolve
    gypsum
    halite
    K-feldspar    dissolve
    Plagioclase   dissolve
    Saponite-Ca   precip
    Saponite-Mg   precip
    Kaolinite
    SiO2(a)precip
    hornblende    dissolve
-minimal
END
INVERSE_MODELING
-solutions 1 7

```

```

-uncertainty .05
-range
-phases
    biotite dissolve
    calcite precip
    CO2(g) dissolve
    gypsum
    halite
    K-feldspar    dissolve
    Plagioclase  dissolve
    Saponite-Ca  precip
    Saponite-Mg  precip
    Kaolinite
    SiO2(a)precip
    hornblende   dissolve
-minimal
END
INVERSE_MODELING
-solutions 1 8
-uncertainty .05
-range
-phases
    biotite dissolve
    calcite precip
    CO2(g) dissolve
    gypsum
    halite
    K-feldspar    dissolve
    Plagioclase  dissolve
    Saponite-Ca  precip
    Saponite-Mg  precip
    Kaolinite
    SiO2(a)precip
    hornblende   dissolve
-minimal
END
INVERSE_MODELING
-solutions 1 9
-uncertainty .07
-range
-phases
    biotite dissolve
    calcite precip
    CO2(g) dissolve
    gypsum
    halite
    K-feldspar    dissolve
    Plagioclase  dissolve
    Saponite-Ca  precip
    Saponite-Mg  precip

```

```

        Kaolinite
        SiO2(a)precip
        hornblende      dissolve
-minimal
END
INVERSE_MODELING
-solutions 1 10
-uncertainty .05
-range
-phases
        biotite  dissolve
        calcite
        CO2(g) dissolve
        gypsum
        halite
        K-feldspar      dissolve
        Plagioclase    dissolve
        Saponite-Ca    precip
        Saponite-Mg    precip
        Kaolinite
        SiO2(a)precip
        hornblende      dissolve
-minimal
END
INVERSE_MODELING
-solutions 1 11
-uncertainty .05
-range
-phases
        biotite  dissolve
        calcite  precip
        CO2(g) dissolve
        gypsum
        halite
        K-feldspar      dissolve
        Plagioclase    dissolve
        Saponite-Ca    precip
        Saponite-Mg    precip
        Kaolinite
        SiO2(a)precip
        hornblende      dissolve
-minimal
END
INVERSE_MODELING
-solutions 1 12
-uncertainty .05
-range
-phases
        biotite  dissolve
        calcite  precip

```

```

CO2(g) dissolve
gypsum
halite
K-feldspar      dissolve
Plagioclase     dissolve
Saponite-Ca     precip
Saponite-Mg     precip
Kaolinite
SiO2(a)precip
hornblende      dissolve
-minimal
END
INVERSE_MODELING
-solutions 1 13
-uncertainty .05
-range
-phases
    biotite      dissolve
    calcite      precip
    CO2(g)       dissolve
    gypsum
    halite
    K-feldspar   dissolve
    Plagioclase  dissolve
    Saponite-Ca  precip
    Saponite-Mg  precip
    Kaolinite
    SiO2(a)precip
    hornblende   dissolve
-minimal
END
INVERSE_MODELING
-solutions 1 14
-uncertainty .07
-range
-phases
    biotite      dissolve
    calcite      precip
    CO2(g)       dissolve
    gypsum
    halite
    K-feldspar   dissolve
    Plagioclase  dissolve
    Saponite-Ca  precip
    Saponite-Mg  precip
    Kaolinite
    SiO2(a)precip
    hornblende   dissolve
-minimal
END

```

INVERSE_MODELING

-solutions 1 15

-uncertainty .05

-range

-phases

biotite dissolve
 calcite precip
 CO2(g) dissolve
 gypsum
 halite
 K-feldspar dissolve
 Plagioclase dissolve
 Saponite-Ca precip
 Saponite-Mg precip
 Kaolinite
 SiO2(a)precip
 hornblende dissolve

-minimal

END

INVERSE_MODELING

-solutions 1 16

-uncertainty .05

-range

-phases

biotite dissolve
 calcite precip
 CO2(g) dissolve
 gypsum
 halite

 K-feldspar dissolve
 Plagioclase dissolve
 Saponite-Ca precip
 Saponite-Mg precip
 Kaolinite
 SiO2(a)precip
 hornblende dissolve

-minimal

END

INVERSE_MODELING

-solutions 1 17

-uncertainty .05

-range

-phases

biotite dissolve
 calcite precip
 CO2(g) dissolve
 gypsum
 halite

K-feldspar	dissolve
Plagioclase	dissolve
Saponite-Ca	precip
Saponite-Mg	precip
Kaolinite	
SiO ₂ (a)precip	
hornblende	dissolve

-minimal
END

A60 – Noname Canyon

Solution 1 snow

units mg/l

pH 5.92

temp 5

Na 0.43

K 0.47

Ca 0.84

Mg 0.19

Si 0.17

C(4) 3.59 as HCO3 charge

Cl 0.47

S(6) 1.14

Sr 0.006

Ti 0.001

Fe 0.028

Al 0.001

Mn 0.001

Solution 2 A60

units mg/l

temp 20.2

pH 7.492

Na 93.5

K 8.29

Sr 0.036

Ca 205.25

Mg 79.75

Mn 0.002

Si 21.9

C(4) 228 as HCO3 charge

Cl 37.45

S(6) 208.8

Ti 0.001

Fe 0.009

Al 0.002

Selected_output

-file A60.csv

-inverse_modeling

-saturation_indices CO2(g) Calcite

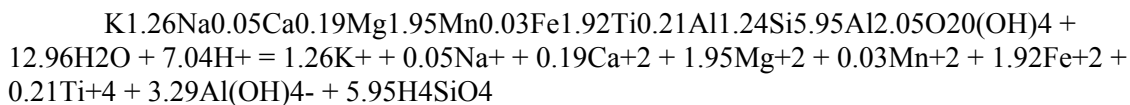
PHASES

Halite

NaCl = Na+ + Cl-

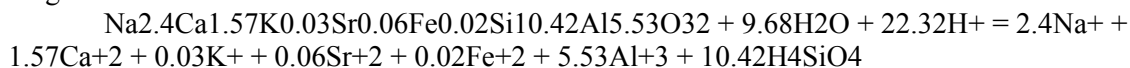
log_k 0.0

Biotite



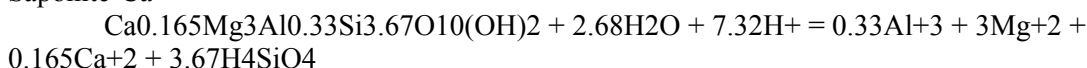
log_k 0.0

Plagioclase



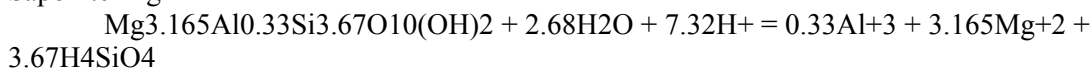
log_k 0.0

Saponite-Ca



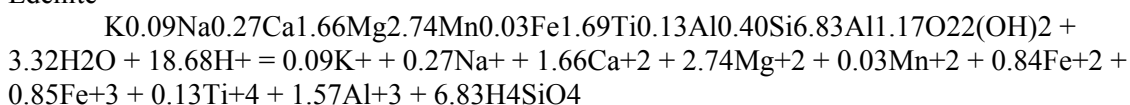
log_k 26.8211

Saponite-Mg



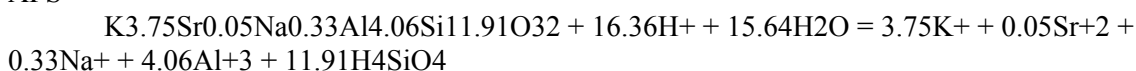
log_k 26.8027

Edenite



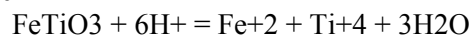
log_k 0.0

AFS



log_k 0.0

Ilmenite



INVERSE_MODELING

-solutions 1 2

-uncertainty .5

-range

-phases

biotite dissolve

calcite

CO2(g) dissolve

gypsum

halite

AFS dissolve

Plagioclase dissolve

Saponite-Ca precip

Saponite-Mg precip

Kaolinite

SiO2(a)precip

Edenite dissolve

Ilmenite precip
-minimal
END

A61 – 5-Mile Canyon

Solution 1 snow

units mg/l	
pH	5.92
temp	5
temp	5
pH	5.92
Li	0.016
Na	0.026
K	0.253
#Sr	0.006
Ca	0.527
Mg	0.103
Mn	0.006
#Fe	0.028
Si	0.025
C(4)	3.59 as HCO ₃
F	0.014
Cl	0.76
Br	0
S(6)	0.611
Al	0.005

Solution 2 A61

units mg/l	
temp	17
pH	7.543
Li	0.151
Na	160
K	18.4
#Sr	0.5
Ca	198.75
Mg	146.25
Mn	0.595
#Fe	0.047

Si	21.9
C(4)	800 as HCO3 charge
F	0.88
Cl	77.44
Br	0.369
S(6)	339.4
Al	0.020

Selected_output

-file A61.csv

-inverse_modeling

-saturation_indices CO2(g) Calcite

PHASES

Halite

NaCl = Na+ + Cl-

log_k 0.0

#Biotite2

#

$$\text{K}1.471\text{Na}0.024\text{Ca}0.081\text{Mg}2.512\text{Mn}0.045\text{Fe}2.596\text{Ti}0.194\text{Al}0.479\text{Si}5.824\text{Al}2.176\text{O}20(\text{O} \\ \text{H})3.974\text{Cl}0.023\text{F}0.003 + 9.942\text{H}_2\text{O} + 10.058\text{H}^+ = 1.471\text{K}^+ + 0.024\text{Na}^+ + 0.081\text{Ca}^{+2} + \\ 2.512\text{Mg}^{+2} + 0.045\text{Mn}^{+2} + 2.596\text{Fe}^{+2} + 0.194\text{Ti}^{+4} + 2.655\text{Al}(\text{OH})4^- + 5.824\text{H}_4\text{SiO}_4 + \\ 0.023\text{Cl}^- + 0.003\text{F}^-$$

log_k 0.0

Biotite

$$\text{KMg}2.25\text{Fe}0.75\text{AlSi}3\text{O}10(\text{OH})2 + 6\text{H}^+ + 4\text{H}_2\text{O} = \text{K}^+ + 2.25\text{Mg}^{+2} + 0.75\text{Fe}^{+2} + \\ \text{Al}(\text{OH})4^- + 3 \text{H}_4\text{SiO}_4$$

log_k 0.0

BiotiteA61

$$\text{K}1.01\text{Mg}1.5\text{Fe}1.5\text{Si}3\text{AlO}10(\text{OH})2\text{F}.01 + 4\text{H}_2\text{O} + 6\text{H}^+ = 1.01\text{K}^+ + 1.5\text{Mg}^{+2} + 1.5\text{Fe}^{+2} \\ + \text{Al}(\text{OH})4^- + 3\text{H}_4\text{SiO}_4 + 0.01\text{F}^-$$

log_k 0.0

Plagioclase

$$\text{Na}0.62\text{Ca}0.38\text{Al}1.38\text{Si}2.62\text{O}8 + 5.52\text{H}^+ + 2.48\text{H}_2\text{O} = 0.62\text{Na}^+ + 0.38\text{Ca}^{+2} + 1.38\text{Al}^{+3} \\ + 2.62\text{H}_4\text{SiO}_4$$

log_k 0.0

Saponite-Ca

$$\text{Ca}0.165\text{Mg}3\text{Al}0.33\text{Si}3.67\text{O}10(\text{OH})2 + 2.68\text{H}_2\text{O} + 7.32\text{H}^+ = 0.33\text{Al}^{+3} + 3\text{Mg}^{+2} + \\ 0.165\text{Ca}^{+2} + 3.67\text{H}_4\text{SiO}_4$$

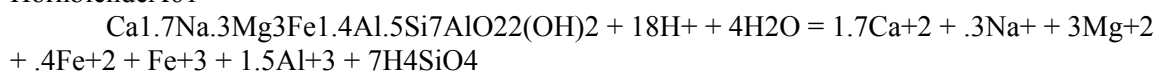
log_k 26.8211

Saponite-Mg

$$\text{Mg}3.165\text{Al}0.33\text{Si}3.67\text{O}10(\text{OH})2 + 2.68\text{H}_2\text{O} + 7.32\text{H}^+ = 0.33\text{Al}^{+3} + 3.165\text{Mg}^{+2} + \\ 3.67\text{H}_4\text{SiO}_4$$

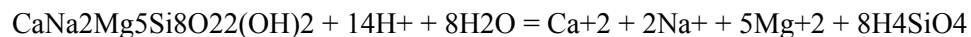
log_k 26.8027

HornblendeA61



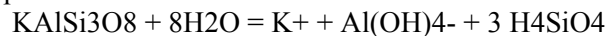
log_k 0.0

Hornblende



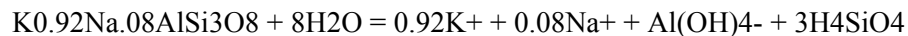
log_k 0.0

K-feldspar



LOG_K 0.0

Kspar



log_k 0.0

INVERSE_MODELING

-solutions 1 2

-uncertainty .15

-range

-phases

biotiteA61 dissolve

calcite precip

CO2(g) dissolve

gypsum

halite

Kspar dissolve

Plagioclase dissolve

Saponite-Ca precip

SiO2(a) precip

Hornblende dissolve

Kaolinite precip

-minimal

END

A62 – Sand Canyon

Solution 1 snow

units mg/l

pH 5.92

temp 5

Na 0.026

K 0.253

Sr 0.006

Ca 0.527

Mg 0.103

Si 0.025 as SiO2

C(4) 3.59 as HCO3

Cl 0.76

S(6) 0.611

Solution 2 A62

units mg/l

temp 19.5

pH 7.63

Na 110.25

K 8.31

Sr 0.375

Ca 128

Mg 31.25

Si 18.6

C(4) 420 as HCO3 charge

Cl 33.89

S(6) 147.7

Selected_output

-file A62.csv

-inverse_modeling

-saturation_indices CO2(g) Calcite

PHASES

Halite

NaCl = Na+ + Cl-

log_k 0.0

Biotite

KMg1.48Fe1.52AlSi3O10(OH)2 + 6H+ + 4H2O = K+ + 1.48Mg+2 + 1.52Fe+2 +

Al(OH)4- + 3H4SiO4

log_k 0.0

Plagioclase

Na0.573Ca0.404Sr0.012K0.011Al1.416Si2.584O8 + 5.664H+ + 2.336H2O = 0.573Na+ + 0.404Ca+2 + 0.012Sr+2 + 0.011K+ + 1.416Al+3 + 2.584H4SiO4

```

log_k 0.0
Saponite-Ca
Ca0.165Mg3Al0.33Si3.67O10(OH)2 + 2.68H2O + 7.32H+ = 0.33Al+3 + 3Mg+2 +
0.165Ca+2 + 3.67H4SiO4
log_k 26.8211
Hbld
Ca2.112Na0.433Mg2.314Fe2.343Al1.343Si7O22(OH)2 + 4H2O + 18H+ = 2.112Ca+2 +
0.433Na+ + 2.314Mg+2 + 2.343Fe+2 + 1.343Al+3 + 7H4SiO4
log_k 0.0
AFS
Na0.085K0.902Sr0.013Al1.013Si2.987O8 + 4.052H+ + 3.948H2O = 0.085Na+ +
0.902K+ + 0.013Sr+2 + 1.013Al+3 + 2.987H4SiO4
log_k 0.0

INVERSE_MODELING
-solutions 1 2
-uncertainty .05
-range
-phases
    biotite dissolve
    calcite precip
    CO2(g) dissolve
    gypsum
    halite
    AFS dissolve
    Plagioclase dissolve
    Saponite-Ca precip
    Kaolinite
    SiO2(a)precip
    hbld dissolve
-minimal
END

```

A63 – Short Canyon

Solution 1 snow

units mg/l	
pH	5.92
temp	5
temp	5
pH	5.92
Li	0.016
Na	0.026
K	0.253
#Sr	0.006
Ca	0.527
Mg	0.103
Mn	0.006
#Fe	0.028
Si	0.025
C(4)	3.59 as HCO ₃
F	0.014
Cl	0.76
Br	0
S(6)	0.611
Al	0.005

Solution 2 A63

units mg/l	
temp	22.4
pH	7.843
Li	0.067
Na	65.7
K	0.948
Sr	0.415
Ca	83.5
Mg	11.6
#Mn	0.002
#Fe	0.02
Si	22
C(4)	244 as HCO ₃ charge
F	0.98
Cl	15.48
Br	0.133
S(6)	76.1
Al	0.020

Selected_output

-file A63.csv

-inverse_modeling

-saturation_indices CO2(g) Calcite

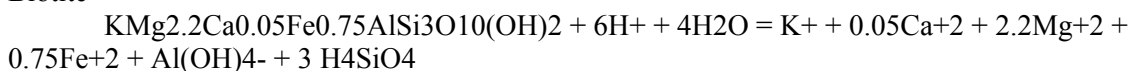
PHASES

Halite



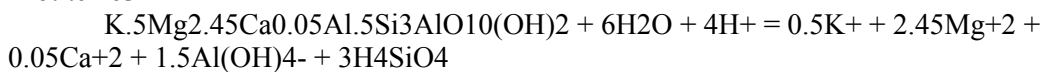
log_k 0.0

Biotite



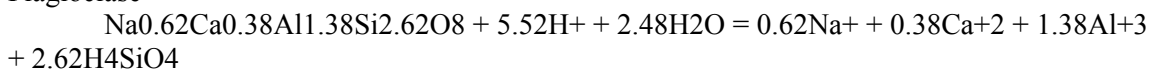
log_k 0.0

BiotiteA63



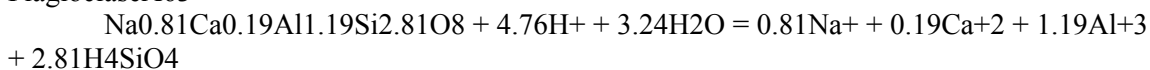
log_k 0.0

Plagioclase



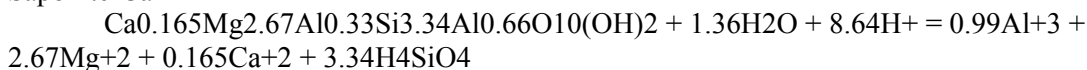
log_k 0.0

PlagioclaseA63



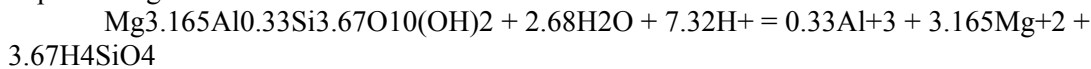
log_k 0.0

Saponite-Ca



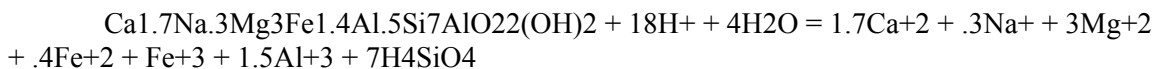
log_k 26.8211

Saponite-Mg



log_k 26.8027

HornblendeA61



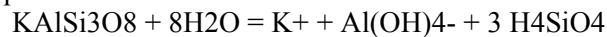
log_k 0.0

Hornblende



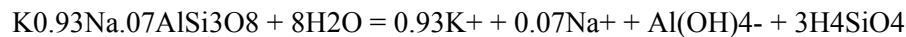
log_k 0.0

K-feldspar



LOG_K 0.0

KsparA63



log_k 0.0

INVERSE_MODELING

-solutions 1 2

-uncertainty .3

-range

-phases

biotite dissolve

calcite

CO2(g) dissolve

gypsum

halite

K-feldspar dissolve

Plagioclase dissolve

Saponite-Ca precip

SiO2(a) precip

Kaolinite precip

-minimal

END

A64 – 5-Mile Canyon

Solution 1 snow
units mg/l
pH 5.92
temp 5
temp 5
pH 5.92
Li 0.016
Na 0.026
K 0.253
#Sr 0.006
Ca 0.527
Mg 0.103
Mn 0.006
#Fe 0.028
Si 0.025
C(4) 3.59 as HCO3
F 0.014
Cl 0.76
Br 0
S(6) 0.611
Al 0.005

Solution 2 A64
units mg/l
temp 19.5
pH 7.63
Li 0.022
Na 154.2
K 17.9
Sr 0.406
Ca 92.2
Mg 37.5
Mn 0.002
Fe 0.008
Si 10.8
C(4) 300 as HCO3 charge
F 3.33
Cl 76.7
Br 0.255
S(6) 278.9

Selected_output

-file A64.csv

-inverse_modeling

-saturation_indices CO2(g) Calcite

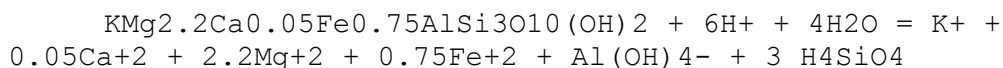
PHASES

Halite



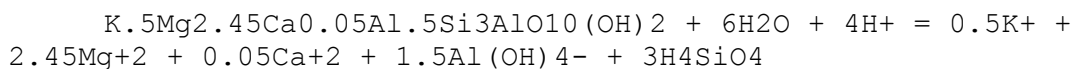
log_k 0.0

Biotite



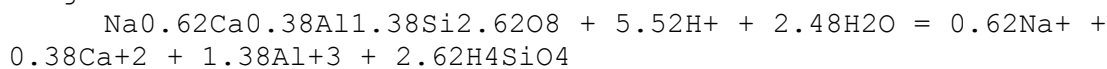
log_k 0.0

BiotiteA64



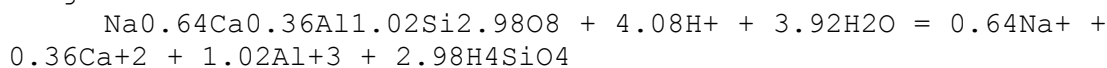
log_k 0.0

Plagioclase



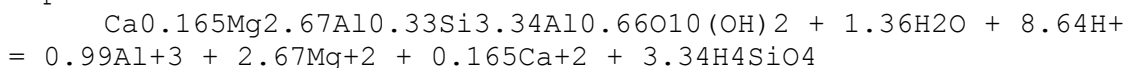
log_k 0.0

PlagioclaseA64



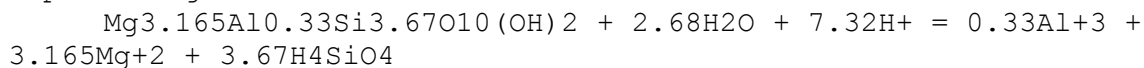
log_k 0.0

Saponite-Ca



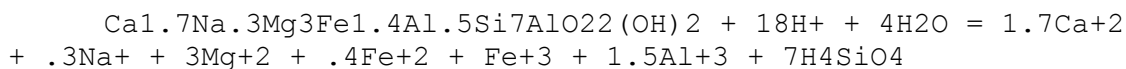
log_k 26.8211

Saponite-Mg



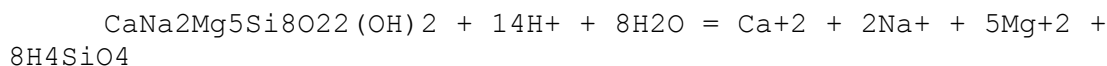
log_k 26.8027

HornblendeA61



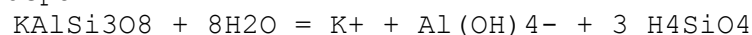
log_k 0.0

Hornblende



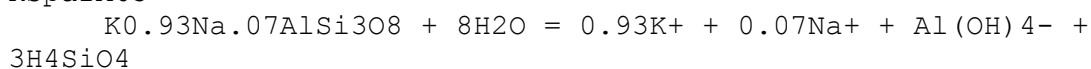
log_k 0.0

K-feldspar



LOG_K 0.0

KsparA63



```
log_k 0.0
```

```
INVERSE_MODELING
```

```
-solutions 1 2
```

```
-uncertainty .05
```

```
-range
```

```
-phases
```

```
biotiteA64 dissolve
```

```
calcite
```

```
CO2(g) dissolve
```

```
gypsum
```

```
halite
```

```
K-feldspar dissolve
```

```
PlagioclaseA64 dissolve
```

```
Saponite-Ca precip
```

```
SiO2(a) precip
```

```
Kaolinite precip
```

```
-minimal
```

```
END
```

Appendix 7: Published Mineral Dissolution Rates

Field Rates (mol/m ² /sec)					
Plag	AFS	Biotite	Hornblende	Source	Comments
3.45E-13				Paces 1986	
1.46E-11	1.46E-11	2.6E-12	9E-13	Swoboda-Colberg and Drever 1993	pH 4
5.2E-12	5.2E-12	6E-13	3E-13	Swoboda-Colberg and Drever 1993	pH 4.5
4.7E-10		8.35E-10		Taylor and Velbel 1991	accounts for bio uptake
2.73E-10		8.2E-11		Mast and Drever 1990	Loch Vale
1.23E-09				Furman et al 1998	Appalachians
10 ⁻¹⁷	10 ⁻¹⁶			White et al 2001	very old=very slow
8.55E-10				Moulton et al 2000	
9E-12	6E-13	2E-13		Clow 1992	
3.2E-11	2E-12	1.2E-12		Clow 1992	
3.16228E-14				Kenoyer & Bowser 1992	labradorite
3.98107E-14				White et al 1995	oligoclase
3.16228E-13				Velbel 1985	oligoclase
	3.1623E-17		7.94328E-17	White et al 1995	pH 4.5-7
	1.9953E-16			White 1995	pH 4.5-7
	7.9433E-15		7.94328E-15	Brantley et al 1993	
	1.5849E-14		3.16228E-14	White et al 1995	pH 4.5-7
			3.16228E-15	Swoboda-Colberg and Drever 1992	2-4.5
1.58489E-12	1.5849E-12			Kirkwood and Nesbitt 1991	
7.94328E-13				Knauss and Wolery 1986	
3.16228E-15				Schnoor 1990	
3.16228E-15	6.3096E-15			suarez and wood 1995	
	1.9953E-15			Brantley et al 1992	
	1.2589E-13			Lee at al 1998	

Laboratory Rates (mol/m ² /sec)						
Plag	AFS	Biotite	Hornblende	Source	Comments	
2.38E-09				Swoboda-Colberg and Drever 1993	pH 4	
1.36E-09				Swoboda-Colberg and Drever 1993	pH 4.5	
	2.08E-09			Swoboda-Colberg and Drever 1993	pH 4	
	1.67E-09			Swoboda-Colberg and Drever 1993	pH 4.5	
			1.8E-10	Swoboda-Colberg and Drever 1993	pH 4	
			1.4E-10	Swoboda-Colberg and Drever 1993	pH 4.5	
		5.93E-09		Swoboda-Colberg and Drever 1993	pH 4	
		3.8E-10		Swoboda-Colberg and Drever 1993	pH 4.5	
1.25893E-12				Swoboda-Colberg and Drever 1993	pH 4.5	
1.75E-12				Chou and Wollast 1985	albite	
				Busenberg and Clemency 1976	albite	
	5.0119E-13			Busenberg and Clemency 1976		
1.32E-12				Busenberg and Clemency 1976	anorthite	
		6E-13		Acker and Bricker 1992	pH 5	
3.98E-09				Sverdrup 1990	pH 7 T 8	
1.58E-08				Sverdrup 1990	pH 7 T 25	
7.08E-09				Wollast and Chou 1985	pH 5-8 T 25	
			1E-11	Sverdrup 1990	pH 7	
			2.51189E-12	Sverdrup 1990	6.2	
			1.99526E-11	Sverdrup 1990	6.8	
1E-11				Welch and Ullman, 1996		
2.51189E-12	7.9433E-12			Holdren and Seyer 1985		
1E-12				Stillings et al 1996		
				Oxburgh et al 1994		